# High Speed Systems Using GaN Visible LEDs and Laser Diodes

by

**Scott Watson**

Submitted in fulfilment of the requirements for the degree of Doctor of Philosophy

**School of Engineering**


**March 2016**

# Declaration of Authorship

This thesis consists of the author's original work, with exception of collaborative work which has been explicitly acknowledged. It has not been previously submitted for any other degree. The copyright of this thesis therefore belongs to the author and due acknowledgement must be made if any material from within is used.

Glasgow, Scotland, UK, 2016.

# *Acknowledgements*

Firstly, I'd like to thank my supervisor, Dr. Tony Kelly, for initially given me the opportunity to do this PhD and for his continuous guidance and support throughout my work. I'd like to thank all my colleagues at the University of Strathclyde, in particular Jonathan McKendry and Shuailong Zhang for their help in getting my measurements up-and-running and for providing devices. Also, my thanks go to other collaborators at the Universities of Edinburgh, St. Andrews, Oxford and Cambridge for providing the CMOS circuitry to drive the devices and some of the colour converting materials.

I'd also like to thank my colleagues and friends at the University of Glasgow for making the process more enjoyable. Thanks go to Chris Martin, Kevin Gallagher, Ross Millar and David Millar for helping to pass the time at lunch and other social activities and to everyone involved at 5-a-sides for keeping me on my toes in-between studying.

Finally, I'd like to thank my family for their support throughout the last few years, my school friends for always being around and to my girlfriend, Victoria, for putting up with me and her desire for me to get this thesis finished!

This research was funded by EPSRC's Doctoral Training Accounts (DTA) Programme.

# Publications

### Journal publications arising from the work in this thesis

1. S. Zhang, Z. Gong, J.J.D. McKendry, **S. Watson**, A. Cogman, E. Xie, P. Tian, E. Gu, Z. Chen, G. Zhang, A.E. Kelly, R.K. Henderson, and M.D. Dawson. *CMOS-controlled colour-tuneable smart display*, IEEE Photonics Journal, vol. 4, issue 5 (2012)

2. S. Zhang, **S. Watson**, A.E. Kelly, J.J.D. McKendry, D. Massoubre, A. Cogman, E. Gu, R.K. Henderdson and M.D. Dawson. *1.5 Gbit/s multi-channel visible light communications using CMOS-controlled GaN-based LEDs*, Journal of Lightwave Technology, vol. 31, issue 8 (2012)

3. ***S.Watson**, M. Tan, S.P. Najda, P. Perlin, M. Leszczynski, G. Targowski, S. Grzanka and A.E. Kelly. *High frequency modulation of a 422nm GaN laser diode*, Optics Letters, vol. 38, no. 19 (2013)

4. J.M.M. Santos, B. Jones, P. Schlosser, **S. Watson**, J. Herrnsdorf, B. Guilhabert, J.J.D. McKendry, J. De Jesus, T. Garcia, M. Tamargo, A.E. Kelly, J. Hastie, N. Laurand and M.D. Dawson. *Hybrid GaN LED with capillary-bonded II-VI MQW color-converting membrane for Visible Light Communications*, Semiconductor Science and Technology (2015)

### Other journal publication contributions

5. J. Herrnsdorf, B. Guilhabert, J.J.D. McKendry, Z. Gong, D. Massoubre, S. Zhang, **S. Watson**, A.E. Kelly, E. Gu, N. Laurand and M.D. Dawson. *Hybrid organic/GaN photonic crystal light emitting diode*, Applied Physics Letters **101** (2012)

6. P. Tian, J.J.D. McKendry, Z. Gong, S. Zhang, **S. Watson**, D. Zhu, I.M. Watson, E. Gu, A.E. Kelly, C.J. Humphreys and M.D. Dawson. *Characteristics and Applications of Micro-pixelated GaN-based Light Emitting Diodes on Si Substrates*, Journal of Applied Physics, vol. 115, issue 3 (2014)

7. P. Tian, J.J.D. McKendry, J. Herrnsdorf, **S. Watson**, R. Ferriera, I.M. Watson, E. Gu, A.E. Kelly and M.D. Dawson. *Temperature-dependent efficiency droop of blue InGaN micro-LEDs*, Applied Physics Letters, vol. 105, issue 17 (2014)

8. D. Tsonev, H. Chun, S. Rajbhandari, J.J.D. McKendry, S. Videv, E. Gu, M. Haji, **S. Watson**, A.E. Kelly, G. Faulkner, M.D. Dawson, H. Haas and D. O'Brien. *A 3 Gb/s Single-LED OFDM-based Wireless VLC Link Using a Gallium Nitride μLED*, IEEE Photonics Technology Letters, vol. 26, issue 7 (2014)

## Conference submissions

1. ***S. Watson**, J.J.D. McKendry, S. Zhang, D. Massoubre, B.R. Rae, R.R. Green, E. Gu, R.K. Henderdson, A.E. Kelly, and M.D. Dawson. *High Speed GaN Micro-Light-Emitting-Diode Arrays for Data Communications*, SPIE Security and Defence Conference (2012)

2. S. Zhang, Z. Gong, J.J.D. McKendry, B.R. Rae, **S.Watson**, E. Gu, Z. Chen, G. Zhang, A.E. Kelly, R.K. Henderson, and M.D. Dawson. *Colour-tuneable inorganic micro-display based on a CMOS-controlled III-nitride micro-LED array*, ISSLED Conference (2012)

3. S. Zhang, J.J.D. McKendry, Z. Gong, B.R. Rae, **S. Watson**, E. Xie, P. Tian, E. Richardson, E. Gu, Z. Chen, G. Zhang, A.E. Kelly, R.K. Henderson, and M.D. Dawson. *Directly color-tunable smart display based on a CMOS-controlled micro-LED array*, IEEE Photonics Conference (2012)

4. S. Zhang, **S. Watson**, J.J.D. McKendry, D. Massoubre, A. Cogman, E. Gu, R.K. Henderdson, A.E. Kelly and M.D. Dawson. *High bandwidth parallel data transmission using GaN/CMOS micro-LED arrays*, IEEE Photonics Conference (2012)

5. J.J.D. McKendry, S. Zhang, **S.Watson**, J. Herrnsdorf, D. Massoubre, A. Cogman, B. Guilhabert, N. Laurand, E. Gu, R.K. Henderson, A.E. Kelly and M.D. Dawson. *Micro-pixelated light emitting diode arrays: novel sources for data communications over POF*, POF21 Conference (2012)

6. J.J.D. McKendry, L. Geng, S. Zhang, **S.Watson**, D. Massoubre, M. Haji, E. Gu, A.E. Kelly, R.V. Penty, I.H. White and M.D. Dawson. *Gigabit data transmission over 10m polymer optical fiber using a blue-emitting light-emitting diode*, UK Nitrides Consortium (2012)

7. S.P. Najda, P. Perlin, T. Suski, L. Marona, M. Bockowski M. Leszczynski, P. Wisniewski, R. Czernecki, R. Kucharski, G. Targowski, **S.Watson**, M. Tan and A.E. Kelly. *Advances in single mode, high frequency and high power AlInGaN laser diode technology*, CLEO Pacific Rim (2013)

8. S.P. Najda, P. Perlin, T. Suski, L. Marona, M. Bockowski M. Leszczynski, P. Wisniewski, R. Czernecki, R. Kucharski, G. Targowski, **S.Watson** and A.E. Kelly. *Advances in AlInGaN laser diode technology for defence applications*, SPIE Security and Defence Conference (2013)

9. ***S.Watson**, M. Tan, S.P. Najda, P. Perlin, M. Leszczynski, G. Targowski, S. Grzanka and A.E. Kelly. *High frequency modulation of a 422nm GaN laser diode*, GRPe Conference (2013)

10. ***S.Watson**, M. Tan, S.P. Najda, P. Perlin, M. Leszczynski, G. Targowski, S. Grzanka and A.E. Kelly. *High frequency modulation of a 422nm GaN laser diode*, ICTON (2013)

11. P. Tian, J.J.D. McKendry, Z. Gong, S. Zhang, **S. Watson**, D. Zhu, I.M. Watson, E. Gu, A.E. Kelly, C.J. Humphreys and M.D. Dawson. *Micro-pixelated InGaN/GaN light emitting diodes on Si substrates*, ICNS (2013)

12. P. Tian, J.J.D. McKendry, Z. Gong, S. Zhang, **S. Watson**, D. Zhu, I.M. Watson, E. Gu, A.E. Kelly, C.J. Humphreys and M.D. Dawson. *Characteristics and applications of InGaN micro-light emitting diodes on Si substrates*, IEEE Photonics Conference (2013)

13. S.P. Najda, P. Perlin, T. Suski, L. Marona, M. Bockowski, M. Leszczynski, P. Wisniewski, R. Czernecki, R. Kucharski, G. Targowski, **S. Watson** and A.E. Kelly. *Advances in AlGaInN laser diode technology*, SPIE OPTO Photonics West Conference (2014)

14. M.A. Watson, P.M. Blanchard, C. Stace, P.K. Bhogal, H.J. White, A.E. Kelly, **S. Watson**, M.Valyrakis, S.P. Najda, L. Marona and P. Perlin. *Assessment of laser tracking and data transfer for underwater optical communications,* SPIE Security and Defence Conference (2014)

15. S.P. Najda, P. Perlin, T. Suski, L. Marona, M. Bockowski, M. Leszczynski, P. Wisniewski, R. Czernecki, R. Kucharski, G. Targowski, **S. Watson** and A.E. Kelly. *AlGaInN laser diode technology for defence, security and sensing applications*, SPIE Security and Defence Conference (2014)

16. S.P. Najda, P. Perlin, T. Suski, L. Marona, M. Bockowski, M. Leszczynski, P. Wisniewski, R. Czernecki, R. Kucharski, G. Targowski, J. Smalc-Koziorowska, S. Stanczyk, **S. Watson** and A.E. Kelly. *Advances in single mode and high power AlGaInN laser diode technology for systems applications*, SPIE OPTO Photonics West Conference (2015)

17. S.P. Najda, P. Perlin, T. Suski, L. Marona, M. Bockowski, M. Leszczynski, P. Wisniewski, R. Czernecki, R. Kucharski, G. Targowski, **S. Watson**, A.E. Kelly, M. A. Watson, P. M. Blanchard and H. J. White. *AlGaInN laser diode technology for free space telecom applications*, SPIE LASE Photonics West Conference (2015)

18. **S. Watson**, S. P. Najda, P. Perlin, M. Leszczynski, G. Targowski, S. Grzanka, M. A. Watson, H. White and A. E. Kelly. *Multi-gigabit data transmission using a directly modulated GaN laser diode for visible light communication through plastic optical fiber and water*, IEEE Summer Topicals Meeting Series (2015)

*****Oral presentation by the author.

# Contents

# List of Figures

# List of Tables

# Abbreviations

| | |
|---|---|
| **APD** | Avalanche photodiode |
| **AR** | Anti-reflection |
| **BER** | Bit-error rate |
| **BERT** | Bit-error rate test system |
| **Cd** | Cadmium |
| **CMOS** | Complementary metal-oxide semiconductor |
| **DC** | Direct current |
| **DMT** | Discrete multi-tone |
| **FWHM** | Full width at half maximum |
| **GaN** | Gallium Nitride |
| **HR** | High-reflector |
| **In** | Indium |
| **IR** | Infrared |
| **LAN** | Local area network |
| **LD** | Laser diode |
| **LED** | Light-emitting diode |
| **LVI** | Light-voltage-current |
| **Mg** | Magnesium |
| **MIMO** | Multiple-input multiple-output |
| **MOCVD** | Metal-organic chemical vapour deposition |
| **MOST** | Media Orientated Systems Transport |
| **MQW** | Multi-quantum well |
| **OFDM** | Orthogonal frequency division multiplexing |
| **OOK** | On-off keying |
| **NRZ** | Non-return to zero |
| **POF** | Plastic optical fibre |

| | |
|---|---|
| **PRBS** | Pseudo-random bit sequence |
| **RCLED** | Resonant-cavity light-emitting diode |
| **RF** | Radio frequency |
| **SDM** | Space division multiplexing |
| **Se** | Selenium |
| **SEM** | Scanning electron microscope |
| **SiC** | Silicon carbide |
| **SI-POF** | Step index plastic optical fibre |
| **SRH** | Shockley-Read Hall |
| **UUV** | Unmanned underwater vehicle |
| **UV** | Ultraviolet |
| **VCSEL** | Vertical-cavity surface emitting laser |
| **VLC** | Visible light communication |
| **WDM** | Wavelength division multiplexing |
| **Zn** | Zinc |
| **4-ASK** | Quaternary-amplitude-shift-keying |

# *Abstract*

Visible light communication is a developing technology making use of light-emitting diodes (LEDs) and laser diodes in the visible spectrum for communication purposes. This thesis looks at the use of gallium nitride (GaN) devices for high speed measurements in free space, through fibre and underwater. Micro-pixellated LEDs (micro-LEDs) have been used as a source for these measurements and the different ways to drive these devices is explored. LEDs are limited in how fast they can be driven and therefore laser diodes are also considered for these high speed measurements. The frequency responses of such devices are measured and data transmission experiments are conducted.

However, these devices can be used for more than just free-space communication. Laser diodes are much more powerful than their LED counterparts and can be modulated much faster making them ideal for fibre communications and underwater communications, where eye-safety is not an issue. By using these devices, a study of step-index plastic optical fibre (SI-POF) and multi-core fibre is carried out, analysing their dispersion properties and transmission characteristics.

Further high speed measurements were conducted under the water as the need to communicate with unmanned vehicles under the ocean continues to be an important issue. Many security and defence companies and oil and gas industries are interested in this technology for that purpose, as the current setup is complex, expensive and limited in bandwidth.

High modulation bandwidths and high data transmission rates are achieved, with some of the leading results in the field presented here. These results highlight the importance of the topic of visible light communication and show the attractiveness of using these visible GaN devices for this purpose.

# Chapter 1

# Introduction

This thesis focuses on the development of high speed communication systems using a variety of optical devices and shows some of the applications where this work can be put into practice. Micro-light-emitting-diodes (micro-LEDs) and laser diodes have been used as high speed sources for communications. This chapter will provide a general introduction to these devices, in addition to a discussion regarding the historical development of the different types of devices. The operation of such devices will be discussed and a comparison between them will be conveyed. An introduction to the fibre measurements will be presented before some words on the underwater measurements will be given. A detailed analysis of the theory will follow in **Chapter 2** with a literature review for each topic highlighting what the state-of-the-art is in contemporary research.

**Chapter 3** will follow on from the literature review by looking specifically at the application of micro-LEDs for visible light communications (VLC). It will explore the ways in which these devices can be driven and the applications that arise as a result. In covering this, detailed measurements and results relating to the different driving options will be outlined and appraised in this chapter. **Chapter 4** will then discuss the use of laser diodes for VLC. Again, the measurements which were carried out will be presented and the results discussed in detail. **Chapter 5** presents the use of fibre in communications. A study of the fibre itself as well as its dispersion properties will be presented. **Chapter 6** looks at another application using such devices: underwater communications. Similar measurements which had been carried out through free space and through fibre were conducted under the water and the results are shown here. Finally, **Chapter 7** will conclude the thesis by examining the outcomes from each of the preceding chapters and discussing some potential future areas of interest in relation to the work carried out.

## 1.1 Light-emitting-diodes

It is reported that the first discovery of electroluminescence was by a British man named Henry Joseph Round in 1907 [1], however Oleg Losev is credited with

the creation of the first ever LED in 1927 [2]. He observed the emission of light from zinc oxide and silicon carbide crystal rectifier diodes in old radio receivers when current was passing through them and published the details in a Russian journal [3]. It was not until 1962 that the first visible spectrum LED was developed by Nick Holonyak Jr. [4]. Early applications of these devices included seven segment displays such as lights for watches, calculators and other electronic equipment, and early computers. However, LEDs were expensive in the 1960s as they emerged as a new technology. Throughout the 1970s, the development of these devices resulted in LEDs ranging in wavelength from red to green with improved light output and efficiency. However, it was not until 1994 that Shuji Nakamura demonstrated the first blue LED based on Indium Gallium Nitride (InGaN) [5]. This, in turn, led to the development of white LEDs where a yellow phosphor material was used as a colour converter so that when the blue light illuminated it, white light was produced. High power white LEDs are rapidly becoming a source for general illumination, replacing incandescent and fluorescent lighting [6]. In addition to their attractive properties for lighting, these devices can be used for visible light communication where the LEDs can be modulated in order to transmit data. This energy-efficient application of dual purpose lighting is one of the many topics concerning communications which will be discussed further in Chapter 3.

### 1.1.1 Different types of LEDs and their structures

Modern LEDs range in wavelength from ultraviolet (UV) through the visible spectrum up to infrared (IR). LEDs have a much longer lifetime than their incandescent counterparts, with some exceeding 100,000 hours. These devices range in size from as small as a few microns wide, up to a few millimetres.

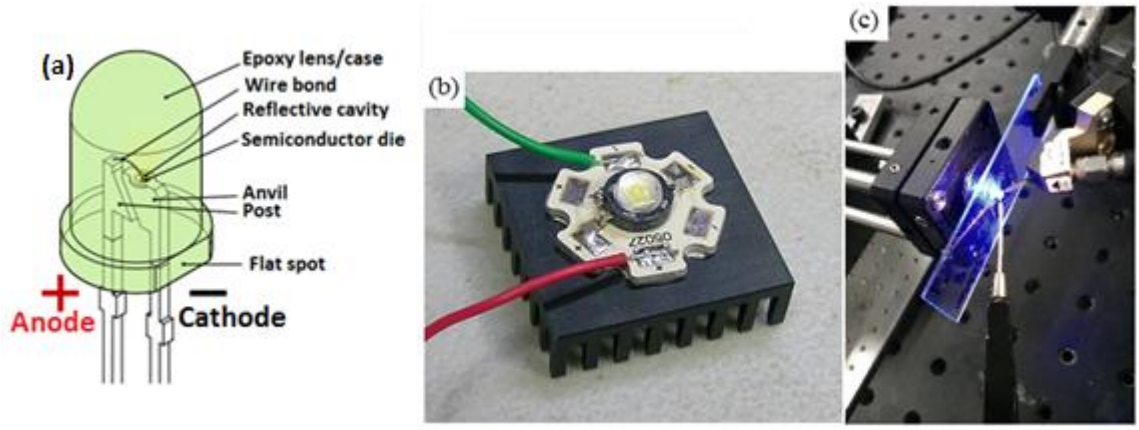


**Figure 1.1.1: (a) Schematic of a typical LED [7], (b) a high power LED connected to a heat sink and (c) a micro-LED in operation.**

Figure 1.1.1(a) shows the typical LED package which is often shown when the word LED is used. It is driven by connecting to the two metal leads: the anode and the cathode. It has a protective coating in the shape of a dome which also helps to direct the light. These devices are very cheap to buy but are limited in their power output and are often only used as indicator lights on electronic equipment. Also, these devices have very low modulation bandwidths and hence are not suited for data transmission. For white LEDs in particular, a yellow phosphor material is used to convert a blue LED to emit white light, as mentioned before. This material is even slower than the LED itself, leading to other processes being considered. High output power LEDs are commercially available, but in order for them to avoid being damaged by heat at higher currents, they require suitable heat sinking. The light output will decrease with an increase of temperature as the quantum efficiency decreases due to more non-radiative recombination in the LED [8]. These devices tend to have more than one LED die in the package to allow more light output, making them ideal candidates for applications of general illumination. A commercial, high power LED can be seen in Figure 1.1.1(b) attached to a heat sink. Devices of this type are still fairly cheap and readily available but again are limited in their communication capabilities. The use of micro-LEDs has rapidly become an interesting research topic. Micro-LEDs, in comparison to broad area LEDs, are made up of an array of separate pixels, each of which is less than 100 μm in size. Micro-LEDs can have hundreds of single transmitters, for example, a 16 × 16 array would consist of 256 individual LED pixels such as the one shown in Figure 1.1.2(a). This device has circular pixels all of the same size but some devices

have varying pixel sizes ranging from diameters as small as 5 μm up to hundreds of μm.

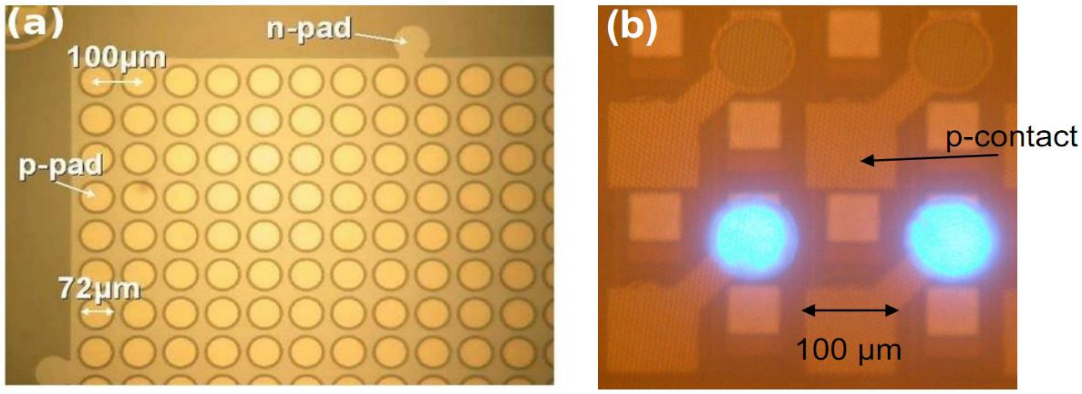


**Figure 1.1.2: (a) Image of a 16 x 16 micro-LED array and (b) a section of an 8 x 8 array in operation.**

Micro-LEDs have a number of advantages over their broad area counterparts. Firstly, they have a higher power density than broad area LEDs. A higher power output is achieved by turning on multiple pixels over the same area than that of a broad area LED [9]. Secondly, they are useful for micro-displays as it is easy to turn on certain pixels in a shape or pattern and image this as a display. The most interesting application is for communications as these micro-LEDs can be modulated at high speeds. LEDs have been used for decades as a source of sending data but the advancement in micro-LED technology has allowed for faster data transmission to be achieved. This will be discussed in greater detail in Chapter 3.

LEDs can have many complex layers or can be simple structures. The simplest LEDs are a special kind of p-n junction diode which has been optimised to increase its light output. Two adjacent layers, one of p-type material and one of n-type material, make up the basis of the diode. Electrons from the n-type material will recombine with the holes in the p-type material producing photons, which causes light to be emitted. This is called electroluminescence. Some LEDs have more complex structures such as the one shown in Figure 1.1.3.

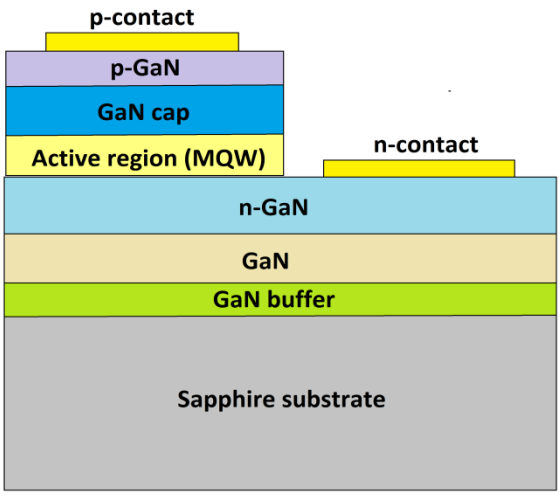


**Figure 1.1.3: Example of an LED structure.**

As mentioned before, there are two main layers: one of p-type material and one of n-type material. In this case, gallium nitride (GaN) is being used. GaN falls into the category of direct, wide bandgap III-V semiconductors. The term, 'wide bandgap' refers to semiconductors with an energy gap of larger than 1.7 eV and GaN has a bandgap of 3.26 eV [10]. For a semiconductor to be suitable for optoelectronic purposes, it must have a direct bandgap. For the applications explored in this work, a direct bandgap results in a much higher brightness from the LEDs in comparison to indirect material such as Silicon Carbide (SiC). The active region is the area where the recombination of electrons and holes takes place, and the light is emitted from here. This area also holds the multi-quantum well (MQW) region. A GaN buffer layer is included directly above the substrate to take into consideration the difference in lattice structure and a cap layer or cladding layer is included to stop electrons from escaping from the active region. Each of these processes can be edited and optimised by changing fabrication techniques.

## 1.2 Laser diodes

LEDs are cost effective and easy to handle, however their performance for VLC is limited by their material carrier lifetime [11], and therefore they cannot be modulated at high speeds. GaN laser diodes are therefore considered as a viable alternative to LEDs in order to achieve higher modulation bandwidths and error-free data transmission. A laser diode is able to output a significantly higher amount of power than an LED, indeed some of the devices used in this thesis

have the capability of producing up to 100 mW of light output power. The first ever functioning laser was reported by Theodore H. Maiman, an American physicist and engineer, who by using ruby crystal alongside a basic flashlight, was able to produce red laser light [12]. As mentioned in section 1.1, Nick Holonyak Jr. was credited with the invention of the first visible LED, however in 1962 he also demonstrated the first visible laser diode where “the current goes in one terminal and out the other terminal, and in the path itself is the light generator because of the current going from minus to plus and generating the light” [13]. The following section will discuss how these devices are structured in order to produce laser operation.

### 1.2.1 Laser diode structure and operation

When a laser diode is lasing, stimulated emission is achieved. Before the laser diode reaches this point, known as the threshold, it behaves like an LED where the emission is spontaneous, as electrons and holes recombine to produce light. In certain conditions, the electron and hole may be in the same area for a matter of microseconds before they recombine. Recombination of these photons could be stimulated if a photon of exactly the same frequency happens within this time, resulting in two photons being emitted together in the same direction, polarisation and phase. This, in itself, results in an amplified output which leads to stimulated emission of coherent light. However, there are two reflective edges, known as facets, which photons can be reflected from a number of times before they are emitted, meaning that the light is amplified further. This stimulated emission results in the diode beginning to lase. The performance of the laser relies on good facet reflectivity which depends on good cleaving of the surface edges.

A double heterostructure laser consists of a low bandgap material between two layers of high bandgap. Without any bias, the electrons and holes exist separately in the n-region and p-region, respectively. When the laser is biased, electrons and holes begin to flow within the device. Figure 1.2.1 shows the band structure of a double heterostructure laser. The active layer is confined to the thin middle layer and when a sufficient voltage is applied, electrons flow into the material of lower bandgap in the conduction band ($E_c$) and become confined. Similarly, holes follow the same process in the valence band ($E_v$). This better

confinement results in a higher chance of radiative recombination, allowing the laser to operate.

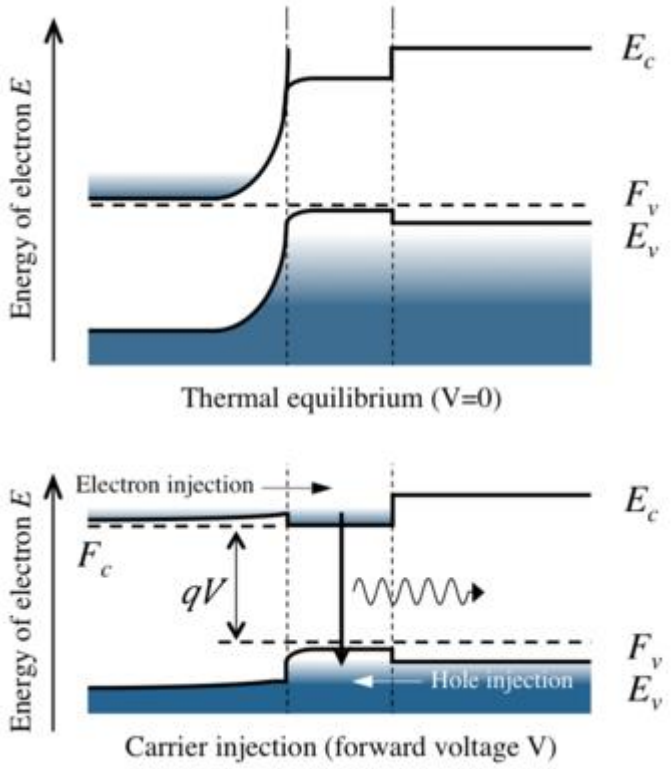


**Figure 1.2.1 Band structure showing how carriers are confined in double heterostructure lasers [14].**

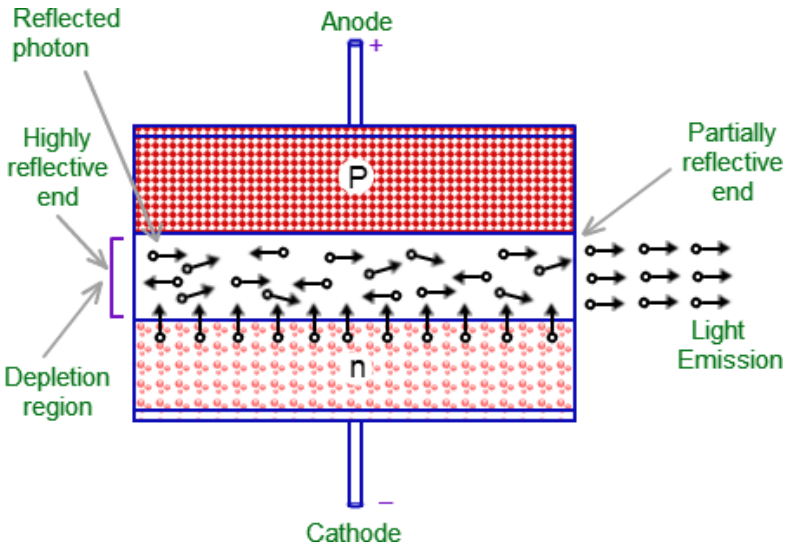


**Figure 1.2.2 Laser diode operation.**

## 1.3 LEDs and laser diodes for communications

A lot of work has been carried out using the devices mentioned above for communication purposes. LEDs and laser diodes can be modulated at high speeds allowing high speed data transmission to be achieved. Free space optical communication using LEDs has been around for a long time now, in applications such as television remote controls and controls of many other pieces of electronic equipment. Infrared (IR) emitting LEDs are used to transmit the data invisibly (to the naked eye) to control the equipment and these LEDs tend to be based on Gallium Arsenide (GaAs) or Gallium Indium Arsenide (GaInAs) structures. However, in the 1950s and 1960s these LEDs were very expensive and were seldom used [15]. As mentioned in Section 1.1, the first visible LED was created in 1962 but was not tailored to communications, rather for indicator lights on electronic equipment. However, it became apparent that using infrared light for fibre communications was potentially a good way to send data, as there are minimal limitations in terms of attenuation and dispersion at these wavelengths. Nowadays, telecommunications technology makes use of light with a wavelength of 1.3 μm and 1.55 μm, as the smallest losses through the fibre are achieved. In Chapter 5, work has been carried out to look at fibre communications using visible light, specifically from the blue part of the spectrum. There is a lack of research on wavelengths from this part of the spectrum applied to fibre communications, so its performance was analysed in depth. Laser diodes have developed over the last decade and are more suited for this purpose. However, LEDs can still play a big part in visible light communications. When a laser diode is emitting above threshold, there are issues with eye-safety, limiting their suitability in terms of general purpose applications without the addition of colour converters or other mechanisms to reduce the power. Laser diodes, as a source for VLC, are explored further in Chapter 4. Micro-LEDs are a recent technology, which have shown great potential for short range visible light communication and the measurements conducted during this PhD are portrayed in Chapter 3. Chapter 6 returns to the topic of laser diodes for another progressive technology: underwater communications. The need for subsea communications is an important issue, especially for security and defence industries. Laser diodes can be exploited here for communication purposes in order to communicate with unmanned

underwater vehicles (UUVs). A higher power output is suited for this application and there are certain wavelengths which result in low losses under the water so the use of VLC for this emerging technology appears to be the best way to replace, or at least compliment the current expensive process of acoustic communication.

The advantages of optical communications are clear to see. Light has enormous bandwidth allowing a significantly higher amount of information to be transmitted over competing techniques. The light can be easily guided, generated and detected [16]. A comprehensive literature review analysing the use of LEDs and laser diodes for communications is given in Chapter 2.

## 1.4 Fibre

There are many different types of optical fibre. Different materials are used for different applications, such as glass or plastic, and can be made up of a single core or multiple cores. Fibre is used for long distance telecommunication but can also be used for shorter, in-room applications such as small networks in a building or a vehicle. The fibre that was used initially in Chapter 5 was step-index plastic optical fibre (SI-POF). Further measurements were then conducted using novel, multi-core plastic optical fibre consisting of 19 cores. No matter what kind of fibre is used, it consists of a core (or multiple cores) and a cladding layer, each with its own refractive index. This difference in refractive index results in total internal reflection, sending the light along the fibre. In Chapter 5, it is shown that there are low levels of attenuation through plastic optical fibre not only in the red part of the spectrum, but also in the blue. By using the blue laser diodes available, experiments were conducted to analyse the performance of the fibre. GaN devices are becoming more readily available and are reducing in price [17], making them ideal sources for this work. Plastic optical fibre is not a competitor of glass fibre in terms of long distance telecommunications, however it has numerous advantages for some applications. Plastic optical fibre is cheap, light and easy to connect to existing setups. It can also be used for high bandwidth data transmission over shorter distances. The Media Oriented Systems Transport (MOST) standard is a network protocol used across the automobile industry. It makes use of plastic optical fibre as a means

of supplying multimedia services in vehicles, and is used by almost every car manufacturer worldwide [18].

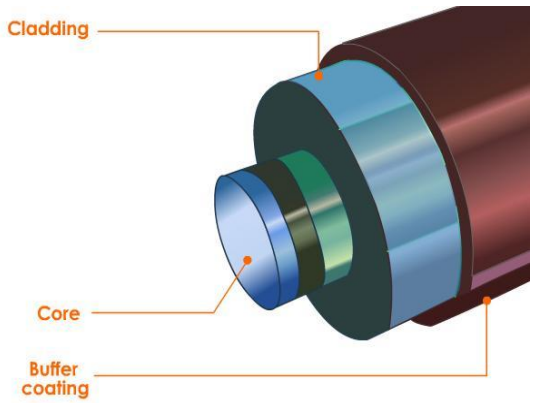


**Figure 1.4.1 Schematic showing the structure of an optical fibre [19].**

Intermodal and material dispersion are two important properties to be considered when working with multi-mode fibre, in terms of factors which may limit the transmission of light. When working with single mode fibre, an additional factor called waveguide dispersion also has to be considered. Much work has been done on fibre communications and some of the headline results in the literature will be presented in the following chapter. Fibre communications have also been implemented underwater for submarine communication [20]. However, the following section will introduce an alternative method of underwater communication using visible light which removes the need for fibre.

## 1.5 Underwater communications

There are many applications which require the use of light under the water. Light can be used for optical assessment of water quality, water turbulence and subsea tracking and imaging [21]. It is also possible to use laser diodes for visible light communication under the water. The ability to communicate with unmanned vehicles under the water or between two underwater vehicles is an important requirement. Currently, acoustic communication is the industry standard, however not only is this limited in bandwidth, it is also an expensive process with many different components involved making it unpractical. This method involves an acoustic modem to transmit data which converts digital signals into acoustic signals. The data is then received by a sensor, and a second acoustic modem converts the acoustic signal back into digital data. Visible light

communication can simplify the setup and dramatically increase the rates at which data can be transmitted. This technology will not completely take over acoustic transmission but can augment it.

There is low loss around the blue/green part of the spectrum when transmitting through water making optical transmission a convenient alternative. There is an attenuation minimum around 420 nm which can be seen in Figure 1.5.1. There are many references in the literature on the spectral absorption of water, all of which show very similar results [22] [23]. As well as the communication between unmanned vehicles, this technology can also be used for divers to communicate with each other. The ability to send light from one diver to another is a simple technique which would allow messages to be sent in a situation where this would not normally be possible.

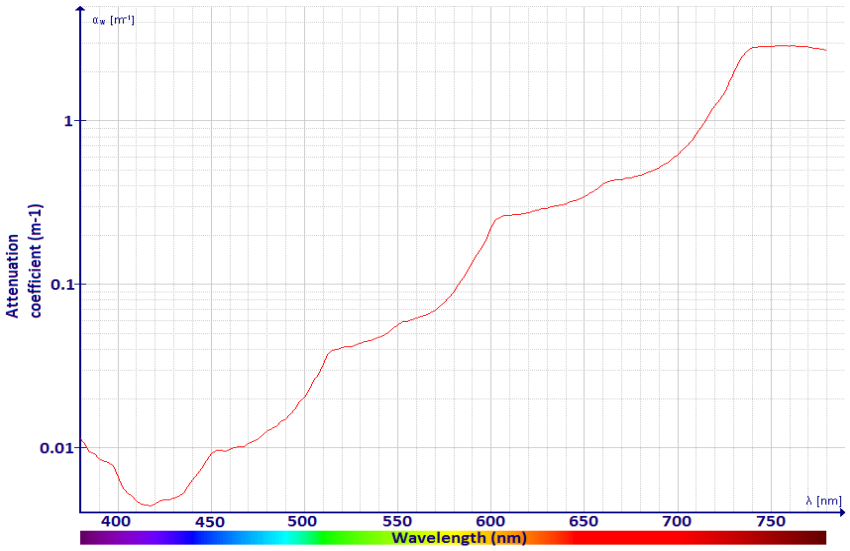


**Figure 1.5.1 Attenuation through pure water vs wavelength for the visible spectrum [22] [23].**

For the experiments described in Chapter 6, a laser diode with a wavelength of 424 nm was used to exploit this low attenuation coefficient. This work will be put in context by comparing the state-of-the-art research concerned with underwater laser diode communication.

## 1.6 Summary

In this chapter, a historical development of LEDs and laser diodes is presented. This leads on to some more modern devices which are commercially available

today, as well as some micro-LEDs which are used for measurements throughout this thesis. The structure of these devices is explored and their operation and limitations analysed.

The use of these micro-LEDs and laser diodes for communications is introduced in section 1.3. This is a particularly important section, as the bulk of this thesis is based around VLC measurements. The following section also explores the possibility of communications through fibre, with the final part of this chapter introducing the concept of underwater communications. Each of these topics will be discussed in detail in the relevant chapters, with further analysis and a review of what techniques are prevalent in the literature, in Chapter 2.

# References


[1] H. J. Round, "A note on carborumdum," *Electrical World*, vol. 19, no. 309, 1907.

[2] N. Zheludev, "The life and times of the LED - a 100 year history," *Nature Photonics*, vol. 1, no. 4, pp. 189-192, 2007.

[3] O. V. Losev, "Luminous carborundum detector and detection with crystals," *Telegrafiya i Telefoniya bex Provodov (Wireless Telegraphy and Telephony)*, vol. 44, pp. 485-494, 1927.

[4] N. Holonyak and S. F. Bevacqua, "Coherent (visible) light emission from Ga(As1-x Px) Junctions," *Applied Physics Letters*, vol. 1, no. 4, pp. 82-83, 1962.

[5] S. Nakamura, T. Mukai, and M. Senoh, "Candela-class high-brightness InGaN/AlGaN double-heterostructure blue light-emitting-diodes," *Applied Physics Letters*, vol. 64, pp. 1687-1689, 1994.

[6] E. Schubert and J. Kim, "Solid-state light sources getting smart," *Science*, vol. 308, no. 5726, pp. 1274-1278, 2005.

[7] SSTPL. (2012) SSTPL LED Lighting. [Online]. http://www.sstpl.com/sstpl_new/product_offering/LED.aspx

[8] C. J. M. Lasance and A. Poppe, *Thermal management for LED applications*, 2nd ed. New York: Springer, 2014.

[9] S. X. Jin, J. Shakya, J. Y. Lin, and H. X. Jiang, "Size dependence of III-nitride microdisk light-emitting diode characteristics," *Applied Physics Letters*, vol. 78, no. 22, pp. 3532-3534, 2001.

[10] R. Szweda, *Gallium Nitride & Related Wide Bandgap Materials and Devices: A Market and Technology Overview 1998-2003*, 2nd ed. Elsevier B. V., 2000.

[11] S. Watson, et al., "Visible light communication using a directly modulated 422 nm GaN laser diode," *Optics Letters*, vol. 38, no. 19, pp. 3792-3794, 2013.

[12] T. H. Maiman, "Stimulated Optical Radiation in Ruby," *Nature*, vol. 187, no. 4736, pp. 493-494, 1960.

[13] N. Hurst. (2012, Sep.) Wired. [Online]. http://www.wired.com/2012/10/holonyak-laser-led-inventor/

[14] K. Inc. (2014) Laser Diode Selection. [Online]. http://ldselection.com/tutorial/basics-of-laser-diode/chapter1-basics-of-laser-diode/

[15] R. Braunstein, "Radiative Transitions in Semiconductors," *Physical Review Letters*, vol. 99, pp. 1892-1893, 1955.

[16] D. J. Klotzkin, *Introduction to semiconductor lasers for optical communications: an applied approach*. New York: Springer, 2014.

[17] C. Jacques. (2012) Lux Research. [Online]. http://www.luxresearchinc.com/news-and-events/press-releases/read/bulk-gallium-nitride-costs-fall-60-2020-leading-more-efficient

[18] M. Otake, "Automotive Fiber: Automobiles make the 'MOST' use of plastic optical fiber," *LaserFocusWorld*, 2012.

[19] C. Freudenrich. (2001, Mar.) How Fiber Optics Work. [Online]. http://computer.howstuffworks.com/fiber-optic.htm

[20] B. Finn and D. Yang, *Communications under the sea: the evolving cable network and its implications*. Cambridge, Massachusetts: The MIT press, 2009.

[21] J. Watson and O. Zielinski, *Subsea optics and imaging*. Philadelphia: Woodhead Publishing, 2013.

[22] R. M. Pope and E. S. Fry, "Absorption spectrum (380-700 nm) of pure water. II. Integrating cavity measurements," *Applied Optics*, vol. 36, no. 33, pp. 8710-8723, 1997.

[23] H. Buiteveld, J. H. M. Hakvoort, and M. Donze, "Optical properties of pure water," in *Proc. SPIE 2258, Ocean Optics XII*, 1994, pp. 174-183.

# Chapter 2

# Background

This chapter will give an in depth analysis of work which has been carried out by other researchers in each of the disciplines featured in this thesis. Some background theory on each topic will be given and a literature review will follow. This chapter is delineated into four key areas: the use of LEDs for communications; the use of laser diodes for communications; fibre communications; and underwater communications.

## 2.1 LEDs for communications

Visible light communication has gathered much interest recently. An LED can be exploited to provide illumination and communication simultaneously making it an ideal energy-efficient light source. There is great potential to use this technology in hazardous environments, defence and security, medical environments, aviation and underwater where other methods of communication can be problematic. Section 2.1 will look specifically at what has been achieved using LEDs for communications and what the limitations may be.

### 2.1.1 LEDs for visible light communication

There has been an extensive amount of work carried out using LEDs for communication purposes. As mentioned in chapter 1, LEDs come in different structures and different pixel sizes. It is possible to use commercial “off the shelf” LEDs for communication purposes but the speed is ultimately limited by a number of factors. The colour converting phosphor within the structure, the capacitance limitations and the carrier lifetime all potentially limit the speed at which data transmission can be achieved. In 2010, researchers at Siemens demonstrated data transmission using commercial, white LEDs at rates up to 500 Mbit/s over 5 m [1]. This is the fastest rate of transmission achieved using “off the shelf” devices and this could be used not only to send raw data between two points, but also to stream video or even an internet signal. The idea of dual purpose lighting was introduced in the early 2000’s. Toshihiko Komine and Masao Nakagawa presented a proposed system which would use white LEDs for optical

wireless communication in a room [2]. Figure 2.1.1 shows their setup exploiting the LED lights in a room.

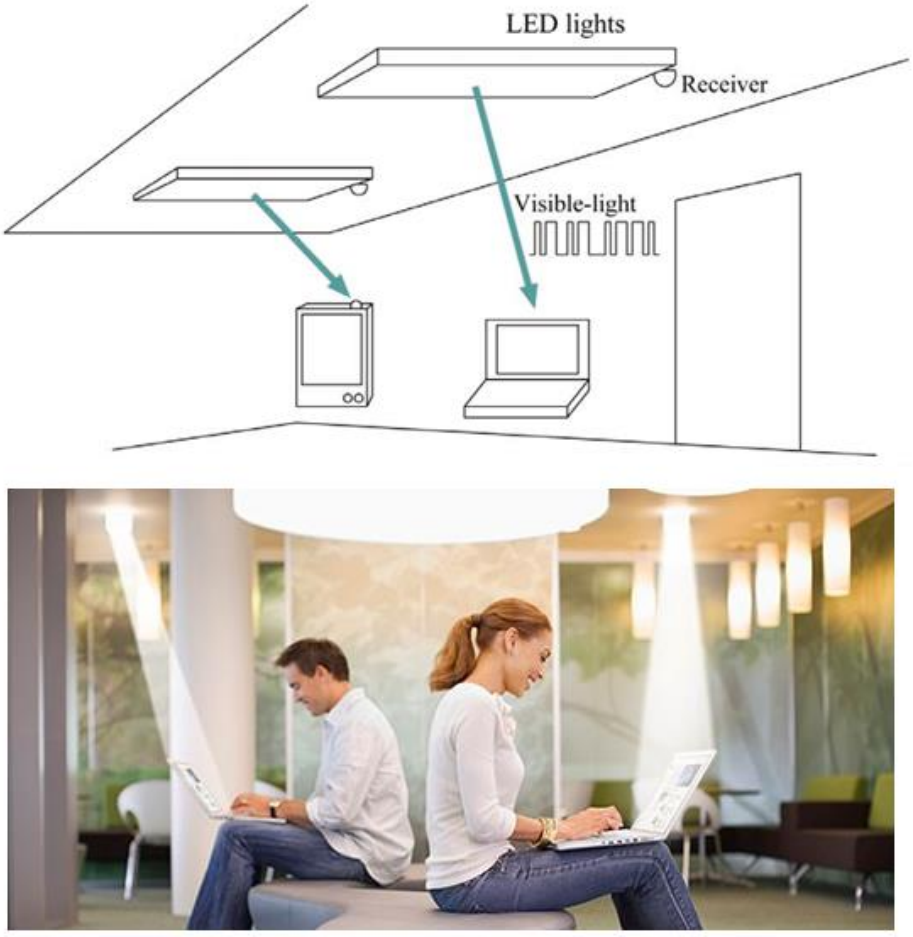


**Figure 2.1.1 A proposed visible light communication system using white LED lighting [2] [3].**

The frequency response of LEDs for optical communications is an important issue which determines how fast the device can be modulated. Kenji Ikeda *et al* have studied the different factors such as hole concentration, layer thickness and injected current density, which effect the overall bandwidth of an LED [4]. Ultimately, such devices are limited to a few megahertz. However, H. L. Minh *et al* have demonstrated that by filtering out the slow effect from the phosphor and detecting only the blue component of the LED, a data rate of 100 Mbit/s can be achieved using on-off keying (OOK) non-return-to-zero (NRZ) modulation after some simple post-equalisation [5]. Other white light VLC networks have been demonstrated using higher modulation schemes such as pulse amplitude modulation, discrete multi-tone and quaternary amplitude shift keying (4-ASK) [6] [7] [8].

Moving towards smaller structures, micro-LEDs are a leading technology for visible light communication due to their high modulation bandwidths and their ability to transmit data at much faster data rates. An example of a micro-LED structure can be seen in Figure 2.1.2. Micro-LEDs are LEDs which are made up of many micron-sized pixels. These pixels can be of equal size within the micro-LED, or be of variable size.

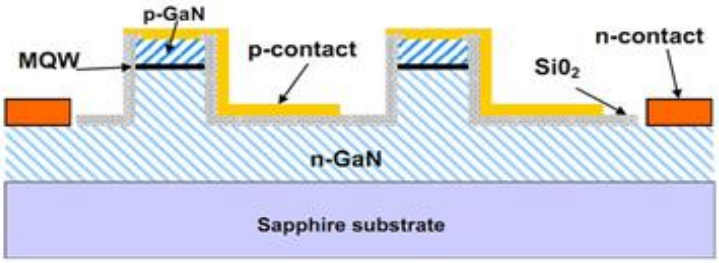


**Figure 2.1.2 Cross sectional diagram of a micro-LED structure.**

An analysis of the size-dependent bandwidth of such pixels has been carried out which shows that smaller pixels have much higher bandwidths [9]. This is attributed to the fact that they can be driven to higher current densities and their reduction in device self-heating [10].

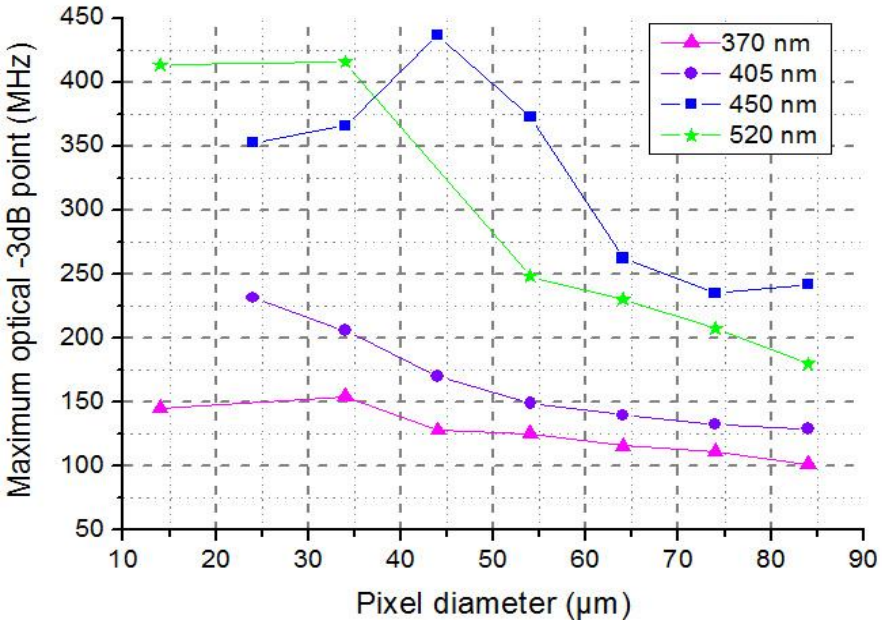


**Figure 2.1.3 Pixel diameter vs optical bandwidth for micro-LEDs of different wavelength [9].**

Smaller pixels have higher modulation bandwidths due to a reduction in carrier lifetime at higher current densities. However, despite the fact that the smaller pixels have a higher bandwidth, the power output is much lower compared to the larger pixels. Pixels with diameters ranging from 14 μm to 84 μm, in steps of 10 μm, were tested with the highest -3 dB modulation bandwidth of over 400 MHz achieved. As mentioned in chapter 1, there are two primary ways to drive the micro-LEDs. This paper has looked at both methods, with the initial size-dependent measurements carried out using high speed probes. A study of different wavelengths was also conducted looking at micro-LEDs emitting at 370 nm, 405 nm, 450 nm and 520 nm. The maximum bandwidths achieved for 450 nm and 520 nm were in excess of 400 MHz whereas the 370 nm and 405 nm devices struggled to reach 150 MHz and 250 MHz, respectively. Further measurements were conducted using a CMOS-controlled micro-LED array for data communications. Despite the CMOS circuitry limiting the system bandwidth, the smaller pixels could still reach bandwidths in excess of 150 MHz. A 24 μm pixel from a 450 nm device was chosen to perform data transmission using a bit-error rate test (BERT) setup. A maximum data rate of 512 Mbit/s was achieved using a single pixel. Further measurements using a single pixel for data transmission have been conducted and show improved transmission rates [11] [12]. It has been shown that a data rate of 1 Gbit/s can be achieved using a single 72 μm pixel emitting at 450 nm and a data rate of 1.2 Gbit/s can be achieved with the same sized pixel emitting at 520 nm. Modern techniques allow higher order modulation schemes to be used to increase data rates even further. Orthogonal frequency-division multiplexing (OFDM) is a method which can be used that encodes the data onto multiple carrier frequencies and ultimately increases the amount of data that can be sent. By exploiting pre- and post-equalisation techniques, data rates exceeding 3 Gbit/s have been achieved [13]. One of the limiting factors with LEDs for communications is their efficiency at higher current densities. The following section explores the “efficiency droop” seen in such LEDs.

### 2.1.2 Efficiency droop in LEDs

There is an on-going study into the recombination mechanisms of LEDs and how their efficiency is affected. The well-known phenomenon of “efficiency droop” is seen in AlInGaN LEDs causing their efficiency to drop off as the current density

increases. There are open-ended debates on the cause of this. Possible reasons for this include Auger recombination, carrier overflow, carrier leakage and unusual defect behaviour [14] [15]. A simple ABC model has been used to describe carrier lifetimes in narrow-gap semiconductors and recent research has been conducted to see if this model can be adapted for GaN LEDs. The rate equation model consists of three terms of interest. The A coefficient relates to a current due to Shockley-Read Hall (SRH) recombination, the B coefficient relates to the radiative recombination of electrons and holes resulting in light, and the C coefficient relates to the Auger current. The A and C coefficients are related to non-radiative recombination which means that when the electron recombines with the hole, its energy is released as heat, not light. Figure 2.1.4 shows how the three recombination processes occur.

Figure 2.1.4 (a) shows an electron and a hole recombining radiatively to produce a photon, resulting in light. Figure 2.1.4 (b) shows that an electron or hole can be trapped in a different state caused by defects in the material resulting in recombination, but giving out its energy as heat. Auger recombination involves three carriers. When an electron recombines with a hole, its energy is not given out as light or heat, but is given to a third carrier which is sent off before thermalising back down to the conduction band edge.

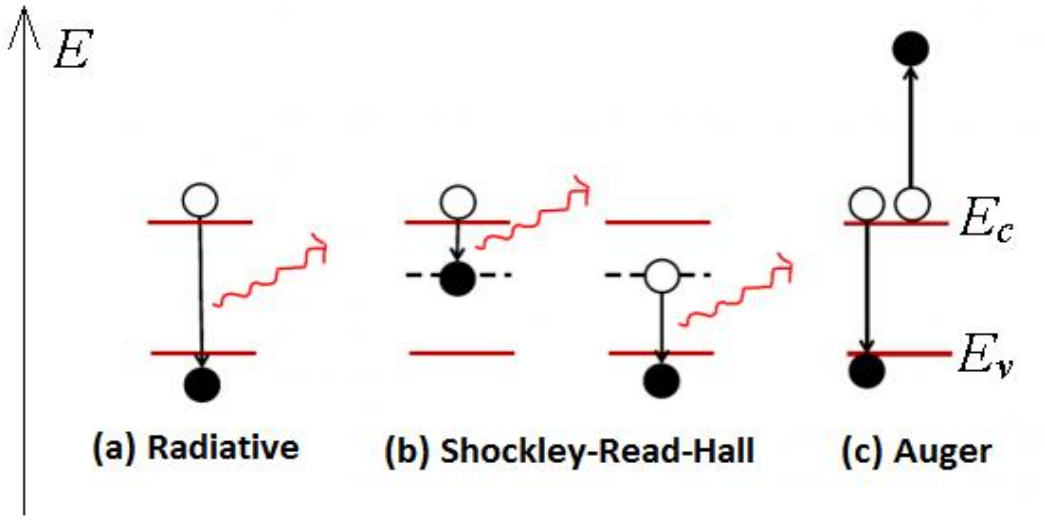


**Figure 2.1.4 Different methods of recombination.**

The total current relating to these three recombination processes is given as:

$$I = I_A + I_B + I_C = ead(AN + BN^2 + CN^3) \quad [2.1]$$

where e is the charge, a is the device area, d is the quantum well thickness, N is the carrier density within the quantum wells and A, B and C are the SRH, radiative and Auger coefficients, respectively. The SRH term is dependent on N as it only involves one carrier which becomes trapped and its energy is lost as heat. The radiative term is dependent on $N^2$ as it involves the recombination of two carriers, an electron and a hole, and its energy is given out in the form of a photon. The Auger term is dependent on $N^3$ as a third carrier is involved, as mentioned before. In order to get the carrier lifetime, the derivative of the recombination rate equation is taken with respect to carrier density:

$$\tau^{-1} = A + 2BN + 3CN^2 \quad [2.2]$$

In order to work out numerical values for each of the coefficients, the carrier versus lifetime data and the L-I data must be available. The most important term in the equation is the B coefficient as this is the part which relates to the emission of light. Typical values can be seen in Figure 2.1.5. The photon can be emitted in different ways whether it is spontaneous emission, absorption/gain or stimulated emission and the recombination rate is given as:

$$R = Bnp \quad [2.3]$$

where B is given as:

$$B(N) = \frac{B_0}{1+\frac{N}{N_0}} \quad [2.4]$$

The terms n and p relate to the electron and hole densities, respectively, therefore a low density will result in a low recombination rate, hence lowering the efficiency of the LED. $B_0$ is the value of B at low values of N and $N_0$ is a fitting parameter that describes how strongly B varies with N. Good agreement with experimental data can be only be shown over a large range of carrier densities if B is a decreasing function of N. A reduction in the optical matrix element reduces the likeliness of recombination [16].

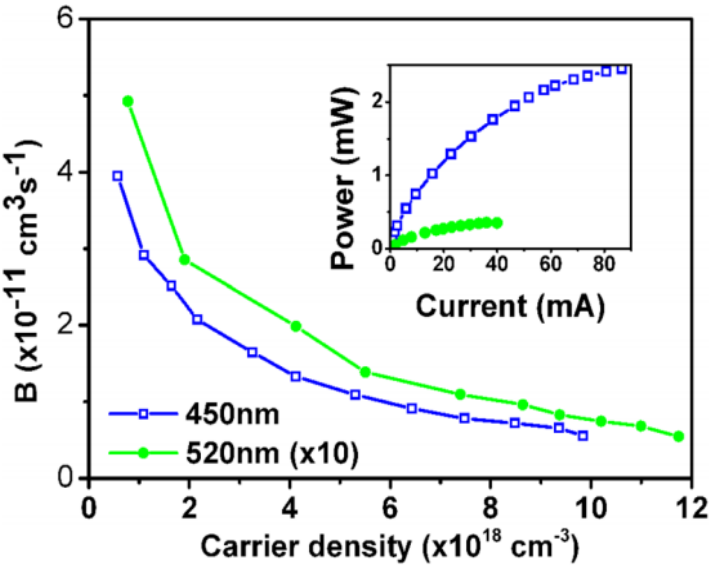


**Figure 2.1.5 Graph showing typical values for the radiative B coefficient for a 44 μm pixel emitting at 450 nm and a 54 μm pixel emitting at 520 nm [15].**

As the carrier lifetime is related to the -3dB bandwidth of the device, it is possible to obtain the quantum well densities corresponding to a certain current using the integral:

$$N(I) = \frac{n_{inj}}{ead}\int_0^I \tau \, dI \qquad [2.5]$$

where $n_{inj}$ is the injection efficiency of the carriers in the quantum wells and the other terms are as before. It is not possible to simply use the A,B,C model to fit this curve so the L-I graph is also used. By plotting B(N) versus N, it is possible to get the value for $B_0$, i.e. the value of B when N = 0. When N = 0, the value of the A coefficient will simply equal the lifetime:

$$\tau^{-1} = \lim_{I\to 0} A \qquad [2.6]$$

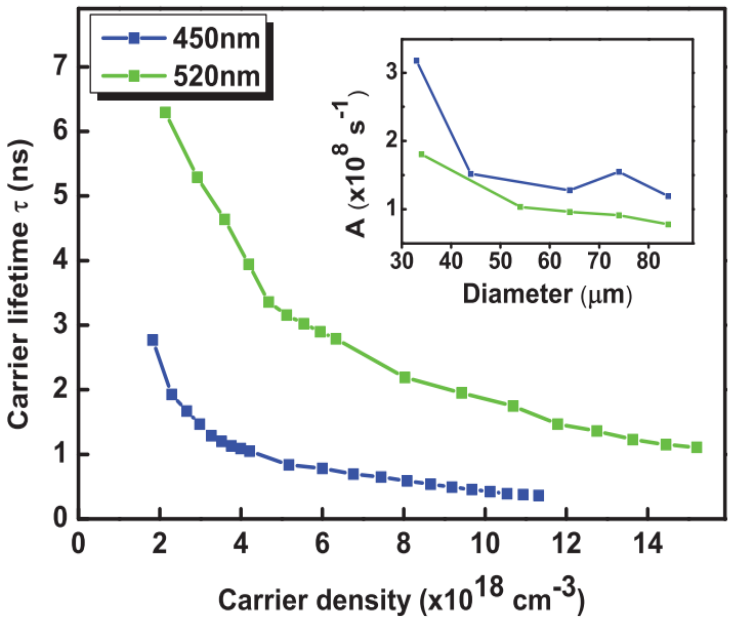


**Figure 2.1.6 Carrier lifetime vs carrier density for a 44 μm pixel emitting at 450 nm and a 54 μm pixel emitting at 520 nm. Inset: The A coefficients calculated from this data at different pixel sizes for the same wavelengths [15].**

Using this method, a presumption is made that all the remaining current is due to Auger recombination, i.e. the C coefficient. The value of C is given as:

$$C = \frac{1}{ead}\frac{dI_C}{d(N^3)} \qquad [2.7]$$

For Auger recombination, the process happens as before where an electron recombines with a hole, however in doing so it gives its energy to a second electron pushing it high into the conduction band. This electron gradually gives off its energy thermally and relaxes back towards the band edge resulting in the LED heating up, again limiting the LEDs efficiency.

This is one of the many ways being explored to extrapolate the A, B and C coefficients when using GaN structures. However, it has been shown in [17] that a fourth coefficient could be included. It has been shown that the recombination rate could become:

$$R = AN + BN^2 + CN^3 + f(N) \qquad [2.8]$$

where f(N) represents carrier leakage from the active region. This fourth term would be expanded into a power series where:

$$f(N) = \alpha N + \beta N^2 + \gamma N^3 + \delta N^4 + \varepsilon N^5 + \ldots \qquad [2.9]$$

It is shown here that f(N) can have higher than third order contributions to the recombination rate, proving that it is an important consideration and would have a large effect. However, this is just one of many explanations regarding this topic, and despite not directly using the analysis from these methods for the basis of the work in this PhD thesis, we assume the first ABC method [15] mentioned to be used.

### 2.1.3 Limitations

In an ideal world, commercial, white LEDs could provide illumination and high speed communication simultaneously. However, these LEDs are limited by a number of different factors. A commercial, white LED is most often made up of a blue LED with a yellow colour converting material. Blue LEDs can achieve bandwidths in the order of 10s of MHz, however, a typical bandwidth (without external circuitry to enhance performance) of a white LED is only a few MHz [18]. This is due to the very slow response of the colour converting material, ultimately limiting the overall bandwidth. This limiting factor is linked to the series resistance and capacitance of such devices.

$$f_{3dB} = \frac{\sqrt{3}}{2\pi\tau} \qquad [2.10]$$

The approximation of the frequency response of an LED can be worked out using equation 2.10 where τ = RC, is the RC time constant of the LED. The time constant is the limiting factor for commercial LEDs as the capacitance value is very high resulting in a low 3 dB frequency. Capacitance values in excess of 500 μF are common for these types of devices, limiting the -3 dB bandwidth to less than 10 MHz. Moving towards using micro-LEDs, this problem is overcome and they begin to be limited by the carrier lifetime which was mentioned in section 2.1.2. Their efficiency drops at higher current densities. Figure 4.1.7 shows the current density plotted against bandwidth for LEDs of different pixel sizes.

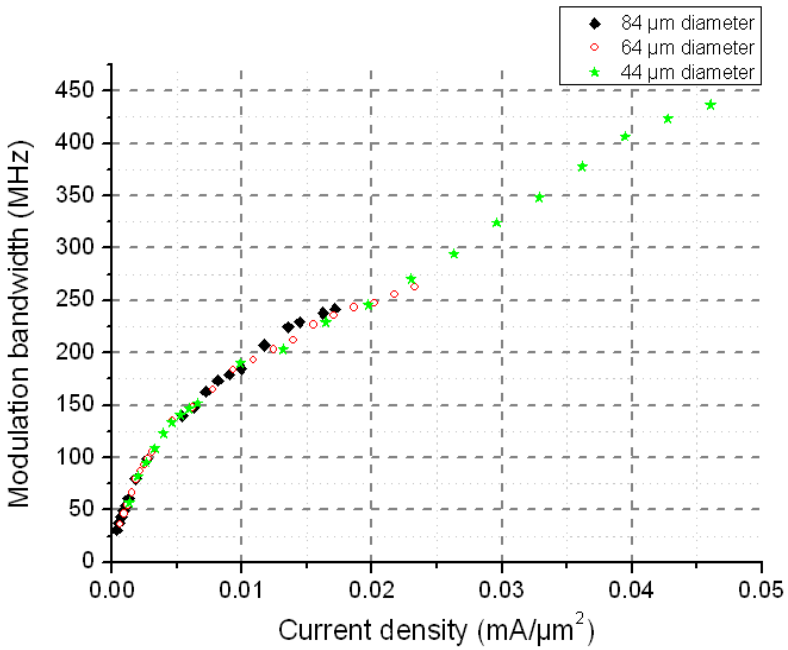


**Figure 2.1.7 Current density vs modulation bandwidth for varying pixel sizes.**

A noticeable deterioration in the LEDs performance is seen as they are driven harder and this "efficiency droop" has been explored in the previous section.

One problem which affects all LEDs is heat sinking. As the current across the LED is increased, the temperature at which it is operating is also increasing which can have an effect on its performance. Heat is generated because some of the energy from the PN junction was not converted to light and is given out as heat instead. Some commercial LEDs are already attached to large heat sink mounts which take the heat away from the device enabling it to work better. However, for some smaller LEDs, such as micro-LEDs which can be as small as a few microns in size, it can be hard to remove the effect of overheating and the pixels tend to die easily.

### 2.1.4 Eye diagrams, bit-error ratio and crosstalk

When carrying out data transmission experiments, the best way to analyse whether the data is being transmitted error-free or not, is to use eye-diagrams. Eye diagrams are the received signals which indicate the performance of the system [19]. There are two main states: the upper level known as the "1" state and the lower level known as the "0" state. If an "open eye" is shown between these two states, i.e. an area of space between the two boundaries, then it can

be confirmed that data transmission can be achieved successfully with a low bit-error rate. The bit-error ratio relates to the number of bit errors divided by the number of transmitted bits over a set time. As the data rate is increased, the "eye" begins to close, i.e. the "0" and "1" states become harder to distinguish and hence, the bit-error ratio increases.

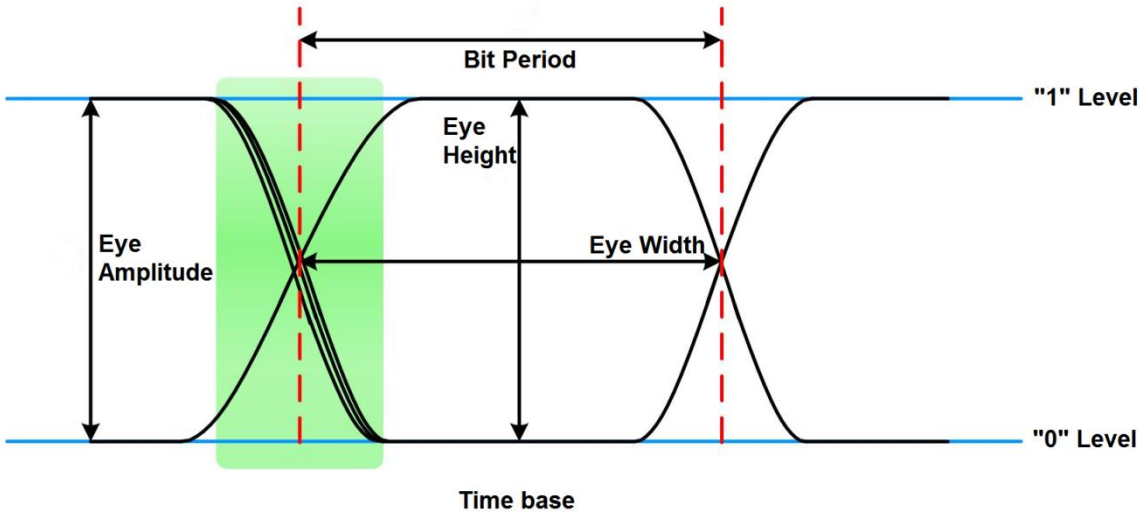


**Figure 2.1.8 Example of an open eye-diagram**

One reason that eye diagrams may begin to close is from crosstalk. It is possible that the signal can become noisier from optical crosstalk caused by other LEDs or other pixels on the same device. If there are two independent signals being sent by two separate LED pixels, then the performance of one can be degraded in the form of crosstalk from the second signal. Furthermore, electrical crosstalk can influence the signal, simply from the electronics used to drive the LEDs. The power penalty due to crosstalk can be calculated [20] [21]. If the two signals at frequencies $\omega_1$ and $\omega_2$ are combined then the field of the individual signals are:

$$E_1 = A_1 e^{j(\omega_1 t + \phi_1(t))} \quad [2.11]$$

$$E_2 = A_2 e^{j(\omega_2(t+\tau) + \phi_2(t+\tau))} \quad [2.12]$$

Therefore the power at the receiver is:

$$P_{rec} = \frac{1}{2} Re[(E_1 + E_2)(E_1 + E_2)] \quad [2.13]$$

If $P = 1/2A^2$ and $R_c = P_2/P_1$ then:

$$P_{rec} = (1 + R_c + 2\sqrt{R_c}\cos(\omega_1 - \omega_2)\,t + \omega_2\tau + \big(\phi_1(t)\big) - \big(\phi_2(t-\tau)\big)) \quad [2.14]$$

Equation 2.14 would simply become:

$$P_{rec} = P_1(1 + R_c) \quad [2.15]$$

if the two signals are at different frequencies and $|\omega_1\text{-}\omega_2|$ exceeds the receiver bandwidth.

The Q factor can be given in terms of extinction ratio and average power, $P_{av}$, as:

$$Q = \frac{2P_{av}(\frac{ER}{ER+1}\big(1+\frac{R_c}{ER}\big)-\frac{1}{1+ER}(1+(ER)R_c))}{2\sqrt{{\sigma_0}^2+{\sigma_{RIN}}^2{i_p}^2}} \quad [2.16]$$

The back to back sensitivity can be expressed as:

$$Q = \frac{2P_{sen_{b-b}}(\frac{ER}{ER+1}-\frac{ER}{1+ER})}{2\sqrt{{\sigma_0}^2+{\sigma_{RIN}}^2{i_p}^2}} \quad [2.17]$$

Therefore the power penalty, defined as $P_{av}/P_{sen}$, is given as:

$$Penalty = \frac{1}{1-R_c} \quad [2.18]$$

and in dB is expressed as:

$$Penalty\ (dB) = \frac{1}{1-R_c} \quad [2.19]$$

### 2.1.5 Colour converters

For both LEDs and laser diodes, the ability to change the wavelength emitted is important, especially as the need for dual purpose lighting of white illumination and communication simultaneously, becomes a realistic prospect. White LEDs tend to be produced in two ways. Firstly, three individual LEDs, one red, one

green and one blue, can be used to from white light. Secondly, a single blue LED can be used with a yellow phosphor material resulting in white light emission as shown in Figure 2.1.9.


**Figure 2.1.9 Diagram showing how a white LED is made up using a blue LED and yellow phosphor.**

Both these methods have advantages and disadvantages. As the first method requires three LEDs, it is hard to keep the luminous efficiency of each colour at the same level and hence the slightest change in temperature could change the colour being emitted. However, the ability to change the amount of light from each colour can be a positive characteristic as you can tune it to a desirable wavelength. Different “shades” of white can be achieved by increasing or decreasing the emission from a certain LED. Phosphor-based LEDs are simpler and cheaper than their RGB counterparts, and are the most commonly used type of white LED used on the market. However, they are limited in their modulation capabilities due to the very slow response of the phosphor material. With RGB LEDs, it is possible to modulate just one of the colours, whilst keeping the white light emission. It was shown that communication was achieved using a panel of RGB LEDs, simply by modulating the red LED, with a data rate of 19.2 kbit/s achieved [22]. Faster data rates could be achieved by modulating multiple LEDs if crosstalk is not an issue.

Further advancements in colour converters have been made, with different colours available and better modulation characteristics. The fastest data transmission using a single blue LED and a colour converter sample was shown and demonstrated 1.68 Gbit/s over 3 cm [23]. Further measurements using this material and some other similar materials were conducted during this PhD and the results are presented in chapter 4. Quantum dots are another colour

converter which can be used in this work. They are most commonly made by colloidal synthesis which involves mixing particles of one component with those of another. They can be in liquid form, however they can be poured onto glass or other materials and solidified and then illuminated for use. These are very small semiconductor materials, typically a few nanometres, and can change the output wavelength of LEDs when placed in front of them. Quantum dots are becoming a popular choice for imaging and displays due to the clear, bright emission which you can get in the visible and near-infrared. Hoshino *et al* have shown how a quantum dot LED can be used for this purpose [24]. Also, organic LEDs (OLEDs) have been used as a source for visible light communication but are again limited in their modulation capabilities. Data transmission at a few megabits per second has been achieved using organic LEDs [25] but typical -3 dB bandwidths of these devices only reach 10's of MHz [26].

## 2.2 Laser diodes for communications

It has been shown that LEDs are a potential candidate for visible light communication. However, their performance is limited by the material carrier lifetime and in order to achieve higher modulation bandwidths, and ultimately higher data transmission rates, laser diodes have to be considered. Laser diodes are important devices for communications in free space, through fibre or underwater and the fact they are limited by stimulated lifetime as opposed to spontaneous lifetime allows them to be modulated at much higher speeds. Chapter 4 will introduce a number of measurements carried out using laser diodes such as frequency response and data transmission measurements. It has been shown that a data rate of 2.5 Gbit/s can be achieved using a blue laser diode in free space and this was the fastest data rate recorded at time of publishing [27]. Further work in chapter 4 shows that the maximum data rate achieved has now reached 3.4 Gbit/s. Lasers exhibit some unusual behaviour when operating at the threshold of the device. Below threshold, lasers act as LEDs with a large linewidth. At 98.6% of threshold, this linewidth begins to decrease as the device begins to lase. Just above threshold (101.3%), the linewidth increases again, causing a change in the modulation bandwidth [28] as well as changes in capacitance, junction voltage and series resistance [29] [30]. This is shown in some of the devices in chapter 4. Chapter 5 will then explore laser diodes as a source for fibre communications. Research has been done to

consider wavelengths outwith the standard telecommunications wavelengths to see if there can be any improvements and this is covered in section 2.2.1. Finally, laser diodes are also becoming a popular source for communications under the water. Chapter 6 presents the measurements that have been carried out for this PhD.

As mentioned in chapter 1, lasers emit light though stimulated emission. This has a number of advantages over LEDs including higher output powers, narrower beams emitted and higher modulation bandwidths. Lasers can be simple structures consisting of a thin active layer between p-type and n-type cladding layers or can consist of many more layers. The lasers used for this work include waveguide layers, multi-quantum well layers and electron blocking layers. A typical structure can be seen in Figure 2.2.1 and a near-field diagram showing the mode profiles for two different ridge waveguide widths is shown in Figure 2.2.2. A detailed laser structure will be shown in Chapter 4.

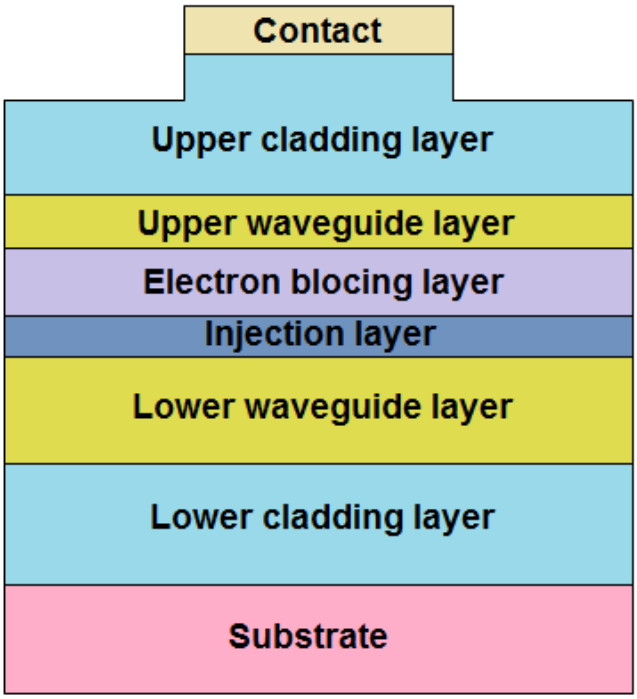


**Figure 2.2.1 Cross section of a typical laser structure.**

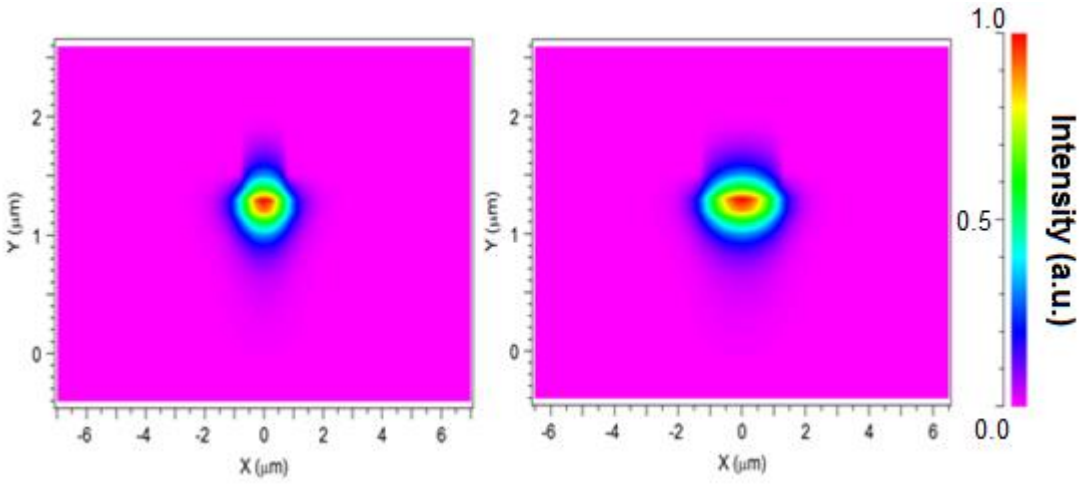


**Figure 2.2.2 Mode profiles at ridge waveguide widths of 1.5 µm and 2.5 µm.**

These laser diodes can reach powers in excess of 80 mW in CW operation; however it has been shown that by pulsing some laser diodes, powers in excess of 1 W can be achieved [31]. With the increase in power, work has been done to assess laser performance for white light illumination and ultimately communication simultaneously. The ability to have high efficiency at high current densities is an obvious advantage over LEDs and it has been shown that stable white light can be produced using a blue laser diode combined with phosphor [32] or by using multiple lasers of different wavelengths [33].

The modulation characteristics of a laser can be analysed using a set of rate equations [34]. When a laser is modulated the current across it is given as:

$$I(t) = I_b + I_m(t) \qquad [2.20]$$

where $I_b$ is the DC bias current and $I_m$ is the current due to the modulation. If there is no modulation, then the laser continues to operate at the bias current. By neglecting the effect of noise, three rate equations are used as a starting point to analyse the lasers modulation characteristics:

$$\dot{P} = (G - \gamma)P + R_{sp} \qquad [2.21]$$

$$\dot{N} = \frac{I}{q} - \gamma_e N - GP \qquad [2.22]$$

$$\dot{\phi} = -(\omega_0 - \omega_{th}) + \frac{1}{2}\beta_c(G - \gamma) \qquad [2.23]$$

where G = $\Gamma v_g g$ is the net rate of stimulated emission and $\gamma = \tau_p^{-1}$ is the photon decay rate related to the photon lifetime inside the laser cavity. $\dot{P}$ relates to the number of photons, $\dot{N}$ is the number of carriers in the active layer and $\dot{\phi}$ is the phase. Equation 2.21 is made up of two parts: the first part corresponds to the rate of stimulated emission and the second part is the rate of spontaneously emitted photons. Equation 2.22 has three parts: I = wLJ where w and L are the width and length of the laser and J is the current density flowing through the active region, and q is the charge. The second and third terms are subtracted and relate to the spontaneous and stimulated emission rates, respectively. It can be seen in that equation 2.23, some of the terms from equation 2.21 reappear. This shows that when the gain changes from its threshold value, the phase will change too. The steady state values of P, N and $\phi$ are obtained by setting the time derivatives to zero. The modulation current creates deviations, $\delta P(t)$, $\delta N(t)$ and $\delta\phi(t)$ which change due to the modulation frequency, $\omega_m$. For small-signal analysis, it is assumed that $I_m(t)$ is small enough to result in small deviations from the steady state. Small signal analysis is only valid if the modulation depth, m, is less than 1 where:

$$m = \frac{(\delta P)_{max}}{P} = \frac{[I_m(t)]_{max}}{I_b - I_{th}} \qquad [2.24]$$

The rate equations for $\delta P$, $\delta N$ and $\delta\phi$ become:

$$\delta\dot{P} = -\Gamma_p \delta P + (G_N P)\delta N \qquad [2.25]$$

$$\delta\dot{N} = -\Gamma_N \delta N - G\delta P + I_m(t)/q \qquad [2.26]$$

$$\delta\dot{\phi} = \frac{1}{2}\beta_c G_N \delta N \qquad [2.27]$$

where $\Gamma_p$ and $\Gamma_N$ are the decay rates of the photon and carrier populations and $G_N$ is the gain derivative. These equations are readily solved using Fourier transformation to show in the frequency domain as:

$$\delta\tilde{P}(\omega) = \frac{G_N P \widetilde{I_m}(\omega)/q}{(\Omega_R + \omega - i\Gamma_R)(\Omega_R - \omega + i\Gamma_R)} \qquad [2.28]$$

$$\delta\widetilde{N}(\omega) = \frac{(\Gamma_P + i\omega)(\frac{\widetilde{I_m}(\omega)}{q})}{(\Omega_R + \omega - i\Gamma_R)(\Omega_R - \omega + i\Gamma_R)} \quad [2.29]$$

$$\delta\tilde{\phi}(\omega) = \frac{\beta_c}{2i\omega}[G_N \delta\widetilde{N}(\omega)] \quad [2.30]$$

where $\widetilde{I_m}(\omega) = \int_{-\infty}^{\infty} I_m(t)\exp(-i\omega t)\,\delta t$ is the Fourier transform of the modulation current. These three equations show that the modulation current changes the population of photons and carriers inside the active region, which also affects the optical phase. The modulation response is frequency dependent due to the intrinsic laser resonance. These equations are important to the work in this thesis as the basis of the laser experiments which have been carried out are analysing the modulated behaviour of such devices. The inclusion of terms relating to the stimulated emission show the reasoning of why lasers are faster than LEDs and why these devices are important for this work.

Extensive work has been carried out using lasers for fibre communications and more recently, underwater communications, however the use of lasers for free space communications is a relatively unexplored topic. Hazardous situations can arise with the power levels emitted from a laser diode, however techniques can reduce this intensity making it appropriate for general illumination. A red laser diode was shown to transmit data at 10 Mbit/s over a 300 m free space link, with the potential of reaching 100 Mbit/s [35]. Also, it has been shown that using a 16-QAM OFDM system, a visible light communication link over 5 m has been achieved using another red laser at much higher data rates. A vertical-cavity surface emitting laser (VCSEL) with a -3 dB bandwidth of 5.2 GHz achieved data transmission rates of up to 10 Gbit/s [36]. Further work making use of laser diodes through fibre and underwater follows in the coming sections.

### 2.2.1 Laser diodes for fibre communications

Fibre communications play a vital role in everyday life from telephone signals to internet connections to cable television. By directing light through optical fibre, it is possible to transmit information from one place to another. Fibre optic communication has developed over a number of years and the wavelength used to transmit the data has also changed over time. Light at wavelengths of 1.3 μm and 1.55 μm are predominantly used for telecommunications due to their low

loss and dispersion values. However, the first working fibre communications systems operated at a wavelength of around 0.8 μm in 1975. GaAs/AlGaAs-based laser diodes and LEDs are used as transmitters. By using a GaAs semiconductor laser, a signal was sent at 45 Mbit/s over 10 km. This was soon increased as the source was changed to InGaAsP lasers emitting at 1.3 μm. Initial problems occurred with multi-mode dispersion but single-mode fibre was introduced to overcome this issue and data was sent at rates up to 1.7 Gbit/s over 50 km by 1987. The lowest losses were discovered when a system operating at 1.55 μm was introduced. Losses of approximately 0.2 dB/km were apparent allowing data transmission at rates of 2.5 Gbit/s over 100 km.

Measurements through fibre have been conducted using both LEDs and laser diodes. Resonant-cavity (RC) LEDs emitting at 650 nm have been used for a number of applications in plastic optical fibre (POF) communication [37]. Work has also shown that high data rates can be achieved using a cyan LED which achieved 1.07 Gbit/s over 50 m of POF [38]. However, more recent research has explored the potential of laser diodes for this work to improve the maximum data rates. By using discrete multi-tone (DMT) modulation techniques it has been shown that 8 Gbit/s can be achieved over 5 m of POF and that 1.62 Gbit/s can be achieved over 100 m of POF [39] [40]. Using wavelengths in the visible spectrum for fibre communications has been explored, however, dispersion becomes a limiting factor. Dispersion will be explored further in chapter 5. Section 2.2.1.1 will introduce the basics of light propagation through fibre.

### 2.2.1.1 Refraction and Total Internal Reflection

When light travels in a fibre, the speed is reduced due to the refractive index. The ratio of the speed of light in a vacuum, $c_v$, to the speed in a medium, $c_m$, is referred to as the refractive index, given as:

$$n = \frac{c_v}{c_m} \qquad [2.31]$$

Light going from a dense medium to a less dense medium, for example from glass to air, will speed up causing the light rays to bend away from the normal. If this angle is less than 90° then the light is refracted. Beyond the critical angle of 90°, the light rays will reflect back into the original medium. This is called total

internal reflection and is the process by which light travels along a fibre [41]. Figure 2.2.3 conveys how this procedure works.

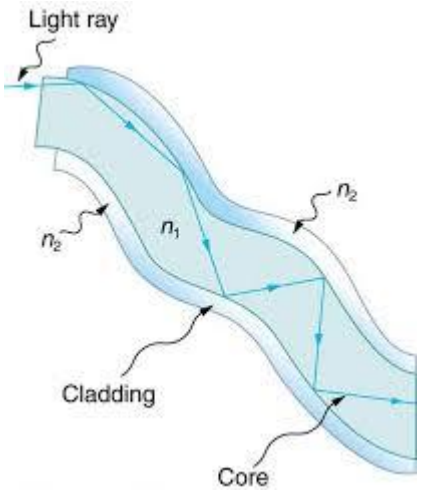


**Figure 2.2.3 Total internal reflection within a fibre.**

The core of the fibre has a higher refractive index, $n_1$, than the cladding of the fibre, $n_2$. This must be the case for total internal reflection to occur and explains why the light is propagated along the fibre. However, not all light that enters the fibre comes out the other end because if a light ray hits the wall of the fibre at an angle below the critical angle, then the light is partly refracted into the cladding.

### 2.2.1.2 Single mode fibre versus multimode fibre

Fibre can be classed as single mode or multimode. Single mode fibre has a small core which only allows one mode of light to propagate through it. Due to this, the path is very direct with fewer reflections, lowering the attenuation and increasing the distance which it can travel and the speed at which it travels at. In contrast, multimode fibre has a much larger core and allows multiple modes of light to propagate. This results in more reflections created which allows more data to be passed through. However, there are much higher levels of dispersion and attenuation in multimode fibre, reducing the quality of the signal when transmitting over longer distances. This type of fibre tends to be used for shorter distances such as the transfer of data, audio and video in local area networks (LANs) [42]. There are two main types of multimode fibre: step-index and graded-index. In step-index fibre, the different rays of lights take alternative paths and arrive at the end of the fibre at different times. Some of

the light can go direct whilst other rays of light take a zigzag route along the fibre. This means that if you are sending data through step-index multimode fibre on different modes, it is important not to overlap data signals as they can get mixed up and be untraceable at the other end of the fibre. This is why step-index multimode fibre is used over short distances as there is a limit to the amount of information that can be sent. Graded-index multimode fibre is slightly different as the refractive index of the centre of the core is higher than the areas closer to the cladding. This means that the light travelling directly in the centre will travel slower than that at the edges. This phenomenon results in the rays of light curving as opposed to zigzagging, reducing the distance the light has to travel. This shorter path combined with the fact that it travels faster at the edges means that it arrives at the end of the fibre at the same time as the straight but slower rays in the centre. This results in lower temporal dispersion, allowing data to be sent with fewer errors. Figure 2.2.4 gives a diagrammatic summary of the three types of fibre.

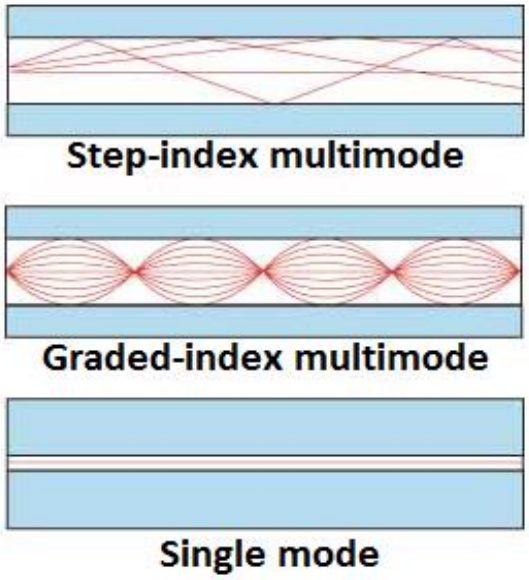


**Figure 2.2.4 Schematic showing the propagation of light in three different types of fibre [43].**

As well as these types of fibre, they can be classed further into single core or multi-core fibre. Single core fibre, as the name suggests, simply consists of one core in the centre of the fibre surrounded by the cladding. Multi-core fibre, however, can have many cores inside a single cladding, which can be advantageous for increasing the amount of data being sent. Space Division Multiplexing (SDM) could be explored as a technique to exploit these different

cores and send data through them to enhance the transmission capacity. Chapter 5 presents measurements carried out for this thesis using multi-core fibre and looks at the benefits and limitations of it. An in depth study of the dispersion properties is addressed and a look at the modulation characteristics of the fibres is presented.

### 2.2.2 Underwater communications

Visible light communication under the ocean is becoming an important emergent technology. The use of visible light from an LED or laser diode to transmit data underwater is developing as a promising method for oil and gas companies and security and defence companies to communicate with unmanned vehicles under the ocean. It has been shown that it is possible to communicate over short distances underwater, and with the advances in tracking and sensor systems, this technology lends itself for this purpose. Hanson and Radic have shown error-free data transmission underwater at 1 Gbit/s over 2 m using light emitted at 532 nm [44]. Gigabit-per-second data transmission underwater is a relatively new phenomenon and this paper shows some of the fastest results recorded underwater. Measurements conducted underwater during this PhD are presented in chapter 6 and show improved results. On a larger scale, it has been shown that longer distances can be achieved with megabit-per-second data rates at distances up to 200 m [45]. An example of an underwater communication system can be seen in Figure 2.2.5 where a ship on the surface of the water can communicate with unmanned vehicles at the bottom of the sea. Also, this technology can be used to create a communication link between two subsea vehicles.

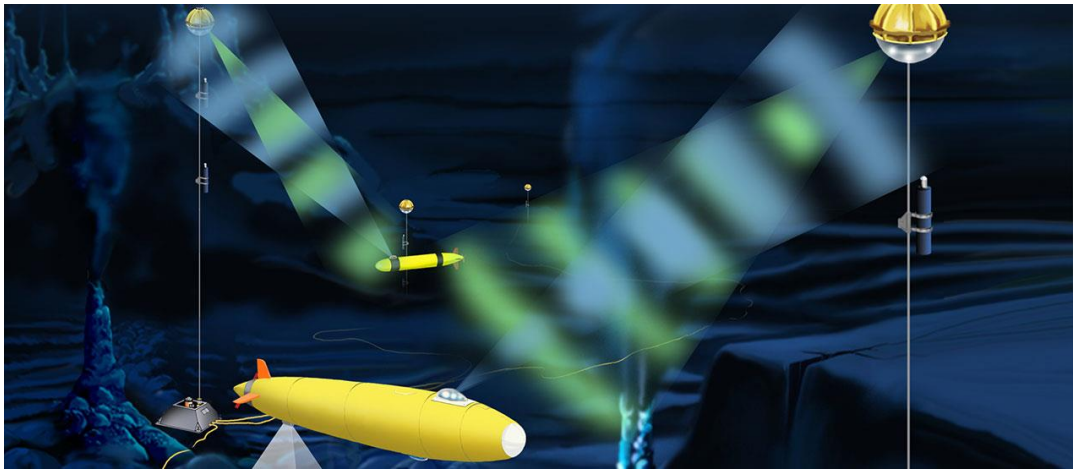

**Figure 2.2.5 Example of an underwater visible light communication system where unmanned vehicles can communicate with other vehicles above and below the water [46].**

Many current systems use acoustics as a means of communicating under the water. However due to the small available bandwidth, the strong signal attenuation underwater and multi-path propagation, amongst other limiting factors, there is great difficulty in this technique. Other methods include the use of very long cables attached to robotic vehicles and sent deep underwater. This cable can be very heavy and expensive, and sometimes may need to go 5000-10,000 metres under the water [47]. Despite the setbacks, a fibre underwater communication system is currently the best way to transmit data over large distances. Thousands of kilometres can be achieved using this method with international links in place worldwide. A system working at 4.8 Tbit/s using six fibre pairs, spanning thousands of kilometres shows how far this technology has developed [48]. Systems like this still operate today, however with the ever-growing running costs and repair costs, visible light communication could be introduced to compliment acoustic systems and provide a robust way of sending data over shorter distances. It has been shown that acoustic systems can reach several kilometres at low bit rates of 1 kbit/s [49] and with the advancements of optical systems, an integrated optical/acoustic system could improve things further.

Another problem which needs to be addressed is the different optical properties of water, as the water type can affect the transmission in different ways. There are many other factors to consider such as location, time of day and turbulence. Sunlight can have an effect on the overall attenuation, however by operating at Fraunhofer lines, this solar background can be  reduced by making use of filters

[50]. There are four main water types which are usually considered [51]: pure seawater, clear ocean water, coastal ocean water and turbid harbour water. Pure seawater has low levels of scattering allowing the beam to propagate almost undisturbed in a straight line. However, this can induce signal loss through absorption. Coastal ocean water, and even clear ocean water, contains dissolved particles resulting in larger amounts of scattering. Coastal ocean water has additional issues with the presence of phytoplankton further limiting the signal by absorption. As expected, turbid harbour water has the highest overall loss. The presence of debris and organic matter such as humic acid, results in high attenuation, especially at blue wavelengths. Figure 2.2.6 shows a graphical representation of the levels of attenuation for each water type. It can be seen that for pure and clear ocean water there is a low level of attenuation, however the attenuation levels seen in harbour water suggests that communication would be hard to achieve over longer distances.

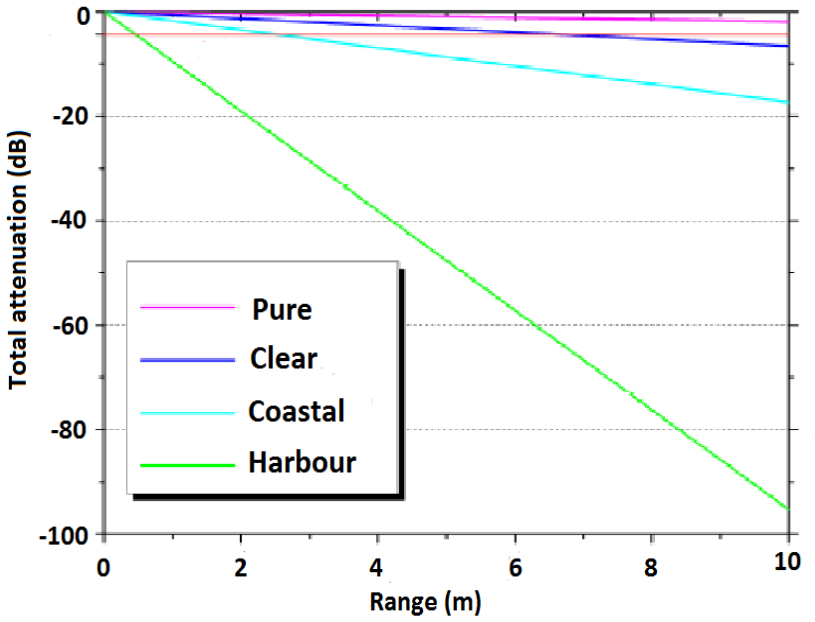


**Figure 2.2.6 Total attenuation over 10 m for various water types at a wavelength of 530 nm [52].**

The total attenuation can be due to absorption, scattering or both. Absorption is a function of the waters refractive index and the wavelength of the light. There is less attenuation due to absorption in sea water at wavelengths between 400 nm and 500 nm. Scattering is when the light shines in other directions other than straight forward – in this case due to the water- hence the beam is spread

reducing the intensity of the light. There are two main types of scattering to consider here, based on the size of the particles: Rayleigh scattering and Mie scattering. Rayleigh scattering is caused by small particles in the water which are much smaller than the wavelength of the light. Organic and inorganic particles are larger and have more effect, resulting in more scattering which is known as Mie scattering.

Chapter 6 will look at the measurements conducted using a blue laser diode underwater. The water quality was similar to that of turbid, coastal water. Maalox antacid was added in controlled amounts to investigate the effect of scattering. The frequency response and data transmission characteristics are presented and the ability to track the signal is shown.

## 2.3 Optical receivers

For all the measurements mentioned in this chapter, an appropriate optical receiver is required in order to convert the optical signal back into an electrical signal and therefore recover the data which has been transmitted through the system. Ideally the photo-detector should have a fast response, high sensitivity, low noise, low cost and high reliability. A p-i-n photo-detector has been used for the measurements conducted throughout this thesis. The photocurrent, $I_p$, is directly proportional to the incident optical power, $P_{in}$, at the detector:

$$I_p = RP_{in} \qquad [2.21]$$

where R is the responsivity of the detector in A/W. The responsivity can be expressed in terms of quantum efficiency, η, as:

$$\eta = \frac{electron\ generation\ rate}{photon\ incidence\ rate} = \frac{{}^{I_p}/_{q}}{{}^{P_{in}}/_{hv}} = \frac{hv}{q}R \qquad [2.22]$$

and therefore:

$$R = \frac{\eta q}{hv} \approx \frac{\eta \lambda}{1.24} \qquad [2.23]$$

where $\lambda = c/v$ in micrometres. The responsivity increases with wavelength as there are more photons present for the same optical power level [53].

The bandwidth of the receiver is another important issue. It is determined by the speed at which it responds to variations in the incident power. The bandwidth limit of the photo-detector used in this thesis was 1.4 GHz which was adequate for micro-LED measurements but became an issue when working with laser diodes. Some of the laser diodes had a faster bandwidth that the detector itself and hence this had to be taken into consideration.

A reverse-biased p-n junction consists of a depletion region where a built-in electric field stops electrons from the n-side getting to the p-side and stops holes getting from the p-side to the n-side. When light is incident on one side of the p-n junction, electron-hole pairs are generated through absorption, however, due to the electric field present the electrons and holes drift to the n- and p-sides, respectively. The resulting current that flows is related to the incident optical power. A p-i-n photodiode contains a layer of undoped semiconductor material between the p-n junction. As the middle i-layer is intrinsic, it has a high resistance and most of the voltage drop occurs here. This results in the depletion region extending in the i-layer and its width is controlled by changing the middle layer thickness. The main difference between the p-n photodiode and the p-i-n photodiode is that most of the light is absorbed in the i-layer and the width of the i-layer can be tailored to create a compromise of speed and sensitivity. A p-i-n photodiode also offers a lower capacitance and hence, is better suited for higher bandwidth applications. However, as it requires reverse bias, a noise current is introduced which reduces the signal to noise ratio. This makes p-n photodiodes better for low light applications [54]. High mobility in photodiodes is desirable as it allows more carriers to get collected and therefore a higher mobility provides a higher efficiency. The detector used for the measurements in this thesis (HSA-X-S-1G4-SI) is a silicon p-i-n detector with a bandwidth of up to 1.4 GHz, as mentioned previously. It covers a range of wavelengths from 320 nm up to 1000 nm. The sensitivity is a function of wavelength. At the lower end of the spectrum, a responsivity value of 0.1 A/W is seen, however at 760 nm the value is 0.5 A/W. Most of the measurements which were carried out were around 420-450 nm which relates to a responsivity of 0.2 A/W.

The performance of a photo-receiver depends heavily on the signal-to-noise ratio (SNR). Noise at the receiver can be problematic when working with small signals. There are two main causes of noise: shot noise and thermal noise. Shot noise is an electronic noise which is related to the stream of electrons created at random times in an electric current. Thermal noise relates to the random movement of electrons in a conductor, resulting in the current fluctuating even without an applied voltage. Obviously, the lower the level of noise present, the easier the signal will be detected and better results can be achieved. Avalanche photodiodes (APD) are another kind of optical receiver which offer increased sensitivity which is helpful when you have a very weak signal. However, they are more complex to use in comparison to p-i-n detectors and require a high bias voltage of between 100-300V [55]. More recently, optical receivers are being made for specific purposes such as in [56] as developments in sensitivity and bandwidth continue. This thesis focuses primarily on the performance of different transmitters in different mediums, however at a systems level, detectors will play an important role. Ultimately, further measurements could be conducted with a detector of higher sensitivity at the appropriate wavelengths and with an increased bandwidth to improve the results.

## 2.4 Summary

This chapter has looked at the background theory and other literature related to the main results sections of this thesis. It began by looking at work which has been carried out using LEDs for communications before analysing the topic of "efficiency droop". An in depth study of the recombination mechanisms was presented and a look at some other limitations of LEDs has been shown. An introduction to eye diagrams is presented and an analysis of the crosstalk encountered in data transmission is explored. Section 2.2 then looked at the use of laser diodes for communications, firstly in free space, then in fibre and finally underwater. Measurements and results from other literature were analysed and the methods for the experiments carried out for this PhD are presented. Section 2.3 looks at different optical receivers and their uses. Micro-LEDs and laser diodes both have advantages and disadvantages. A brief comparison of their performance is shown in Table 2.4.

| | **Micro-LED** | **Laser diode** |
|---|---|---|
| Emission | Surface | Edge |
| Output power | ~mW | ~100mW |
| Modulation bandwidth | ~400 MHz | >2 GHz? |
| Alignment tolerances | High | Low |

**Table 2.4 Micro-LED and laser diode comparison.**

The following chapters will look at each of the main topics in detail, starting with micro-LEDs for communications in chapter 3.

# References


[1] Siemens, "500 Megabits/Second with White LED Light," Press Release, 2010.

[2] T. Komine and M. Nakagawa, "Findamental Analysis for Visible Light Communication System using LED Lights," *IEEE Transactions on Consumer Electronics*, vol. 50, no. 1, pp. 100-107, 2004.

[3] F. HHI. (2015) Fraunhofer: Optical Wireless Communication. [Online]. https://www.fraunhofer.de/en/fields-of-research/communication-knowledge/broadband-communications/visible-light-communication.html

[4] K. Ikeda, S. Horiuchi, T. Tanaka, and W. Susaki, "Design Parameters of Frequency Response of GaAs-(Ga,Al)As Double Heterostructure LED's for Optical Communications," *IEEE Transactions on Electron Devices*, vol. 24, no. 7, pp. 1001-1005, 1977.

[5] H. L. Minh, et al., "100-Mb/s NRZ Visible Light Communications Using a Postequalized White LED," *IEEE Photonics Tecnhology Letters*, vol. 21, no. 15, pp. 1063-1065, 2009.

[6] J. Grubor, S. Randel, K.-D. Langer, and J. W. Walewski, "Broadband Information Broadcasting Using LED-Based Interior Lighting," *Journal of Lightwave Technology*, vol. 26, no. 24, pp. 3883-3892, 2008.

[7] J. Vucic, C. Kottke, S. Nerreter, K.-D. Langer, and J. W. Walewski, "513 Mbit/s Visible Light Communications Link Based on DMT-Modulation of a White LED," *Journal of Lightwave Technology*, vol. 28, no. 24, pp. 3512-3518, 2010.

[8] C. H. Yeh, et al., "Investigation of 4-ASK modulation with digital filtering to increase 20 times of direct modulation speed of white-light LED visible light communication system," *Optics Express*, vol. 20, no. 15, pp. 16218-16223, 2012.

[9] J. J. D. McKendry, et al., "Visible Light Communications using a CMOS-Controlled Micro-Light-Emitting-Diode Array," *Journal of Lightwave Technology*, vol. 30, no. 1, pp. 61-67, 2012.

[10] Z. Gong, et al., "Size-dependent light output, spectral shift and self-heating of 400 nm InGaN light-emitting diodes," *Journal of Applied Physics*, vol. 107, no. 1, 2010.

[11] J. McKendry, et al., "High Speed Visible Light Communications Using Individual Pixels in a Micro Light-Emitting Diode Array," *IEEE Photonics Technology Letters*, vol. 22, no. 18, pp. 1346-1348, 2010.

[12] S. Watson, et al., "High speed GaN micro-light-emitting diode arrays for data communications," in *SPIE Security and Defence*, 2012.

[13] D. Tsonev, et al., "A 3 Gb/s single-LED OFDM-based wireless VLC link using a gallium nitride uLED," *IEEE Photonics Technology Letters*, vol. 26, no. 7, pp. 637-640, 2014.

[14] G. P. Agrawal and N. K. Dutta, *Long-wavelength semiconductor lasers*. Van Nostrand Reinhold, 1986.

[15] R. P. Green, et al., "Modulation bandwidth studies of recombination processes in blue and green InGaN quantum well micro-light-emitting diodes," *Applied Physics Letters*, vol. 102, no. 9, 2013.

[16] F. Stern, "Calculated spectral dependence of gain in excited GaAs," *Journal*

*of Applied Physics*, vol. 47, no. 5382, 1976.

[17] Q. Dai, et al., "Carrier recombination mechanisms and efficiency droop in GaNInN/GaN light-emitting diodes," *Applied Physics Letters*, vol. 97, no. 133507, 2010.

[18] D. H. Kwon, S. H. Yang, and S. K. Han, "Modulation Bandwidth Enhancement of White LED based Visible Light Communications using Electrical Equalizations," in *SPIE Broadband Access Communication Technologies IX*, vol. 9387, 2015.

[19] E. F. Schubert, *Light-Emitting Diodes*, 2nd ed. Cambridge University Press, 2006.

[20] C. Jorgensen, "Optical Amplifiers and processing in High-Capacity Photonic Networks," PhD Thesis, Technical University of Denmark, 1997.

[21] A. Tzanakaki, "Tunable Wavelength Conversion in Optical Networks," PhD Thesis, University of Essex, 2000.

[22] N. Shrestha, M. Sohail, C. Viphavakit, P. Saengudomlert, and W. S. Mohammed, "Demonstration of visible light communications using RGB LEDs in an indoor environment," in *Electrical Engineering/Electronics Computer Telecommunications and Information Technology*, Chiang Mai, 2010, pp. 1159-1163.

[23] H. Chun, et al., "Visible light communication using a blue GaN uLED and fluorescent polymer color converter," *Photonics Technology Letters*, vol. 26, no. 20, pp. 2035-2038, 2014.

[24] K. Hoshino, A. Gopal, M. S. Glaz, D. A. Vanden Bout, and X. Zhang, "Nanoscale fluorescence imaging with quantum dot near-field electroluminescence," *Applied Physics Letters*, vol. 101, no. 4, 2012.

[25] P. A. Haigh, S. Rajbhandari, and I. Papakonstantinou, "Visible Light Communications using Organic Light Emitting Diodes," *IEEE Communications Magazine*, vol. 51, no. 8, pp. 148-154, 2013.

[26] I. A. Barlow, T. Kreouzis, and D. G. Lidzey, "High speed electroluminescence modulation of a conjugated-polymer light emitting diode," *Applied Physics Letters*, vol. 94, 2009.

[27] J. Watson and O. Zielinski, *Subsea optics and imaging*. Philadelphia: Woodhead Publishing, 2013.

[28] R. Hui, S. Benedetto, and I. Montrosset, "Near threshold operation of semiconductor lasers and resonant-type laser amplifiers," *IEEE Journal of Quantum Electronics*, vol. 29, no. 6, pp. 1488-1497, 1993.

[29] L. F. Feng, et al., "Simultaneous sudden changes of electrical behaviour at the threshold in laser diodes," *Journal of Applied Physics*, vol. 102, no. 6, 2007.

[30] L. F. Feng, et al., "Sudden Change of Electrical Characteristics at Lasing Threshold of a Semiconductor Laser," *IEEE Journal of Quantum Electronics*, vol. 43, no. 6, pp. 458-461, 2007.

[31] C. Skierbiszewski, et al., "High power blue-violet InGaN laser diodes grown on bulk GaN substrates by plasma-assisted molecular beam epitaxy," *Semiconductor Science and Technology*, vol. 20, no. 8, pp. 809-813, 2005.

[32] K. A. Denault, M. Cantore, S. Nakamura, S. P. DenBaars, and R. Seshadri, "Efficient and stable laser-driven white lighting," *AIP Advances*, vol. 3, no. 7, 2013.

[33] A. Neumann, et al., "Four-color laser white illuminant demonstrating high

color-rendering quality," *Optics Express*, vol. 19, no. S4, 2011.

[34] G. P. Agrawal and N. K. Dutta, "Rate Equations and Operating Characteristics," in *Semiconductor Lasers*. Van Nostrand Reinhold, 1993, ch. 6.

[35] G.-y. Hu, C.-y. Chen, and Z.-q. Chen, "Free-space optical communication using visible light," *Journal of Zhejiang University Science A*, vol. 8, no. 2, pp. 186-191, 2007.

[36] C.-Y. Lin, et al., "A hybrid CATV/16-QAM-OFDM visible laser light communication system," *Laser Physics*, vol. 24, no. 10, 2014.

[37] M. M. Dumitrescu, M. J. Saarinen, M. D. Guina, and M. V. Pessa, "High-speed resonant cavity light-emitting diodes at 650 nm," *IEEE Journal on Selected Topics in Quantum Electronics*, vol. 8, no. 2, 2002.

[38] J.-M. Wun, et al., "GaN-Based Miniaturized Cyan Light-Emitting Diodes on a Patterned Sapphire Substrate With Improved Fiber Coupling for Very High-Speed Plastic Optical Fiber Communication," *IEEE Photonics Journal*, vol. 4, no. 5, 2012.

[39] S. C. J. Lee, F. Breyer, S. Randel, H. P. A. van den Boom, and A. M. J. Koonen, "High-speed transmission over multimode fiber using discrete multitone modulation," *Journal of Optical Networking*, vol. 7, no. 2, pp. 183-196, 2008.

[40] S. C. J. Lee, et al., "Discrete Multitone Modulation for Maximising Transmission Rate in Step-Index Plastic Optical Fibers," *Journal of Lightwave Technology*, vol. 27, no. 11, pp. 1503-1513, 2009.

[41] O. Ziemann, J. Krauser, P. E. Zamzow, and W. Daum, *POF Handbook: Optical Short Range Transmission Systems*, 2nd ed. Springer, 2008.

[42] Multicom Inc. (2015) Multicom. [Online]. http://www.multicominc.com/training/technical-resources/single-mode-vs-multi-mode-fiber-optic-cable/

[43] T. F. O. Association. The FOA Reference Guide to Fiber Optics. [Online]. http://www.thefoa.org/tech/ref/basic/fiber.html

[44] F. Hanson and S. Radic, "High Bandwidth Underwater Optical Communication," *Applied Optics*, vol. 47, no. 2, 2008.

[45] C. Pontbriand, N. Farr, J. Ware, J. Preisig, and H. Popenoe, "Diffuse high-bandwidth optical communications," in *OCEANS 2008*, Quebec City, 2008, pp. 1-4.

[46] I. Lumasys. (2014) Lumasys, Inc.. [Online]. http://www.lumasys.com/

[47] P. Ross. (2013) International Business Times. [Online]. http://www.ibtimes.com/scientists-develop-underwater-wireless-internet-deep-sea-communication-1425518

[48] G. P. Agrawal, "Lightwave Systems," in *Fiber-Optic Communication Systems*. John Wiley & Sons, Inc., 2002, ch. 5, pp. 200-202.

[49] N. Farr, A. Bowen, J. Ware, C. Pontbriand, and M. Tivey, "An integrated, underwater optical/acoustic communications system," in *IEEE OCEANS 2010*, Sydney, 2010.

[50] R. L. Kurucz, I. Furenlid, J. Brault, and L. Testerman, "Solar Flux Atlas from 266 to 1300 nm," National Solar Observatory, Technical Report, 1984.

[51] B. M. Cochenour, L. J. Mullen, and A. E. Laux, "Characterization of the Beam-Spread Function for Underwater Wireless Optical Communication Links," *IEEE Journal of Oceanic Engineering*, vol. 33, no. 4, pp. 513-521,

2008.

[52] C. D. Mobley, *Light and Water: Radiative Transfer in Natural Waters*. Academic Press Inc, 1994.

[53] G. P. Agrawal, "Optical Receivers," in *Fiber-Optic Communication Systems*. John Wiley & Sons, Inc., 2002, ch. 4, pp. 133-182.

[54] I. Poole. Radio-Electronics. [Online]. http://www.radio-electronics.com/info/data/semicond/photo_diode/pin-pn-photodiode.php

[55] J. Gowar, "Sources and Detectors," in *Optical Communication Systems*. Prentice Hall International, 1993, ch. 13.

[56] J. Liu, Y. Zhou, G. E. Faulkner, D. C. O'Brien, and S. Collins, "Optical receiver front end for optically powered smart dust," *International Journal of Circuit Theory and Applications*, vol. 43, no. 5, 2014.

# Chapter 3

# Micro-LEDs for visible light communications

Following the analysis of the theory in Chapter 2, this chapter will present the use of micro-LEDs for communication purposes. The different ways to drive to these devices will be explored and the different LEDs available and applications of them will be discussed. The measurements which have been carried out at the University of Glasgow will be explained in detail which includes basic characterisation, spectral measurements, frequency response measurements and bit-error rate measurements. After analysing the two main ways to drive these devices, there are two experimental sections which make up the bulk of this chapter. Firstly, the ability to modulate more than one pixel at a time allows parallel data transmission to be achieved. There are some issues with crosstalk between pixels which has been explored before the results which were achieved are portrayed. Secondly, work carried out using a colour tuneable micro-LED exploits the advantages of micro-displays as well as communication. This is explored in the second part of this chapter.

## 3.1 Different ways to drive the micro-LEDs

Micro-LEDs can be driven in two different ways. They can be driven directly by using a high speed probe or they can be connected up to CMOS circuitry and be controlled externally. Both ways have their advantages and disadvantages which will be covered in the next section.

### 3.1.1 High speed probe

In order to measure the frequency response of the micro-LEDs or carry out data transmission experiments, the apparatus to drive the LEDs must be fast enough so that they are not the limiting factor for the overall system bandwidth. One way to do this is to use a high speed probe (Picoprobe Model 10 in this case) to address each of the individual pixels of the micro-LED. The probe tips themselves have two probe points, one for the signal and one for the ground. Depending on the LED structure, there may be separate pads which can be probed to in order to connect with the p and n contacts, however sometimes it

is only possible to probe directly to the LED itself. The distance between the two probe tips can be adjusted to suit the separation of the p and n contacts of the device. A layout of the probe structure can be seen in Figure 3.1.1 and a photograph of the experimental setup shown in Figure 3.1.2.

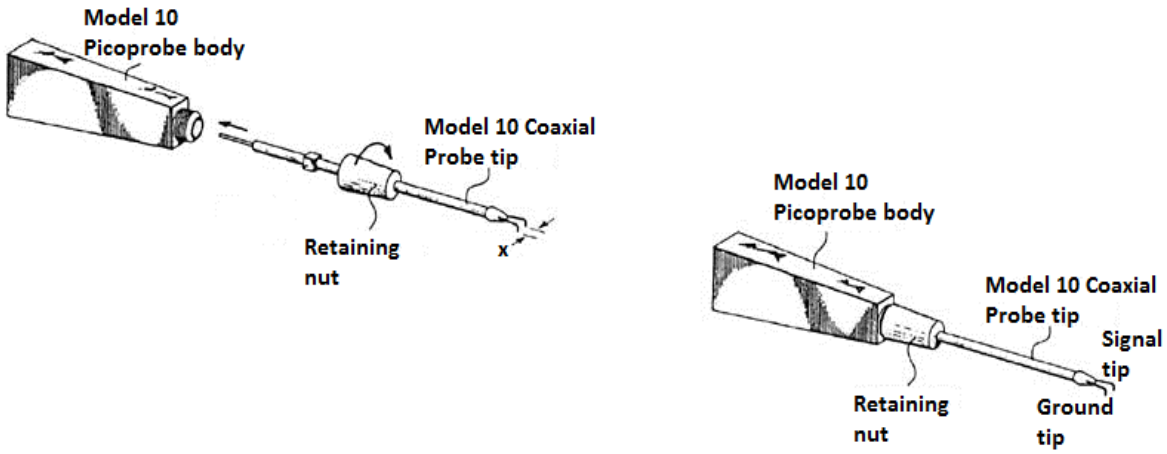


**Figure 3.1.1 A schematic of the probe structure [1].**

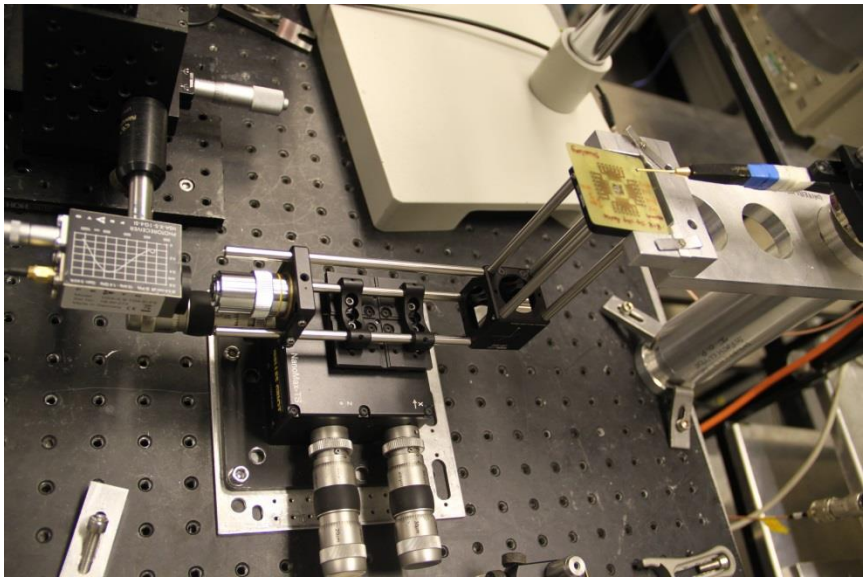

**Figure 3.1.2 Photograph showing the experimental setup when using the probe.**

For high speed measurements, usually a DC current is combined with an RF signal using a bias-tee and the output is supplied to the probe. The probe has an SMA connector allowing this signal to be connected easily. There is a smaller, high speed, 50 ohm connector at the other end where the probe tips can be connected to. The bandwidth of these probes can be in excess of 10 GHz which is a lot faster than the bandwidth of any micro-LED in the literature. However, a

disadvantage of these probes is the potential of scratching or damaging the device when making contact with it. Most micro-LEDs are very delicate and the slightest defect could affect the performance, therefore care must be taken when placing the probe tips onto the device. One way to remove this aspect is to have external circuitry which can control the micro-LEDs as mentioned in section 3.1.2.

### 3.1.2 Complementary Metal Oxide Semiconductor (CMOS) technology

The ability to automate the control of a micro-LED makes things a lot easier than probing to it. The micro-LED can be computer controlled via a standard USB interface and each individual pixel can be turned on with the click of a button. This lends itself to parallel data transmission which is discussed in detail in section 3.2. There have been many additions and redesigns of the CMOS circuitry used to drive the devices, with the one used for these measurements known as the “fourth generation” board, supplied by the University of Edinburgh. Special attention has been paid to the layout and routing of the parallel and common inputs. This CMOS board allows individual connections to be made to modulate single pixels or alternatively multiple pixels at the same time. The layout of the CMOS board is seen below in Figure 3.1.3.

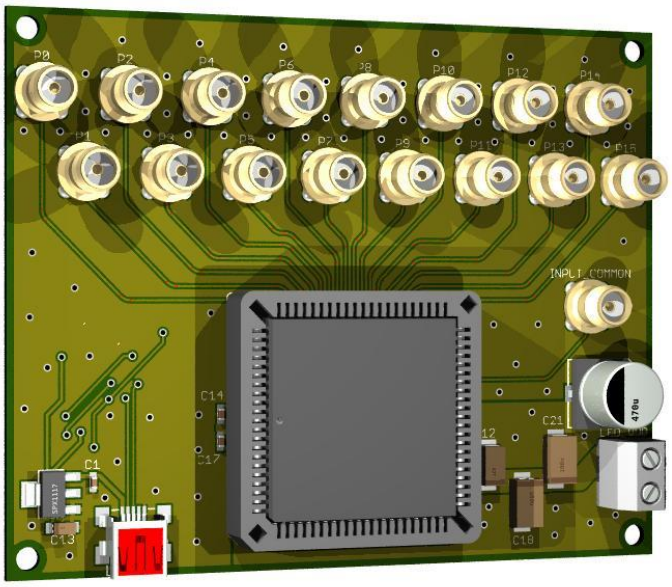


**Figure 3.1.3 Layout of the CMOS board used to drive the micro-LEDs.**

The SMA connections at the top of the board are labelled P0 to P15. Each of these connections relates to one column of LED pixels. For example, a 16 × 16 micro-LED device has 256 individual pixels. If a high speed signal was connected to P0, the first column of micro-LEDs, i.e. 16 pixels, would be modulated, but only this column. The SMA connector on the right hand side of the board, below these connectors is the common input. This means that if a high speed signal is applied here, it will take effect on all the LED pixels. The micro-LED itself is placed in the grey square in the middle of the board and is flip-chip bump bonded allowing the connection to be made. The integration of the micro-LEDs with the CMOS board is crucial and for this work, gold bump bonds are used to interconnect the two chips. The tracks on the board have been optimised to reduce reflections and interference by careful spacing and control of the track widths. The power supplied by the USB cable provides the 3.3V required for the board to operate. Once the USB cable has been connected, the software can be loaded. The software provides an interface allowing different pixels to be turned on and off simply by clicking on the corresponding box. A layout of the software window can be seen in Figure 3.1.4. You simply select the board name from the drop down menu, select whether you want to use the parallel inputs or the common input and then it is ready to go.

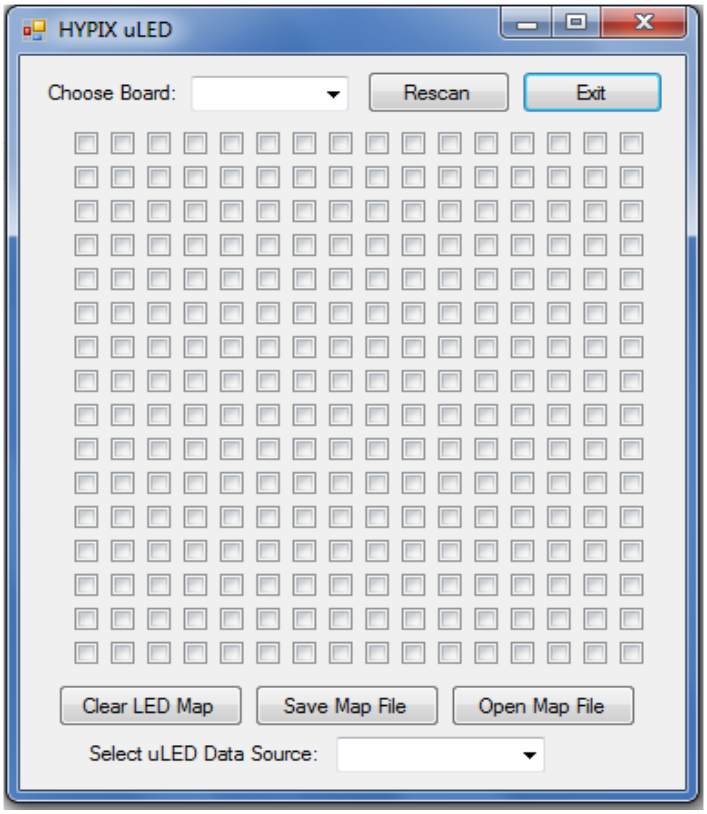


**Figure 3.1.4 Layout of the software used to control the micro-LED pixels.**

## 3.2 Parallel data transmission

By making use of the CMOS board shown in Figure 3.1.2, multiple pixels from the micro-LED array can be modulated. Section 3.2 introduces the concept of parallel visible light communication using a blue GaN micro-LED. The optical bandwidth of the device is measured and then four pixels are modulated simultaneously to see if the overall data transmission rate can be increased. Analysis of the electrical and optical crosstalk has been investigated and all of the results are portrayed in the following section. Further measurements were conducted using the same setup but with a faster device to try and improve the data transmission rate. These improved results are also presented here.

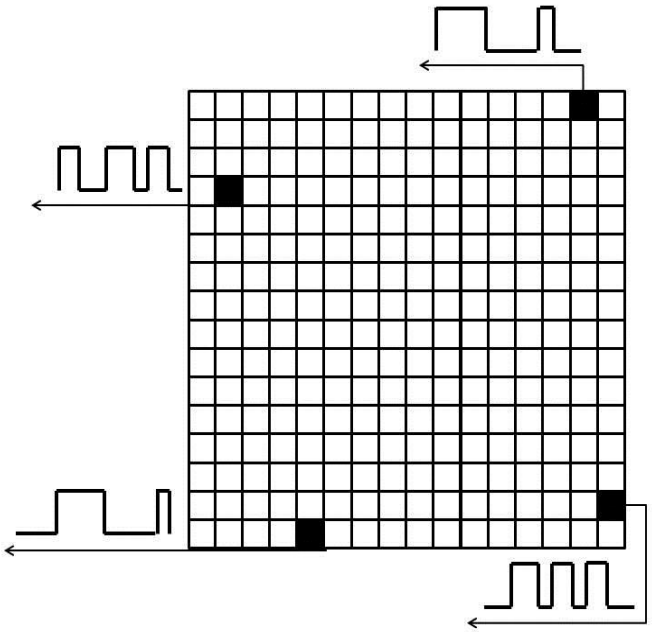

**Figure 3.2.1 Schematic of CMOS driver chip layout showing the four pixels being modulated with independent data.**

### 3.2.1 Characterisation of crosstalk vs. pixel separation

There are two main kinds of crosstalk. Firstly, despite the fact that only one pixel is aligned to the detector at one time, the detector could pick up undesired optical signals from other active pixels. This is called optical crosstalk. Secondly, the presence of electrical crosstalk can be a limiting factor where the desired signal is affected by the CMOS driver circuitry itself. The degradation of eye diagrams with increased pixels and the power penalty seen in bit-error rate plots can be put down to this electrical crosstalk. The methods used to analyse this crosstalk are shown in this section.

The beams of light from the modulated pixels were collected using a 0.68 numerical aperture aspheric lens and focussed onto a photo-detector using a ×10 microscope objective. In order to measure the effect of optical crosstalk, one pixel was aligned to the detector and its optical power was measured. This pixel was then turned off but left aligned to the detector while adjacent, non-aligned pixels were turned on individually to see what effect they had. The power of each of these non-aligned pixels was measured and compared to the original measurement from the aligned pixel in order to assess the optical crosstalk in relation to pixel distance from the detector. Figure 3.2.2 shows the

experimental setup and Figure 3.2.3 shows the optical crosstalk as a function of pixel separation.

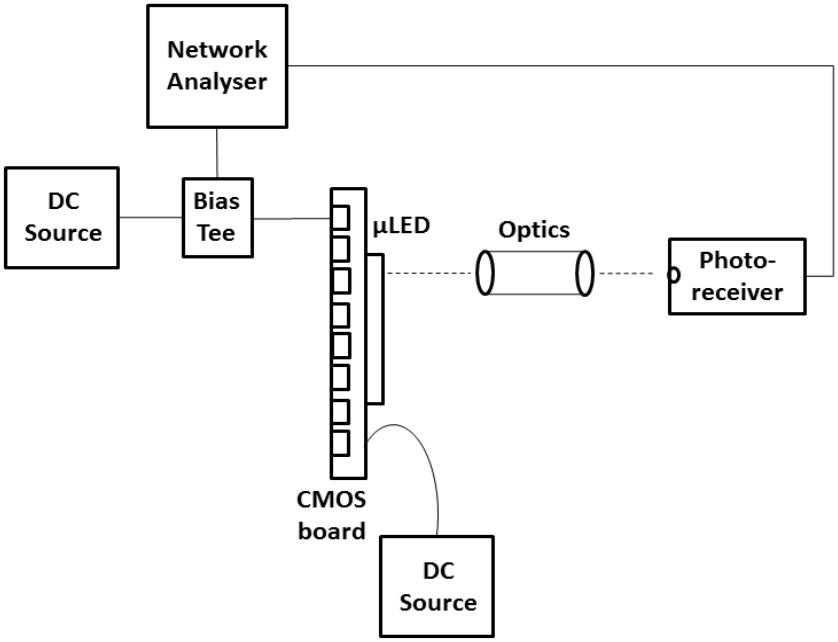


**Figure 3.2.2 Experimental setup for crosstalk measurements.**

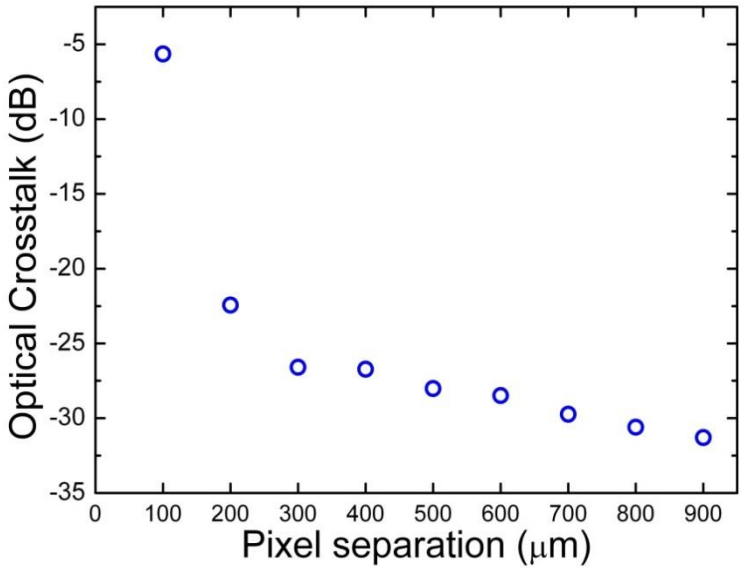


**Figure 3.2.3 Optical crosstalk vs pixel separation between the aligned pixel and the other non-aligned pixels.**

As you can see in Figure 3.2.3, when using two pixels which are next to each other, i.e. a pixel separation of 100 µm, the optical crosstalk is -6 dB. This is a large effect and could have an influence on the system performance for parallel

data transmission. However, as the pixel separation goes above 200 μm, the effect from optical crosstalk is less than -25 dB. We can therefore neglect the effect of optical crosstalk by selecting pixels with a minimum spatial separation of 200 μm. If this same system was realised using lasers then this level of crosstalk would still be deemed too high due to beat noise and other causes of interference [2]. For a system like this to work, crosstalk levels would have to be less than -40 dB to remove this effect and allow parallel signals to be sent and received successfully. As the crosstalk encountered by LEDs is coherent, -25 dB is deemed low enough to allow successful parallel data transmission.

When the pixels are spatially separated to neglect the effect of optical crosstalk, there is still the presence of electrical crosstalk. This is caused by the integration of the micro-LED with the CMOS circuitry. A small voltage drop occurs when you have one pixel on and you turn on a second pixel. This is due to the power routing resistance of the CMOS board itself. By modulating an unaligned pixel with the aligned pixel in DC operation, a signal is picked up on the detector. This should not be the case and shows the presence of electrical crosstalk. Further experimental data is shown later in the following section.

Multiple-input multiple-output (MIMO) systems have shown that it is possible to overcome the effects of crosstalk by isolating each channel using spatial light modulators and/or lenses. This idea, as the name suggests, has many transmitters, each which is detected by a different receiver. A working system has been shown using a vertical-cavity surface emitting laser (VCSEL) to provide transmission [3]. This could be put in to practice using the CMOS-controlled micro-LED array and multiple detectors to improve the results further. However, these measurements are analysing the transmitters and the optical crosstalk for this particular system, and hence the lenses are not optimised for this purpose. By finding the point where optical crosstalk is an issue in this setup, it is then possible to remove this factor and then analyse the electrical effect from the CMOS circuitry.

### 3.2.2 Experimental results

The frequency response of a single micro-LED pixel was measured using a network analyser and high speed detector as in Figure 3.2.2. Figure 3.2.4 shows

the frequency response of this pixel at a bias of 6.5 V. Each pixel on the device used for this experiment was 99 × 99 $\mu m^2$. It can be seen that this pixel has a -3 dB optical bandwidth of approximately 150 MHz. A sudden drop in the frequency response is seen at around 500 MHz which is caused by the limitations of the CMOS board itself as the CMOS drivers cannot modulate their output in response to signals higher than this frequency. A number of different pixels across the array were measured to test the uniformity of the array. Each pixel was within 10 MHz of each other, confirming that they all have similar behaviour.

The CMOS-controlled pixels have a lower bandwidth than pixels driven by high speed probes which is ultimately down to the frequency response of the CMOS board itself and the high modulation depth of the CMOS driver output.

Data transmission experiments were carried out using a number of pixels from this array, using the same optics as before to collect the light. Four micro-LED pixels were chosen to prove the concept of parallel data transmission. Four separate data patterns were supplied to the four different pixels however all had a common clock frequency as seen in Figure 3.2.5. The four data signals were all on-off keying (OOK) non-return-to-zero (NRZ) pseudo random bit sequences supplied from the BERT. They were $2^7$-1 bits in length and had a peak-to-peak voltage of 2V. These patterns were supplied to the four micro-LED pixels resulting in them all being modulated simultaneously. The pixels chosen for this experiment were all separated by more than 600 μm in order to remove the effect of optical crosstalk. As shown earlier in Figure 3.2.3, the crosstalk is less than -25 dB and therefore negligible.

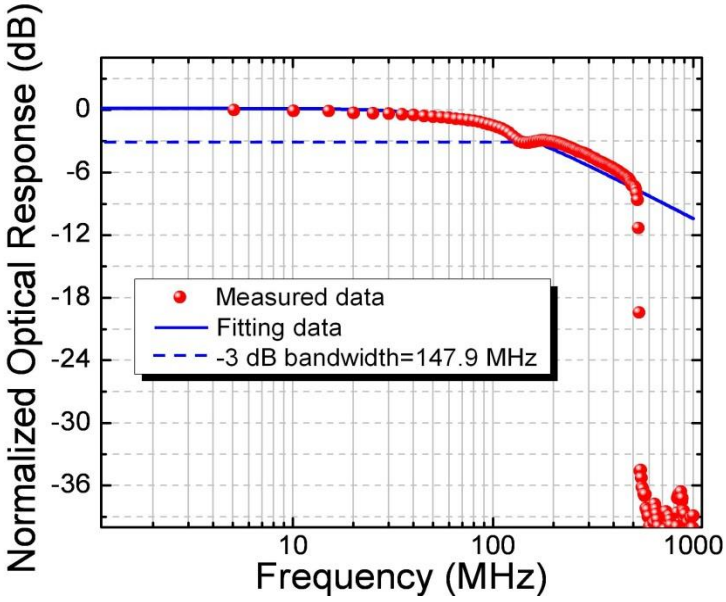


**Figure 3.2.4 Frequency response of a CMOS driven micro-LED pixel at 6.5V.**

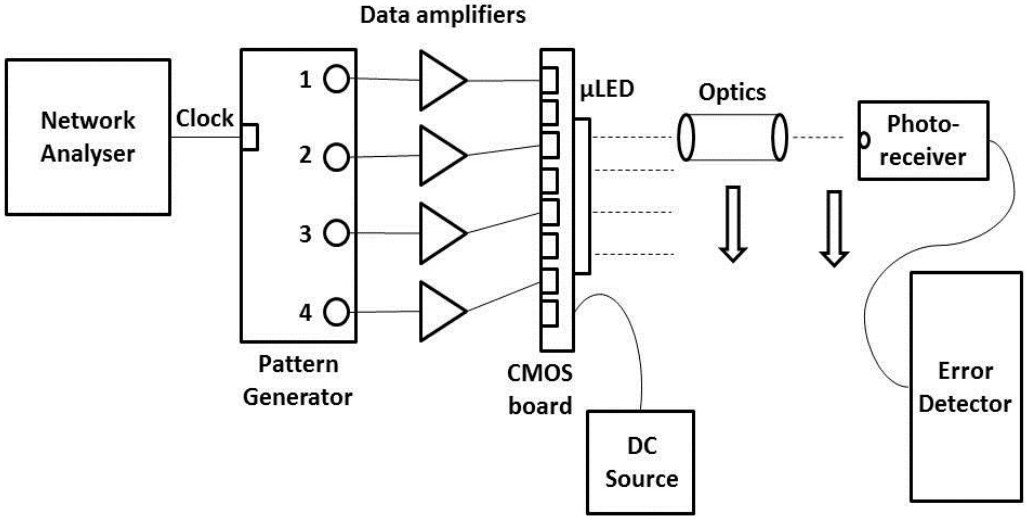


**Figure 3.2.5 Experimental setup for parallel data transmission.**

The eye diagrams recorded from this experiment are shown in Figure 3.2.6. A typical eye diagram from an individual pixel being modulated at 375 Mbit/s with an applied voltage of 6.5 V is shown in Figure 3.2.6 (a). This pixel is aligned to

the detector in order to obtain the eye diagram and then the second, third and fourth pixels are modulated, with the corresponding eye diagrams shown in Figure 3.2.6 (b), (c) and (d).

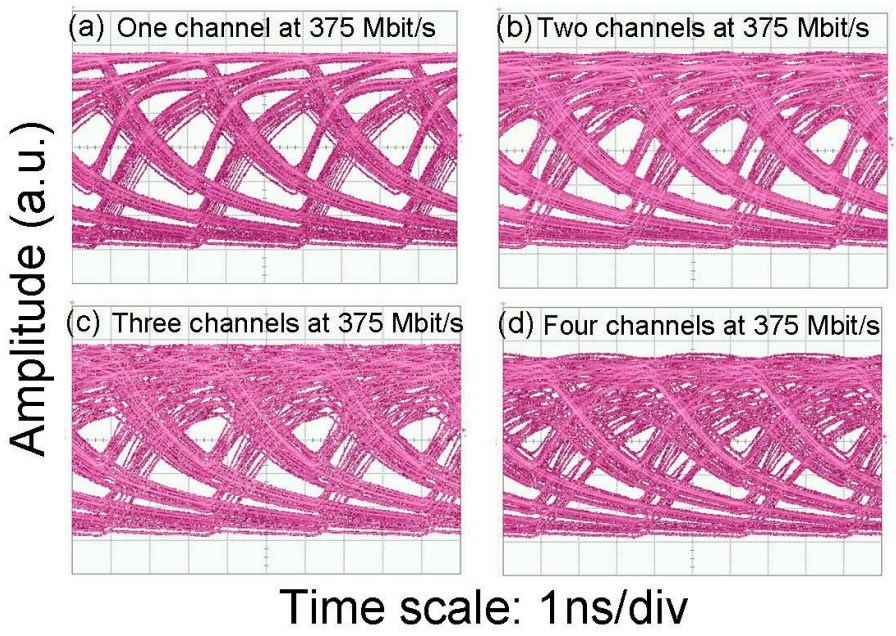


**Figure 3.2.6 Eye diagrams from CMOS-controlled micro-LED pixels being modulated at 375 Mbit/s for (a) one channel, (b) two channels, (c) three channels and (d) four channels at a bias of 6.5V.**

It can be seen that the eye quality degrades as the number of pixels is increased which indicates the presence of electrical crosstalk, as we have shown that optical crosstalk has a negligible effect. With four pixels modulating simultaneously at 375 Mbit/s, the total bit rate of data being transmitted from the device is 1.5 Gbit/s. The bit-error rates were measured as a function of received optical power for each of the four cases as seen in Figure 3.2.7.

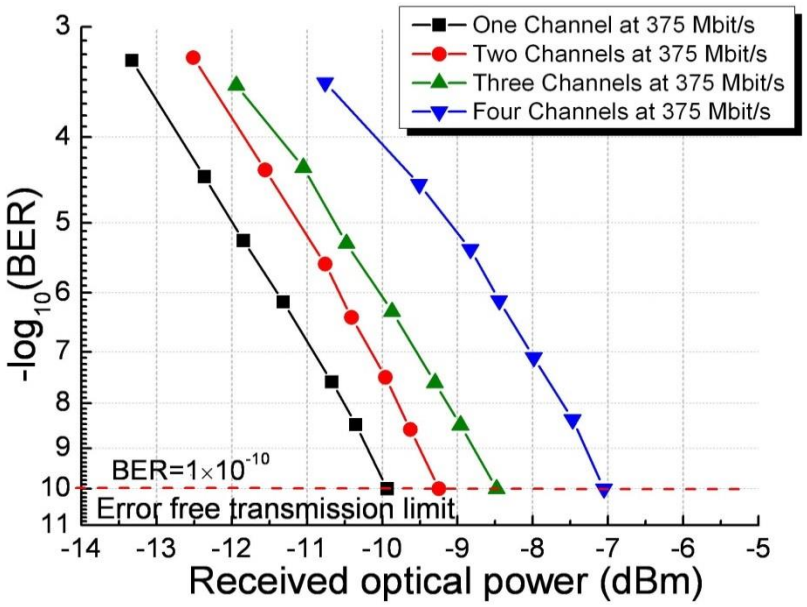


**Figure 3.2.7 Bit-error rate vs received optical power for one, two, three and four pixels in operation, transmitting at 375 Mbit/s.**

As the number of pixels is increased, more power is required to achieve the same bit-error rates at the same bit-rate. This was also apparent in the eye diagrams. Compared to one pixel modulating for error-free transmission, a power penalty of 0.69 dBm is seen as the second pixel is added. Similarly, a power penalty of 1.46 dBm and 2.88 dBm for the addition of the third and fourth pixels respectively, is seen. In an ideal case with no crosstalk between channels or limitations from the CMOS board, no power penalty would be evident and the sensitivities for each of the subsequent channels would be unchanged. However, this is not the case and ultimately, with an increase in the number of channels, this power penalty would keep increasing.

Further experiments were carried out to analyse the effect of electrical crosstalk. Two pixels, which were separated by more than 600 μm, were chosen in order to neglect the effect of optical crosstalk. The frequency response of the system was investigated under a number of different drive conditions. The first scenario was to align a pixel to the detector but only to operate it in DC, i.e. not modulating, to measure the system noise floor. This is shown by the blue inverted triangles in Figure 3.2.8. Following this, the pixel was then modulated on its own by sending signals from the network analyser to be collected by the detector. The frequency response was acquired and is shown by the black

diamonds. As expected, it is very similar to the frequency response seen in Figure 3.2.4.

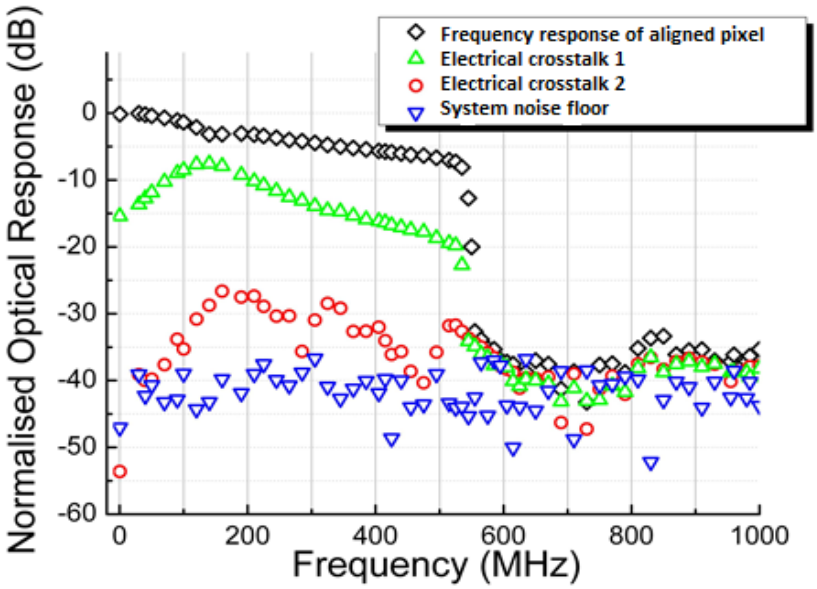


**Figure 3.2.8 Frequency response of the system under different operating conditions: Blue - System noise. Red - Electrical crosstalk due to mutual inductance/capacitance. Green - Electrical crosstalk due to the "ground bounce" effect. Black - Frequency response of aligned pixel at 6.5V.**

The red circles are the frequency response of the aligned pixel in DC mode again, with the driving signal to the second pixel on but the pixel switched off. This, ideally, should be the same as the noise floor, however it can be seen that there is a slight increase at low frequencies. This is potentially caused by the mutual inductance/capacitance between the CMOS electronics, which could cause interference between channels [4]. However, this level of crosstalk does not explain the power penalties seen in Figure 3.2.7. The final test, shown by the green triangles, represents the frequency response of the aligned pixel when it is in DC operation and the second pixel is turned on and modulated. If there was no issue with electrical crosstalk, this plot should be the same as the noise floor as the aligned pixel is only operated in DC. However, the response shown here proves that the aligned pixel is being modulated by the electrical crosstalk caused by modulating the second pixel. This signal is large enough to influence the parallel data transmission measurements. This effect is caused by the power routing resistance of the CMOS circuitry and is known as the “ground bounce” effect [4]. By modulating the second pixel, the bias applied to the first pixel fluctuates causing amplitude noise. One way to resolve this issue would be to

reduce the power routing resistance which can be done by increasing the thickness and/or width of the tracks on the CMOS board.

Further data transmission experiments were carried out using the same setup to see if the data rate could be improved. A similar blue micro-LED, with similar pixels, was used for the experiment. Four pixels were chosen from the array, two which were 60 µm and two which were 50 µm, due to the design on the micro-LED. The frequency response of one of the 50 µm pixels at 6.3V is shown in Figure 3.2.9.

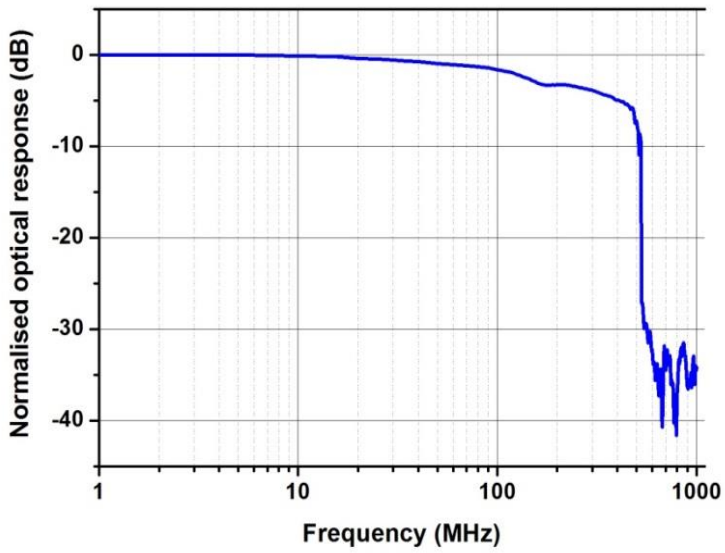


**Figure 3.2.9 Frequency response of a 50 µm pixel driven at 6.3V.**

The -3 dB optical bandwidth of this pixel is 158 MHz which is slightly higher than that seen in the initial measurements. The pixels were spatially separated again in order to neglect the effect of optical crosstalk and independent, uncorrelated data was sent to each pixel. This time, four pixels were modulated, all at 500 Mbit/s, resulting in a combined data rate of 2 Gbit/s. The eye diagrams and bit-error rate plots are shown in Figure 3.2.10 and Figure 3.2.11, respectively.

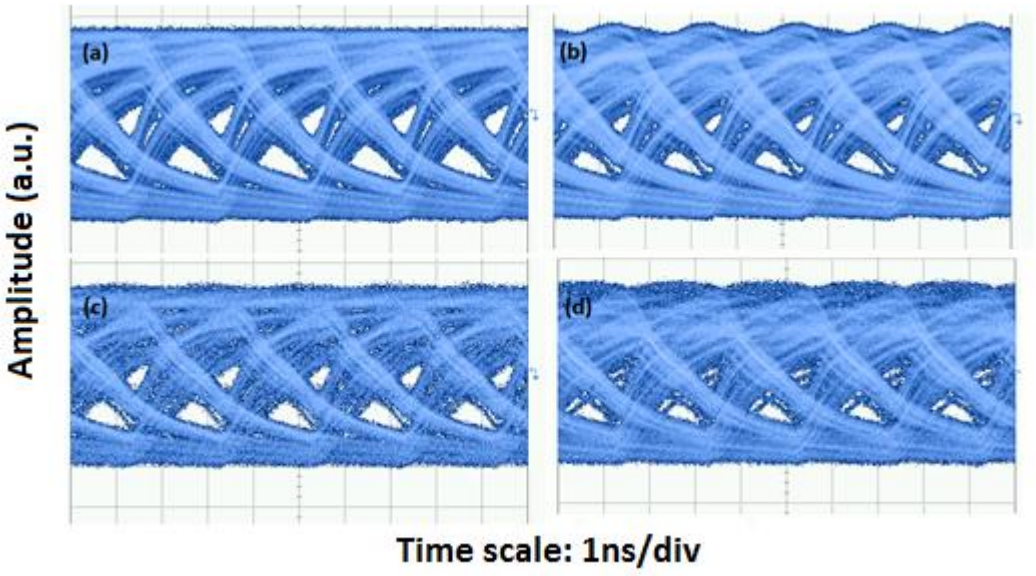


**Figure 3.2.10 Eye diagrams at 500 Mbit/s for (a) 1 pixel, (b) 2 pixels, (c) 3 pixels and (d) 4 pixels modulating.**

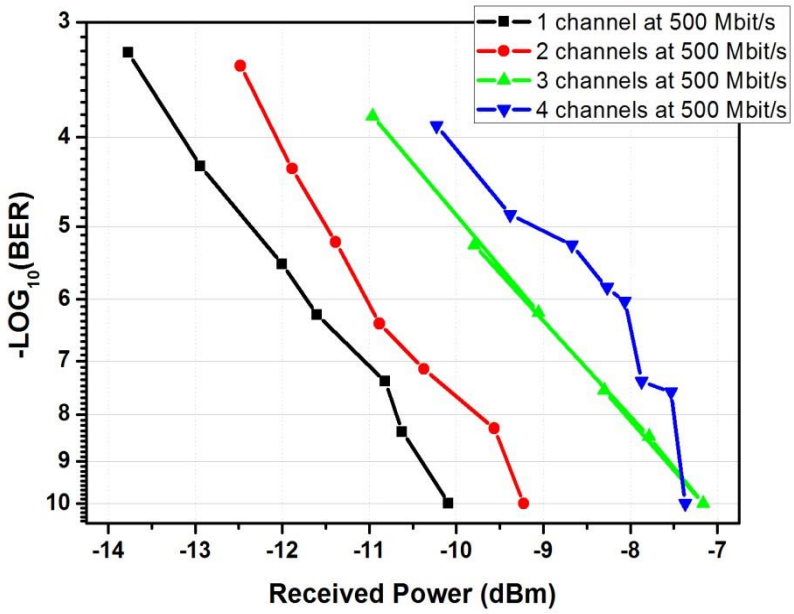


**Figure 3.2.11 Bit-error rate vs received optical power for single and multiple channels modulating at 500 MHz.**

Like before, it can be seen that the increasing number of channels increases the power penalty. This is also the reason that the eye diagrams begin to close as the data rate increases, however, error free data transmission at 2 Gbit/s is still achieved. For this particular case, a power penalty of 0.87 dBm is seen as the second channel is added and then power penalties of 2.93 dBm and 2.72 dBm are seen for the addition of the third and fourth channels. Usually, the power

penalty increases as the number of channels is increased so it can be noted that the final point on the four channel bit-error rate plot is due to experimental error. By using smaller pixels, the bandwidth is higher but the optical power output is smaller. A 10 μm pixel may, in theory, allow faster data transmission rates however the power is too weak in order to carry out these experiments in the first place. By using these pixels at 50 μm and 60 μm, it allows a compromise of bandwidth of power, improving on the earlier result. It is hoped that the number of channels could be increased to ultimately increase the overall data rate. In theory, a 16 × 16 micro-LED which has 256 pixels could be used, and if crosstalk and current consumption were not an issue, a combined data rate of 128 Gbit/s could be achieved.

## 3.3 Novel CMOS controlled colour tuneable micro-LED

As mentioned earlier, one of the applications of micro-LEDs is for smart displays. By exploiting a micro-LED array made from an InGaN structure, the emission wavelength can be changed from red to green by tailoring the current density applied to the pixel. This then allows a range of different colours to be applied to the display. There have been a number of publications on different growth methods to achieve colour tuneable inorganic devices [5], [6], however, none of these have been realised at a systems level where they have been shown in working colour displays. The work here demonstrates a novel structure, fabricated at the Institute of Photonics, which can be CMOS controlled and used as an inorganic micro-display. It is capable of displaying animated images ranging in colour from red to green at comparable output powers. In addition to this, the pixels on this device show modulation bandwidths of up to 100 MHz, which would make them a suitable source for visible light communications. Error-free data transmission can be achieved at up to 250 Mbit/s per pixel [7], which will be discussed in more detail in the following section.

### 3.3.1 Device structure

This device was grown on a sapphire substrate by metal organic chemical vapour deposition (MOCVD). The epitaxial structure consists of the following layers:

- A 1.5 μm thick GaN buffer layer

- A 4 μm thick n-doped GaN layer

- A five-period $In_{0.18}Ga_{0.82}N$ (2.5 nm)/GaN (12 nm) multi-quantum well layer emitting at 460 nm

- A five-period $In_{0.4}Ga_{0.6}N$ (2.5 nm)/GaN (12 nm) multi-quantum well layer emitting at 600 nm

- A 210 nm thick p-GaN cap layer

The quantum well layer emitting at 600 nm is the main quantum well layer producing a higher intensity. The quantum wells at 460 nm act as an electron reservoir and pre-strain/relaxation layer for improving the radiative efficiency of the main quantum wells [8] [9]. The device was fabricated into a 16 × 16 array of micro-LEDs with each pixel having an individual p-contact and a common n-contact. The performance of the device is explained in the following section.

### 3.3.2 Experimental details and results

The experimental setup is shown in Figure 3.3.1. The CMOS board containing the micro-LED is driven by a RF signal from the network analyser combined with a bias current from a constant current source. A 0.68 numerical aperture collection lens is used to collect the light and a ×10 microscope objective then focuses the light onto the photo-detector, before the signal is sent back to the network analyser to calculate the bandwidth. Similarly, the network analyser could be replaced with a bit-error rate test (BERT) system in order to carry out data transmission experiments.

The spectrum of a typical pixel from this device was measured as a function of drive current. A significant blueshift is seen as the injected current increases which can be seen in Figure 3.3.2. There are two main peaks in the spectra: one from the blue quantum wells and a more dominant peak from the red/green quantum wells.

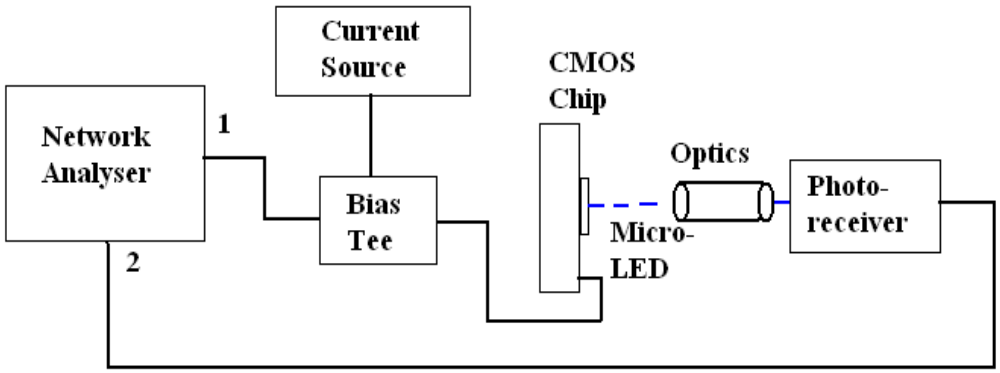


**Figure 3.3.1 Experimental setup for a CMOS-controlled micro-LED.**

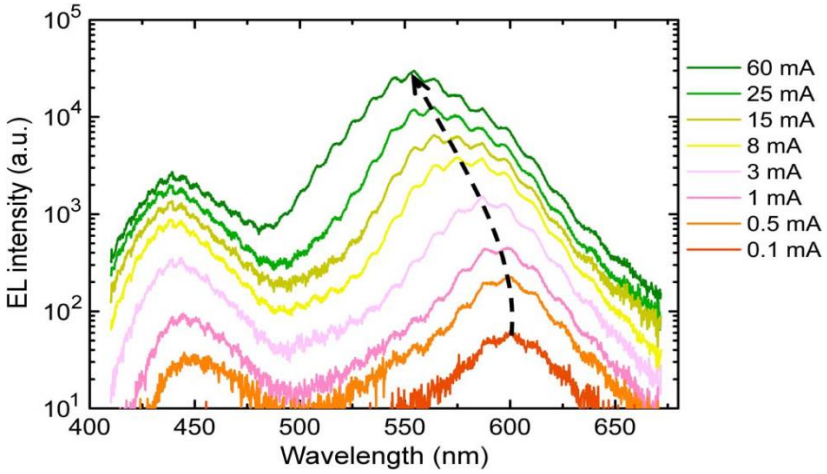


**Figure 3.3.2 Spectra from one pixel of the CMOS controlled colour tuneable micro-LED taken at a range of currents from 0.1mA up to 60mA [7].**

For most applications, a spectral shift would be seen as a disadvantage as a constant wavelength is usually desirable. However, by utilising this characteristic of the device, a multi-colour display becomes a realistic prospect using a single micro-LED array. This feature has a number of advantages over the alternative options. Firstly, it reduces the need for colour converters which have a short lifetime and can increase production costs. Also, these colour converters have a very low bandwidth which would limit such devices in terms of communications. Ultimately, the device reported here keeps the system more compact and easier to run.

In order to have a multi-colour display, the current would have to be varied for different pixels if it was under CW operation. However, by making use of pulsed

operation, the duty cycle can be varied on different pixels to give a uniform output. By working under pulsed conditions, the device is not affected by a temperature increase and therefore less of a spectral shift is apparent.

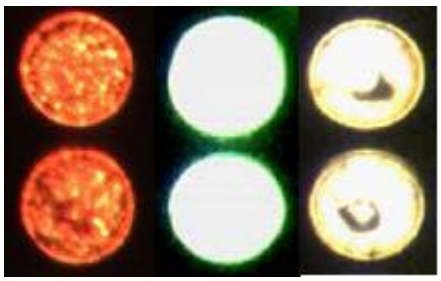

**Figure 3.3.3 Controlled emission from different pixels of the micro-LED array by varying the duty cycle.**

Approximately the same average output power for each colour was achieved by driving the pixels with different duty cycles. The red pixel is being driven in DC at 0.5 mA with an output power of 0.93 μW, the green pixel has a duty cycle of 0.5% at 80 mA with an output power of 1.03 μW and the yellow pixel has a 2% duty cycle at 18 mA with an output power of 0.97 μW. Obviously, this is very low power but the uniformity continues at higher current densities. The power density per pixel can reach up to 25.6 mW $cm^{-2}$, which is still enough for practical applications such as head-up displays, head-mounted displays and contact lens displays [10], [11].

As well as multi-colour displays, these CMOS controlled micro-LED pixels have high modulation bandwidths, showing that they can also be used for optical data transmission. There is the potential to have a smart display which shows an animated image but at the same time one or several of the pixels are being modulated for communication purposes. The images will appear as normal, as the speed at which they are modulating is a lot faster than the human eye can interpret. However, there could be additional information being sent to a receiver on a phone or a laptop via the light. The -3 dB optical bandwidth of one of these pixels is in excess of 100 MHz, which can be seen in Figure 3.3.4 (a). A drop in the frequency response can be seen around 450 MHz as it is limited by the CMOS board itself, as seen previously in Section 3.2.2.

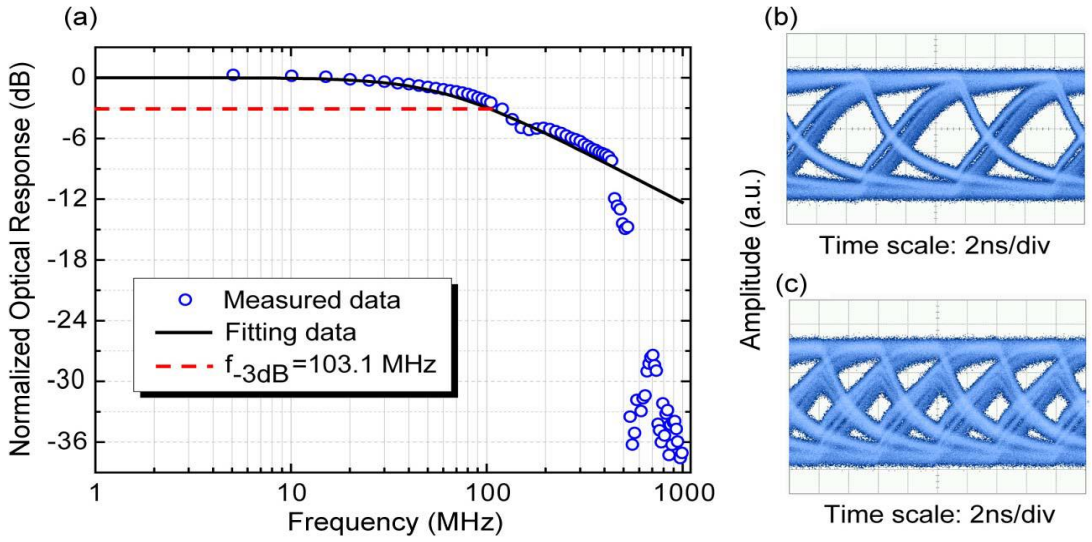


**Figure 3.3.4 (a) Frequency response plot of a CMOS controlled micro-LED pixel at 6.5V and eye diagrams taken at (b) 155 Mbit/s and (c) 250 Mbit/s [7].**

Data transmission was also carried out using a single pixel from the micro-LED array using a bit-error rate test (BERT) setup. A pseudo-random bit sequence (PRBS) with a length of $2^7$-1 bits and peak-to-peak amplitude of 2V was sent to modulate the pixel. The light emitted from this pixel was collected using optics and focussed onto a high speed photo-detector. As the light from one pixel is relatively small, an amplifier was put in place to amplify the electrical signal from the detector before it reaches the BERT. In this case, error-free data transmission is defined as a bit-error rate of less than $1\times10^{-10}$ and successful transmission was achieved up to 250 Mbit/s. The corresponding eye diagrams at 155 Mbit/s and 250 Mbit/s are shown in Figure 3.3.4 (b) and (c), respectively.

## 3.4 Summary and conclusions

This chapter has covered the topic of micro-LEDs for visible light communication. It began by introducing the different ways to drive to the LEDs. Using a high speed probe means that the probe tips have to be carefully placed onto the device itself which can be problematic at times, however, ultimately this allows for high speed measurements to be conducted. The ability to control the turning on and off of pixels easily using a computer makes this process easier, however in doing so, limits the maximum bandwidth that can be achieved due to the components on the CMOS circuitry. Individual pixels can be turned on at the click of a button which helped for the experiments carried out in this chapter.

The concept of parallel data transmission was explored showing that higher data rates could be achieved by modulating multiple pixels on the LED array. The presence of crosstalk was explored in detail to see how this affects the overall transmission rate but ultimately, using four individual micro-LED pixels, it was shown that 2 Gbit/s can be achieved. Moving towards a system which could be implemented in a real life scenario, MIMO can be considered to further advance the data transmission rate and practicality of this technology.

Following this, a colour tuneable micro-LED was used to show its potential for micro-display purposes but also its ability to provide communication. By adjusting the current applied to the device, the wavelength emitted changed. This allows a micro-display to be realised simply using one LED where each pixel can be different colours. As well as this, this device showed that it has a modulation bandwidth of over 100 MHz and can transmit data at 250 Mbit/s. The concept of visible light communication using LEDs is an ever-growing topic, where the potential of having a room lit by LED lighting whilst providing a communication link to phones and laptops is becoming a realistic prospect. Micro-LEDs have shown great potential to be used as sources for high speed communication, however the next chapter explores the use of laser diodes for communications and the advantages and disadvantages this has over LEDs.

# References


[1] G. I. Inc. Picoprobe by GGB Industries Inc.. [Online]. http://www.ggb.com/10.html

[2] L. G. C. Cancela and J. J. O. Pires, "Quantifying the influence of crosstalk-crosstalk beat noise in optical DPSK systems," in *IEEE Eurocon - International Conference on Computer as a Tool*, 2011, pp. 1-4.

[3] H.-H. Lu, et al., "A multiple-input-multiple-output visible light communication system based on VCSELs and spatial light modulators," *Optics Express*, vol. 22, no. 3, pp. 3468-3474, 2014.

[4] R. J. Baker, *CMOS: Circuit Design, Layout and Simulation*, 2nd ed. Wiley Interscience, 2007.

[5] Y. Hong, et al., "Visible-color-tunable light-emitting diodes," *Advanced Materials*, vol. 23, no. 41, pp. 3284-3288, 2011.

[6] B. Damilano, et al., "Blue-green and white color tuning of monolithic light emitting diodes," *Journal of Applied Physics*, vol. 108, no. 7, p. 073115, 2010.

[7] S. Zhang, et al., "CMOS-Controlled Color Tunable Smart Display," *IEEE Photonics Journal*, vol. 4, no. 5, pp. 1639-1646, 2012.

[8] N. Otsuji, K. Fujiwara, and J. K. Sheu, "Electroluminescence efficiency of blue InGaN/GaN quantum-well diodes with and without an n-InGaN electron reservoir layer," *Journal of Applied Physics*, vol. 100, no. 11, 2006.

[9] C.-F. Huang, C.-Y. Chen, C.-F. Lu, and C. C. Yang, "Reduced injection current induced blueshift in an InGaN/GaN quantum-well light-emitting diode of prestrained growth," *Journal of Applied Physics*, vol. 91, no. 5, 2007.

[10] D. Vettese, "Microdisplays: Liquid crystal on silicon," *Nature Photonics*, vol. 4, pp. 752-754, 2010.

[11] A. R. Lingley, et al., "A single-pixel wireless contact lens display," *Journal of Micromechanics and Microengineering*, vol. 21, no. 12, p. 125014, 2011.

# Chapter 4

# Laser diodes for visible light communications

This chapter will look at some measurements carried out using GaN laser diodes for communication purposes. It will begin with a look at the device structure and characterisation of the devices used for these measurements. This will be followed by the work I have carried out throughout my PhD using these blue laser diodes. The high speed measurements which have carried out are presented and discussed in detail. The use of colour converters is explored briefly before an insight is given into the reliability of the laser diodes.

## 4.1 Visible light communications using laser diodes

There has been a significant recent interest in using laser diodes as a means of visible light communication [1]. There are many applications for sub-sea and fibre communications, but the potential to use laser diodes for free space communications is also an important topic. The power output from a laser diode can be hazardous, particularly with regard to eye-safety, however, it is possible to use colour converter materials to not only limit the power but also change the wavelength, with the favourable option of producing white light. Like LEDs, lasers of different wavelengths can be combined to create white light or a blue laser and a yellow phosphor can be used to create white light. The main advantage of using lasers instead of LEDs is that they do not suffer from droop [2] and therefore their efficiency is much better at higher drive currents. By using blue laser diodes and converting the light to white light, it becomes eye-safe [3] and companies such as BMW are beginning to use blue lasers as a source for car headlights [4]. Blue laser diodes have shown potential for high speed measurements and some of the fastest free space data transmission results are presented here.

## 4.2 Blue laser diode measurements

### 4.2.1 Setup and characterisation

The devices used for these measurements are gallium nitride (GaN) laser diodes emitting at a wavelength of around 422 nm. They were designed, grown and

fabricated by TopGaN in Poland. These devices are grown by metal-organic chemical vapour deposition (MOCVD) on a c-plane GaN substrate. The wafers have the following AlGaInN epitaxy layers:

(1) 0.8 µm $Al_{0.08}Ga_{0.92}N$ lower cladding layer

(2) 50 nm GaN lower waveguide layer

(3) 50 nm $In_{0.02}Ga_{0.98}N$ injection layer

(4) $In_xGa_{1-x}N/In_{0.02}Ga_{0.98}N$ quantum wells ×3

(5) 20 nm $Al_{0.2}Ga_{0.8}N$ electron blocking layer

(6) 80 nm GaN waveguide

(7) 350 nm $Al_{0.08}Ga_{0.92}N$ upper cladding layer

The laser structure was processed into ridge waveguide laser diodes with a cavity of 700 µm and a stripe width of approximately 3 µm. Figure 4.2.1 shows a picture of a typical structure using a scanning electron microscope (SEM). After cleaving, the laser diodes were high-reflector (HR) coated (5× $ZrO_2/SiO_2$ quarter-wavelength layers) with 95% reflectivity and anti-reflection (AR) coated with 10% reflectivity. For the measurements conducted here, the devices were mounted p-side up in standard TO56 packages.

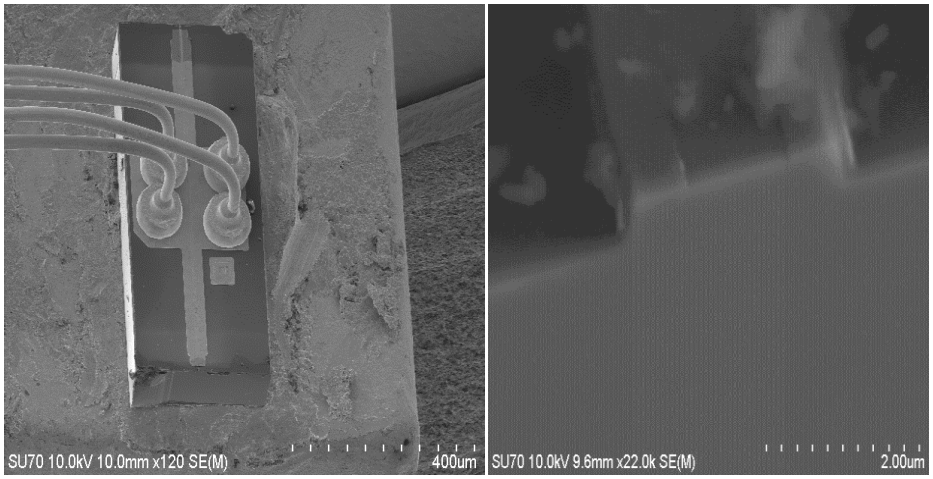


**Figure 4.2.1 SEM picture of a ridge waveguide laser diode showing cavity length and stripe width.**

The measurements were conducted using the experimental setup in Figure 4.2.2. For the LVI and spectral measurements, no RF component is connected, just a DC bias. For the bandwidth measurements, the RF component is provided from the network analyser and for the bit-error rate measurements, the network analyser is replaced with a BERT system.

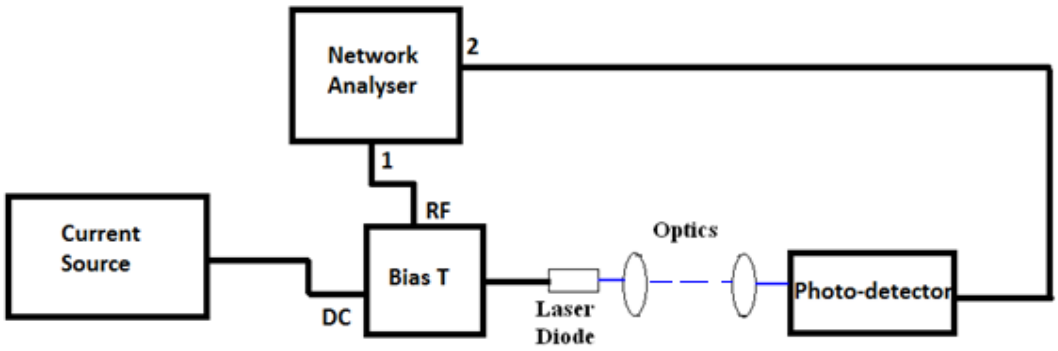


**Figure 4.2.2 Experimental setup using the laser diode.**

The LVI characteristics of one of these devices were measured at 25°C and are shown in Figure 4.2.3. This device has a threshold current of around 70 mA and a threshold voltage around 5V. The laser diode emitted over 20 mW of power; however similar devices have achieved output powers of 50-100 mW CW at room temperature [5]. For the high speed measurements, we were not concerned with maximising the power output, so the experimental setup was not completely optimised in terms of light collection and heat sinking. However, for the purpose

of these measurements, we had more than enough light to conduct the experiments.

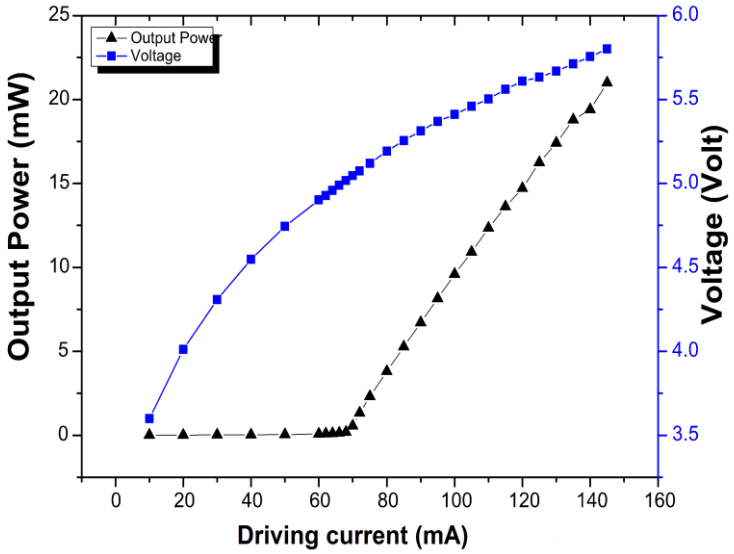


**Figure 4.2.3 LVI characteristics of the GaN laser diode used for these experiments at 25°C.**

The optical spectra at different drive currents were measured using an Ocean Optics USB 4000 Miniature Fibre Optic Spectrometer. This spectrometer has an optical resolution of 1.5-2.3 nm for full width at half maximum (FWHM). As shown in Figure 4.2.4, the peak wavelength changes slightly with increasing drive current which is caused by the heating up of the device.

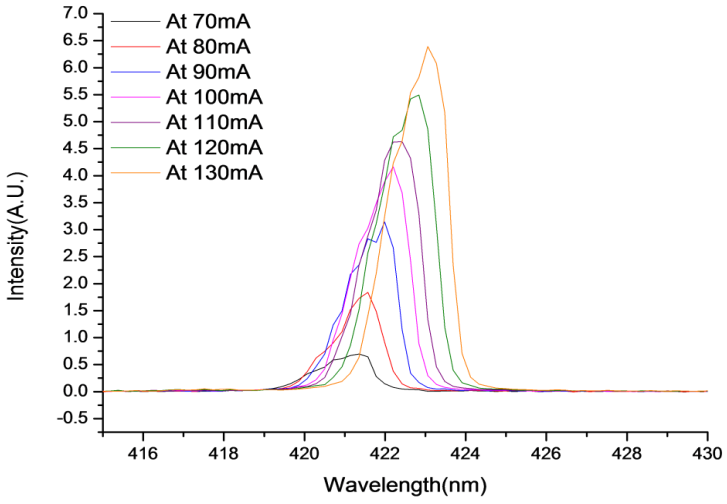


**Figure 4.2.4 Optical spectra of the laser diode with increasing drive currents.**

This red-shift which is observed is due to a reduction in the bandgap energy and is seen in LEDs as well as lasers [6]. It is mainly associated with a rise in the junction temperature and therefore larger devices result in a larger red-shift than their smaller counterparts. In the next section, frequency response measurements were carried out, with the best results shown from 60 to 71 mA, which relates to an emission wavelength of 421-422 nm.

### 4.2.2 High speed measurements

The frequency response of this device was measured using a network analyser. Light from the laser diode was collected using a 0.3 NA lens and focussed onto a high speed silicon PIN photo-receiver (HSA-X-S-1G4-SI) with an effective active diameter of 0.8 mm. The setup was approximately 0.5 m in length, and the frequency response was taken as a function of drive current in order to work out the -3 dB bandwidths.

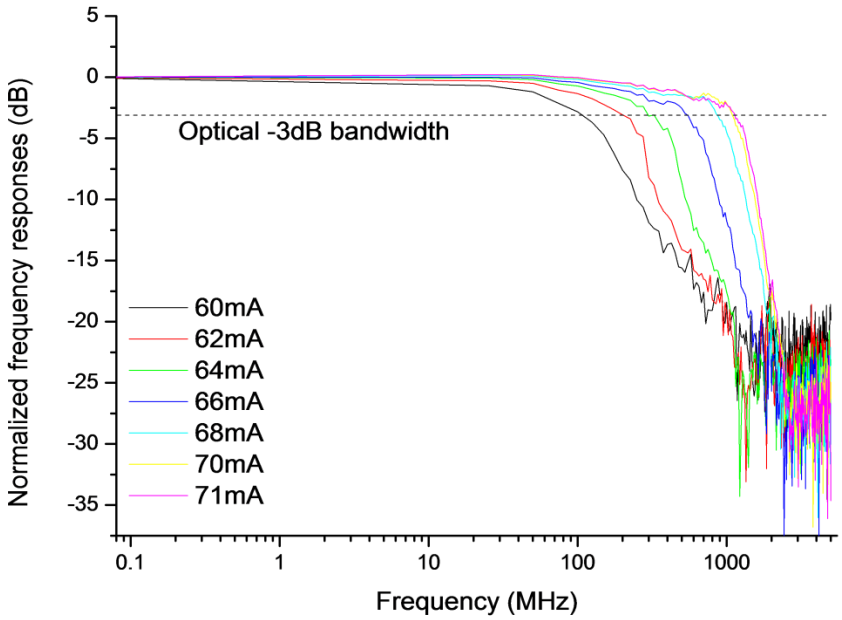


**Figure 4.2.5 Frequency response at different drive currents.**

It can be seen from Figure 4.2.5 that the frequency response is dependent on the injection current [7]. The maximum optical -3 dB bandwidth is found to be 1.416 GHz. The bandwidth of the silicon photo-receiver was 1.4 GHz, but the results have been calibrated to take this roll-off into account by subtracting the frequency response of the photo-receiver from the results. Figure 4.2.6 shows

the increase of bandwidth with increasing current more clearly. Data points at higher currents began to flatten off and roll over as the system started to become the limiting factor.

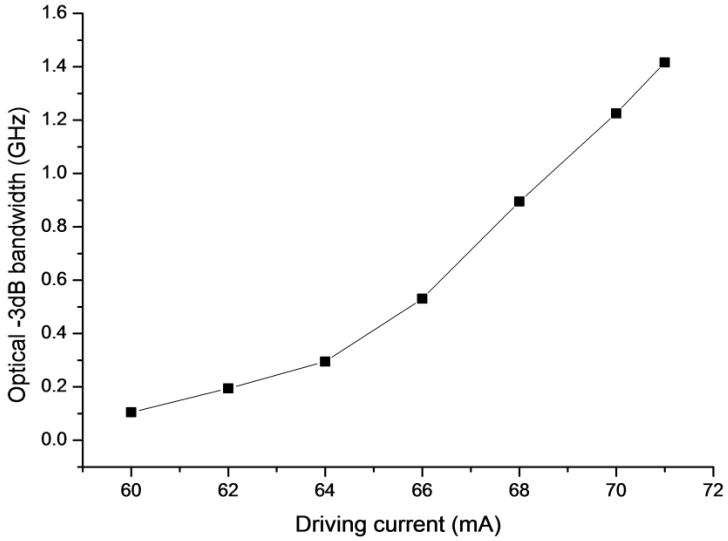


**Figure 4.2.6 Optical -3 dB bandwidth versus drive current.**

Eye diagrams were measured using a 12.5 GHz digital sampling oscilloscope as shown in the setup in Figure 4.2.7. The eye diagrams are shown in Figure 4.2.8. These figures show the eye diagrams achieved before any amplification of the signal.

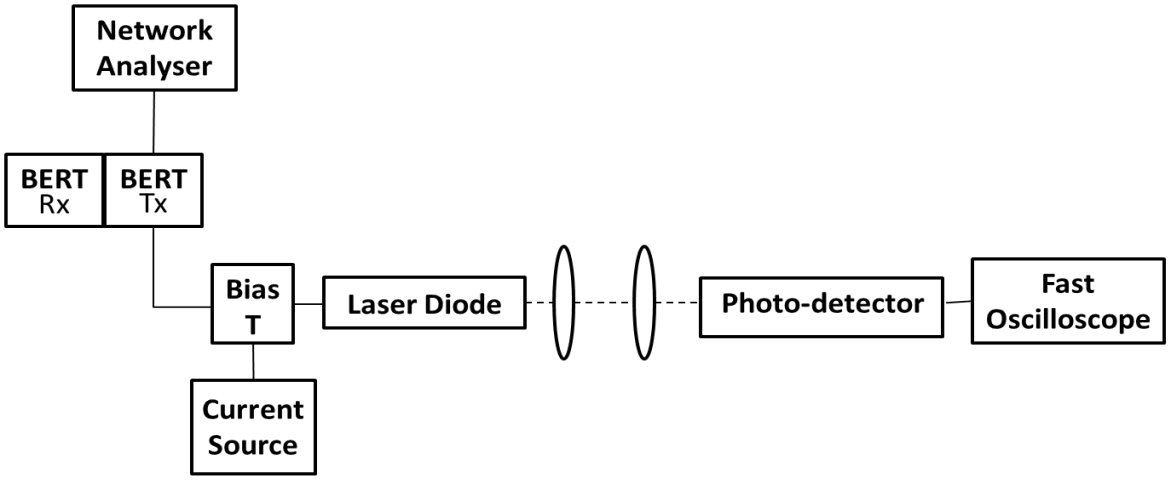


**Figure 4.2.7 Setup used to measure the eye diagrams.**

The current was set to 115 mA at 1 Gbit/s and 120 mA at 2.5 Gbit/s, at which points the highest Q factor values were measured by analysing the signal-to-noise ratio on the oscilloscope.

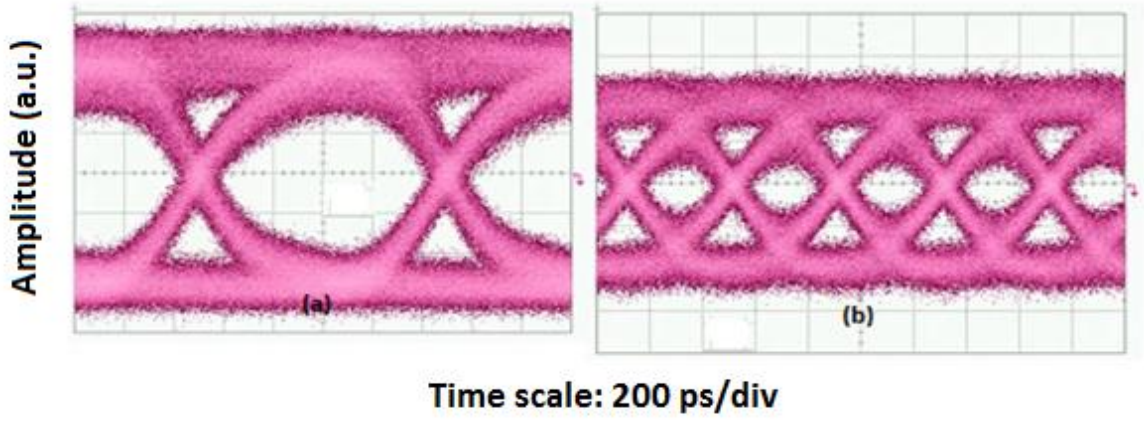


**Figure 4.2.8 Eye diagrams at (a) 1 Gbit/s and (b) 2.5 Gbit/s at the photodetector output.**

When a limiting amplifier was added to the setup, the Q factors were improved to 14.3, 12.4 and 10.4 dB for 1.4, 2 and 2 Gbit/s, respectively. At 2.5 Gbit/s, although the Q factor has decreased due to the bandwidth limit of the photodetector, it still gives an open eye and error-free transmission.

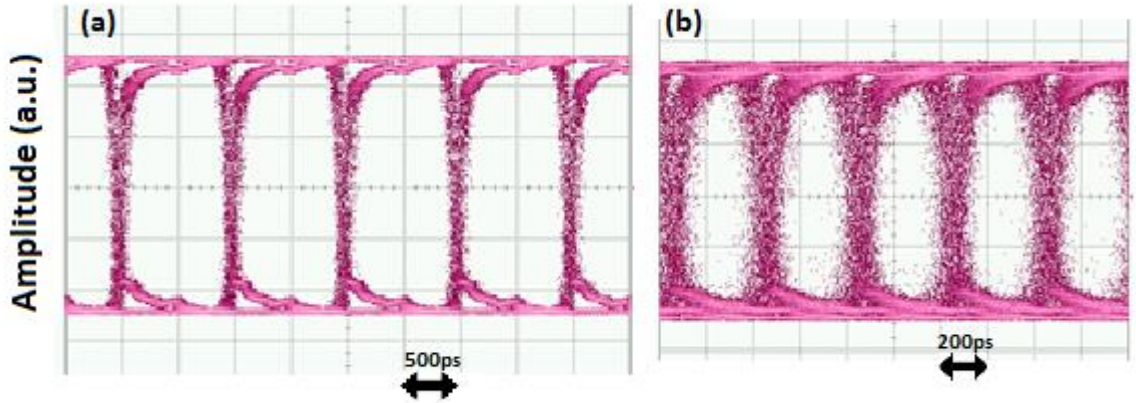


**Figure 4.2.9 Eye diagrams at (a) 1 Gbit/s and (b) 2.5 Gbit/s at the photodetector output with the limiting amplifier included.**

Ultimately, better results may be achieved with a faster photo-receiver or by using further amplification. A data amplifier could be used to amplify the signal coming from the signal generator, which would increase the RF power sent to

the device. Also, a preamplifier could be inserted to help improve the sensitivities.

Data transmission experiments were carried out in free space using a bit-error rate test (BERT) system. The laser diode was driven by a combination of DC current and a non-return-to-zero (NRZ) pseudo random bit sequence (PRBS) supplied from the BERT as shown in Figure 4.2.10.

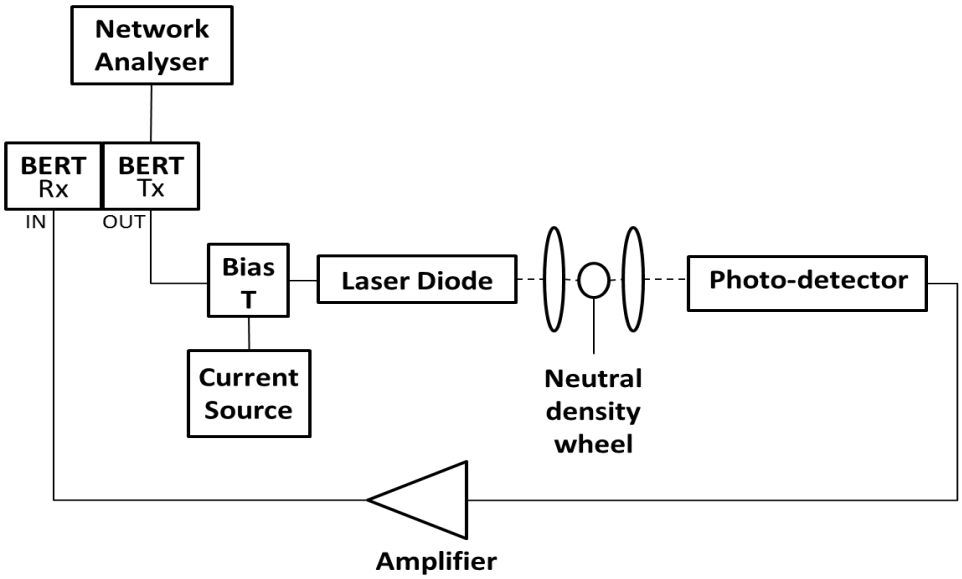


**Figure 4.2.10 Setup used for bit-error rate measurements.**

This bit sequence was $2^7$-1 bits in length with a peak-to-peak voltage of 2V. This pattern length is used for many applications such as gigabit Ethernet and fibre channel, which use 8-B/10-B and other related coding schemes. The received optical power was attenuated by a variable neutral density filter placed in front of the receiver, which allowed the bit-error rate to be measured as a function of received power. A limiting amplifier was placed after the detector to provide low noise amplification in order to retrieve a good signal.

Figure 4.2.11 shows the bit-error rate plotted against the received optical power for bit rates from 1 Gbit/s up to 2.5 Gbit/s. The current was varied from 73 mA to 95 mA to obtain the optimum for each bit rate.

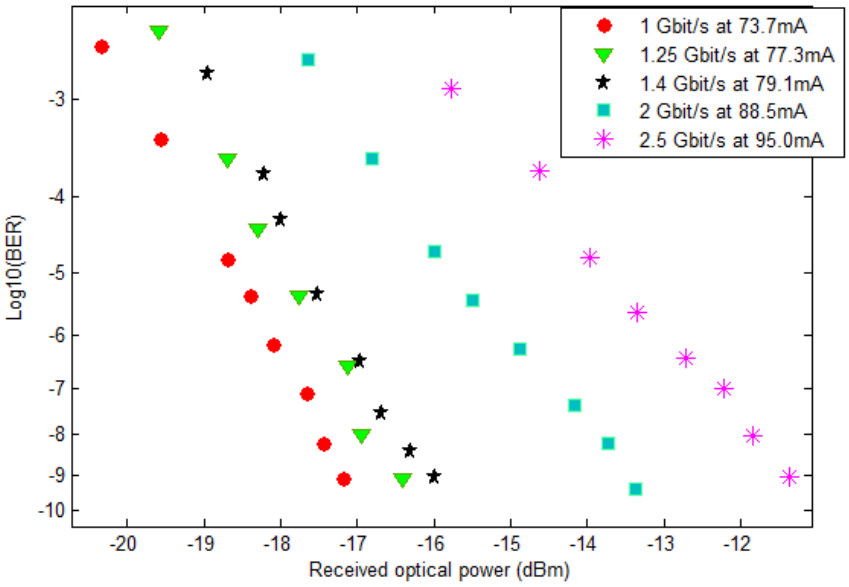


**Figure 4.2.11 Bit-error rates versus received optical power at 1, 1.25, 1.4, 2 and 2.5 Gbit/s at optimum bias current for each bit rate.**

The sensitivities at 1, 1.25, 1.4, 2 and 2.5 Gbit/s are -17.4, -16.5, -16.0, -13.5 and -11.5 dBm, respectively. The sensitivities at 2 and 2.5 Gbit/s show an additional power penalty of approximately 1 and 2 dB, respectively, compared to the performance at 1 Gbit/s. This is caused by the bandwidth limitations of the system, not only from the photo-receiver but from the laser diode itself.

These results not only show the potential for free space VLC over short distances, but also through single-mode plastic optical fibre (POF), if the fibre can be designed to be low-loss at these wavelengths. This will be explored further in Chapter 5. Also, the use of these GaN laser diodes for underwater communications is an important topic as there is low loss underwater at these wavelengths. Furthermore, as mentioned briefly before, these devices could be used as high speed sources for a white light VLC system, given the correct colour converter material.

Further data transmission experiments were carried out using a different laser diode from the same batch to see if there were any differences in frequency response or data transmission rate. Due to variance across the lasers in this batch, some diodes performed better than others. The same setup and measurement techniques were used but this laser diode performed better than the previously mentioned one. The LVI plot is shown in Figure 4.2.12.

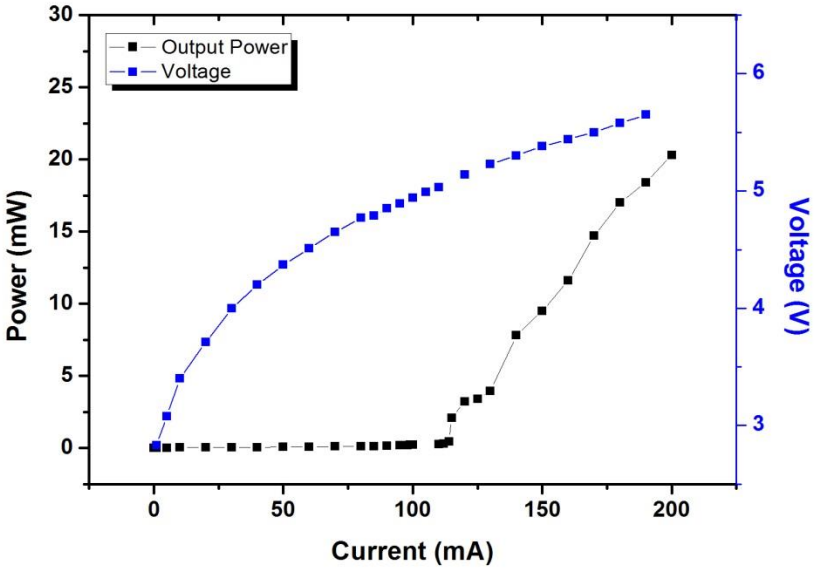


**Figure 4.2.12 LVI characteristics for laser diode.**

It can be seen that the threshold current is 115 mA for this device which is much higher than the one used earlier which was around 70 mA. Despite this, it still reaches output powers over 20 mW as seen before. The frequency response was measured and was found to be in excess of 2 GHz, which is the highest -3 dB bandwidth measured in this work.

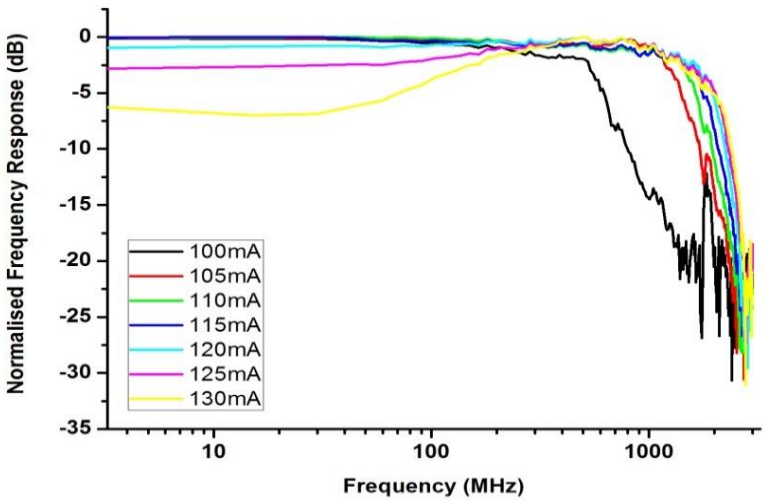


**Figure 4.2.13 Frequency response at different bias currents.**

The optical bandwidth of the device continues to increase as a function of drive current with a maximum bandwidth of 2.3 GHz achieved at 130 mA. Like before, this measurement was conducted using a photo-detector with a bandwidth limit

of 1.4 GHz but this roll-off is taken into consideration and subtracted from the data.

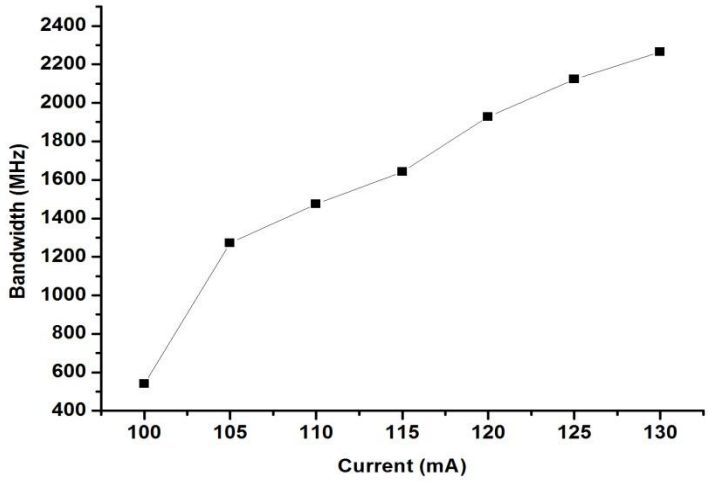


**Figure 4.2.14 Optical bandwidth as a function of drive current.**

It can be seen in Figure 4.2.13 that a resonance begins to appear as higher currents are reached. This pushes the frequency response plot out to higher frequencies, ultimately resulting in higher -3 dB bandwidth values. As this device exhibited higher bandwidth, eye diagrams and bit-error rate experiments were conducted to see if the data rate could be increased. Figure 4.2.15 shows the eye diagrams achieved with a maximum data rate of 3.4 Gbit/s shown in Figure 4.2.15 (d).

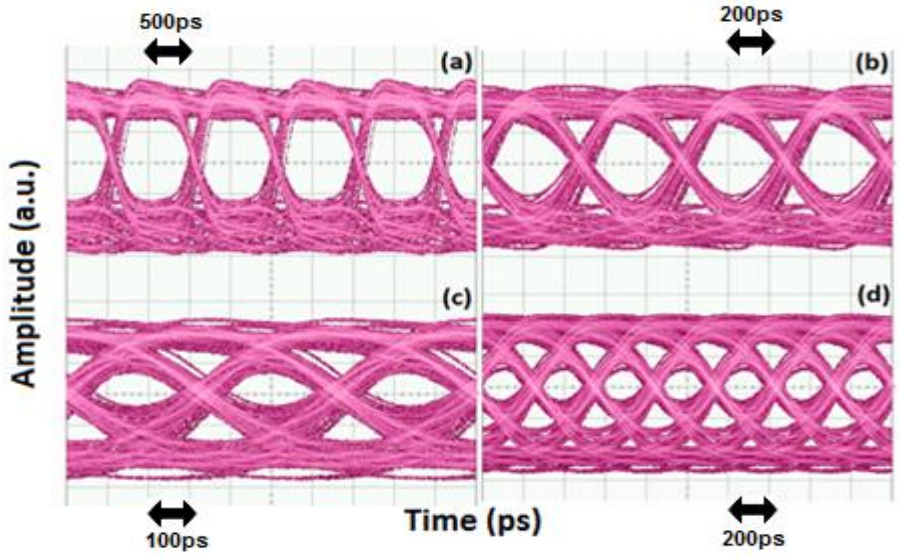


**Figure 4.2.15 Eye diagrams at (a) 1 Gbit/s, (b) 2 Gbit/s, (c) 3 Gbit/s and (d) 3.4 Gbit/s.**

Error-free data transmission was confirmed by carrying out data transmission experiments using the BERT system. Figure 4.2.16 shows the bit-error rate plotted against the received optical power, which was controlled using a neutral density wheel.

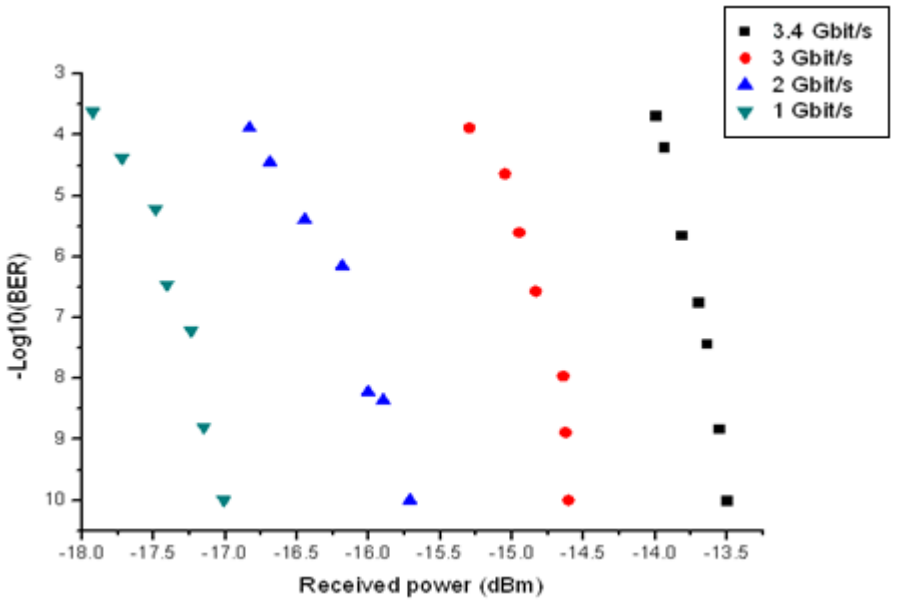


**Figure 4.2.16 Bit-error rate plotted against received optical power for different data rates.**

The sensitivities at 1, 2, 3 and 3.4 Gbit/s are -17, -15.7, -14.6 and -13.5 dBm, respectively. These improved results again show the potential for this technology to become a leading source for visible light communications. These data rates exceed the typical cable internet speeds by an order of magnitude. However, these laser diodes have reliability issues and their performance tends to drop off over time. This issue will be explored further in section 4.2.4.

## 4.2.3 Colour converter materials

It has been shown that colour converters can be used alongside GaN LEDs to extend their wavelength coverage whilst keeping their high modulation performance. A ZnCdSe/ZnCdMgSe multi-quantum well (MQW) colour converting sample has been shown to have an intrinsic response of 145 MHz which is considerably faster than conventional phosphors [8]. With the increase in power and modulation performance of a laser diode in comparison to an LED, measurements were carried out with various colour converting samples to analyse their performance. A III-V material which produces peak emission at a wavelength of 640 nm (red), an organic, yellow fluorescent material known as

“super-yellow” emitting at 580 nm [9] and a green emitting organic material called “swager” emitting at 540 nm were the three colour converters used [10]. These samples were provided by the Institute of Photonics at the University of Strathclyde. The emission spectrum for each is shown in Figure 4.2.17.

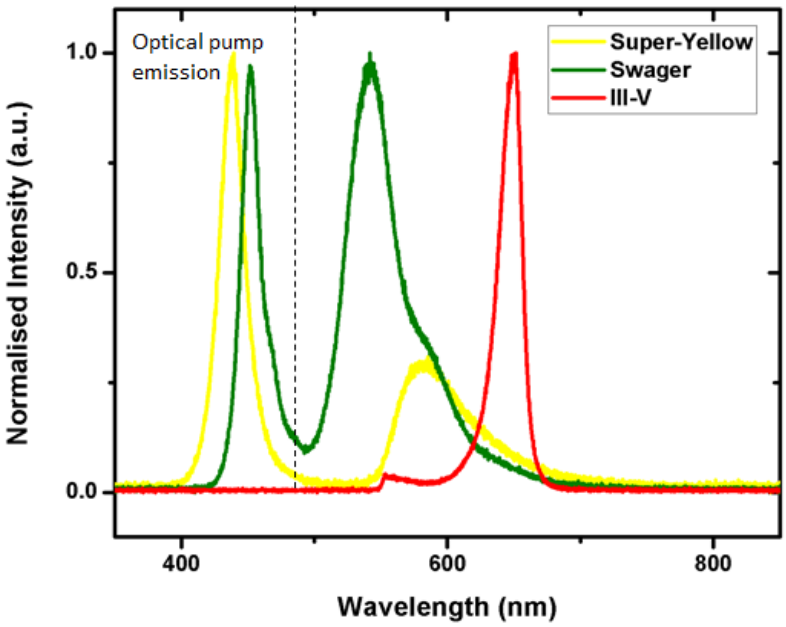


**Figure 4.2.17 Spectral response for each of the colour converting materials.**

The peaks shown at around 450 nm are from the blue device used to pump the colour converter samples, which have not been filtered out for the super-yellow and swager measurements. The other three peaks indicate the emission wavelength of each sample. The setup shown in Figure 4.2.18 was used to measure the bandwidth of these different samples.

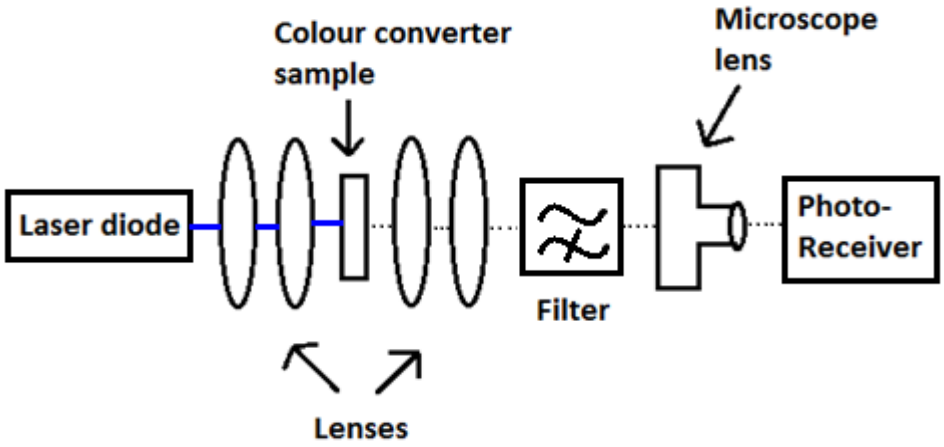


**Figure 4.2.18 Experimental setup showing the layout required to measure the characteristics of the different colour converter materials.**

The first two lenses are used to focus the light onto the colour converting sample and then this emission is then collimated and re-focussed using the next two lenses. A long pass filter is added to remove the residual blue light. For the III-V sample, an “FEL550” filter is used to remove everything below 550 nm and an “FEL500” filter is used when working with the super yellow and swager samples to remove everything below 500 nm as shown in Figure 4.2.19 (a) and (b), respectively. A final microscope lens is used to focus the light onto the photo-receiver. As in previous bandwidth measurements, such as the setup shown earlier in Figure 4.2.3, an RF signal from the network analyser is combined with a DC bias from a constant current source. This signal is used to modulate the laser diode. The signal received on the photo-receiver is then input to the network analyser to allow analysis of the bandwidth characteristics.

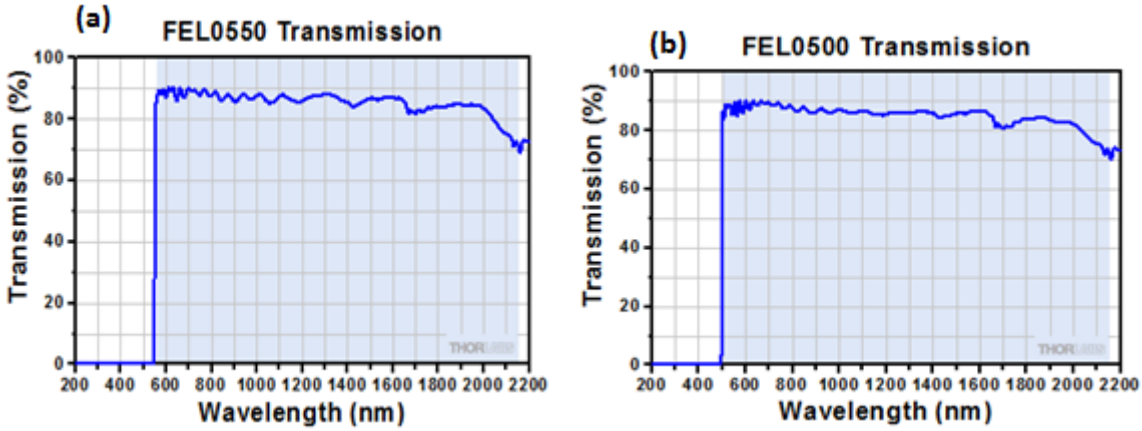


**Figure 4.2.19 Long pass filters used to block the light below (a) 550 nm and (b) 500 nm.**

Initial measurements were conducted using a blue micro-LED made up of 100 × 100 $\mu m^2$ pixels. However, as seen in Figure 4.2.20, the current versus bandwidth data is very similar for the LED on its own and with the colour converters. This suggests that the bandwidth of the LED is the limiting factor. It shows that the maximum bandwidth achieved for each case is very similar. So, by using a faster device, i.e. a laser diode, it is possible to subtract the device response and only analyse the response of the colour converting sample. It is not possible to get an accurate subtraction simply using this data due to the noise seen at higher frequencies when using the LED.

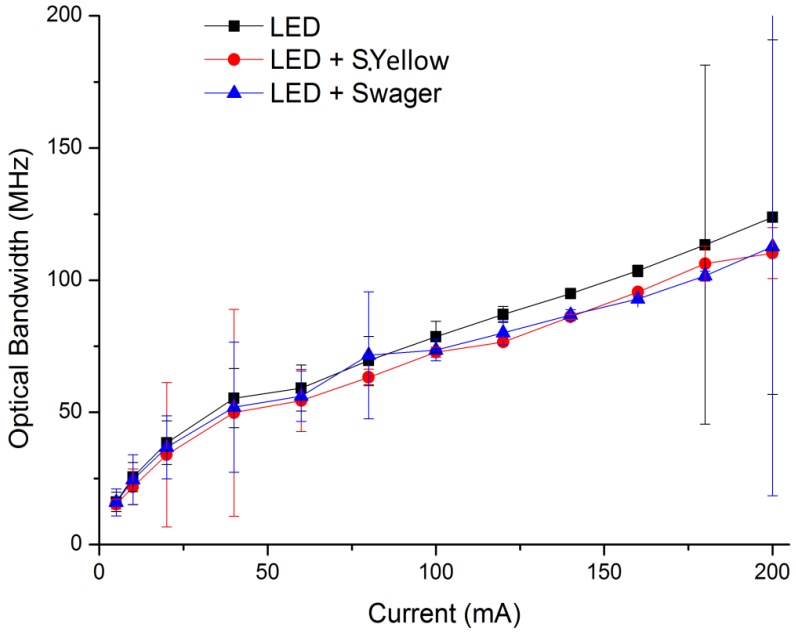


**Figure 4.2.20 Bandwidth vs current for the micro-LED on its own and with the super yellow and swager colour converting samples.**

Bandwidth measurements were conducted using a laser diode which reached a maximum bandwidth value of 1.4 GHz. This measurement was restricted by the bandwidth limit of the photo-receiver. However, this laser diode is fast enough to characterise the bandwidth of the colour converter samples. A plot showing the bandwidth of the laser plotted against bias current is shown in Figure 4.2.21. Unlike other bandwidth plots in this thesis, the first point is unusually high for what appears to be below threshold. Whilst unexpected, this is likely to be caused by the continual degradation of the device during the measurement, where the original threshold value was below 100 mA, however over time has shifted to the right. The graph in Figure 4.2.21 appears to show a high

bandwidth point below threshold, however the device is acting as it would above threshold and hence appears higher than it should.

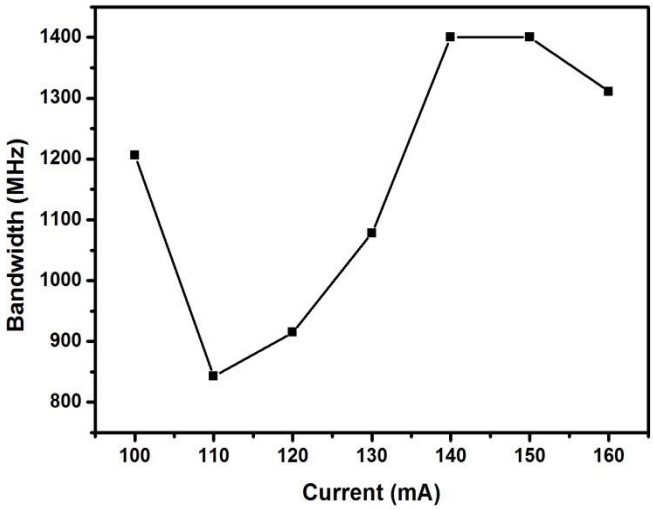


**Figure 4.2.21 Laser diode pump bandwidth as a function of bias current.**

A drop in bandwidth is seen around the 'new' threshold value of the laser before it rises up again up to reach a maximum bandwidth of 1.4 GHz. As discussed in section 2.2 of chapter 2, this drop occurs due to the unusual modulation behaviour exhibited around threshold. The colour converter samples were then included in the measurement so that the laser diode was pumping the converter and the bandwidth of the emission was measured. This allows the laser response to be compared to the combined response. Following this, by subtracting the laser diode response from those in Figure 4.2.22 at each of the currents, the bandwidth of the colour converting samples (on their own) can be calculated. This should be a flat line indicating that there is no effect from the current.

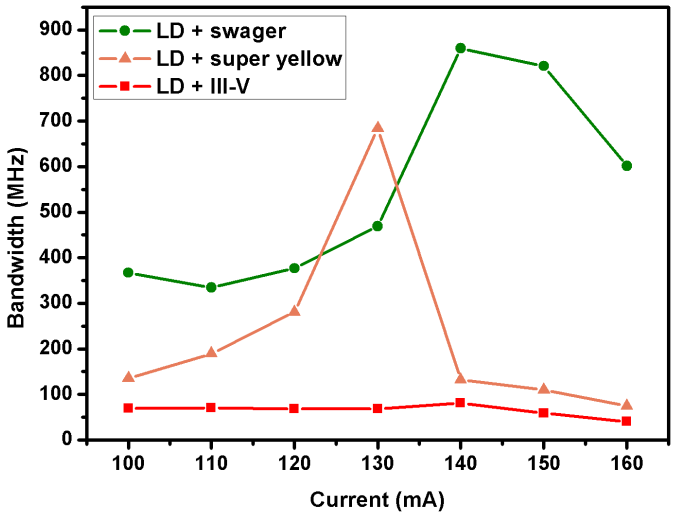


**Figure 4.2.22 Bandwidth vs bias current for the laser diode and the different colour converters combined.**

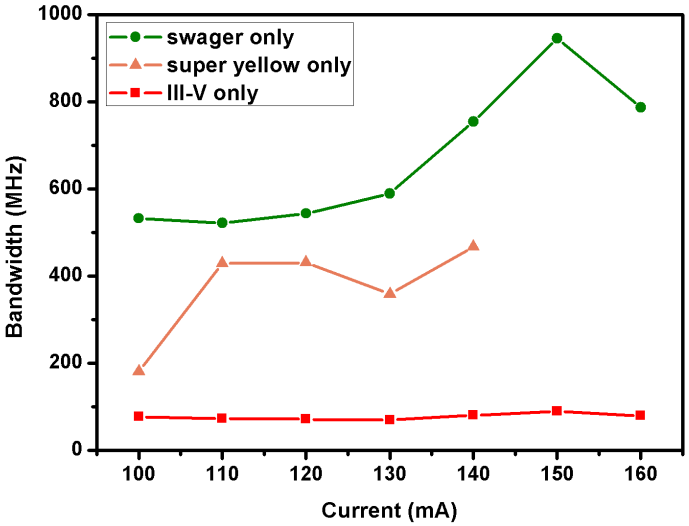


**Figure 4.2.23 Subtracted data showing bandwidth of the different colour converter samples.**

It can be seen that the bandwidth of the colour converter samples is fairly consistent with current, as expected. There is a slight fluctuation which occurs due to errors in the subtraction which can be due to noise in the original measurements or it could be the degradation of the laser diode. Another potential reason could have been that some of the blue light from the laser was leaking through, however further measurements proved this not to be the case. The colour converter sample was removed and the blue light was used again, however none of the light bypassed the filter and no response was picked up on

the photo-detector showing that the blue light had no effect. The III-V sample was shown to be slower than the LED and has a bandwidth of ~70 MHz. This could be due to the intrinsic properties within the semiconductor. The super yellow sample varies slightly but seems to have a bandwidth of around 425 MHz and the swager sample is the fastest of the three at around 550 MHz. These organic materials exhibit much higher bandwidths in comparison to the III-V semiconductor material. These are promising results which show that high speed modulation characteristics are apparent in these colour converting samples and that high speed data transmission across the visible spectrum could be achieved.

### 4.2.4 Reliability

Over time, the laser diodes used for these experiments begin to degrade as their threshold value changes. The power output is reduced and its bandwidth characteristics are affected. If the laser is left on above threshold for a period of time, the drop in performance can be characterised. Even after leaving the laser on for a period of three hours, it can be seen from the power-current (LI) graph that the laser is beginning to degrade. The laser diode used for this reliability measurement had a threshold current of ~65 mA, however within three hours, this had shifted by over 10 mA.

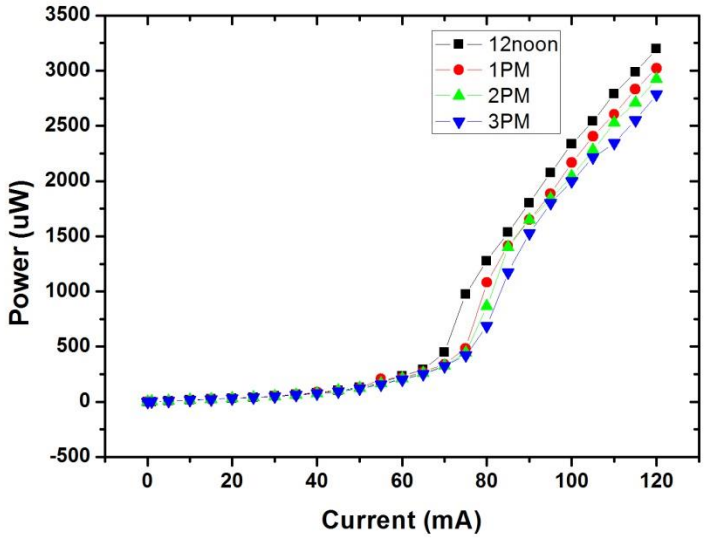


**Figure 4.2.24 LI graph showing the change in the power-current characteristics over time.**

The laser is kept at a constant temperature and therefore it can be assumed that the degradation is due to the laser structural defects present. This can be

problematic as ideally the laser performance would be consistent throughout all measurements. However, in order to keep the laser stable for longer periods of time, the laser is switched off in between measurements so that it does not have the chance to degrade as quickly. A reduction in these structural defects in GaN based laser diodes is important in terms of improving the efficiency and ultimately, the reliability of the devices. There are three main stages of degradation: rapid degradation, gradual degradation and catastrophic failures [11]. Rapid degradation tends to occur within 100 hours of operation and is due to the way the recombination mechanisms behave in the device. Catastrophic failure is usually due to a large current surge, and the heat caused by this results in the device dying straight away. Also, damage to the laser facet can cause the device not to work at all. This can be from physical damage to the device or by catastrophic optical damage (COD). Catastrophic optical damage occurs when the maximum power density of the laser diode is exceeded and positive feedback occurs where increased heat results in increased absorption which ultimately leads to the facet heating up and melting. The recombination velocity determines how quickly the facet heats up due to surface recombination [12] [13].

Gradual degradation is to do with the laser diode wearing out over time. This is related to the point defect reaction in the epitaxial layers [14]. The third option is most likely the case for the laser diodes used for this work.

## 4.3 Summary and conclusions

This chapter has looked at the use of laser diodes for communication purposes. It began by looking at the structure of such devices before presenting the characterisation of the devices used for the high speed measurements. The frequency response of these laser diodes was shown, with bandwidths in excess of 2 GHz achieved. Data transmission experiments were carried out and error-free transmission was achieved at 2.5 Gbit/s, which at the time of publishing was the highest data rate achieved for VLC using a directly modulated GaN blue laser diode [15]. Further work showed improved data rates of 3.4 Gbit/s which is the fastest data rates using these devices without higher order modulation schemes. The use of colour converters was explored before a look at the reliability of these devices was given towards the end of the chapter. The

following chapter will look at the use of these laser diodes for fibre communications.

# References


[1] W.-Y. Lin, et al., "10m/500Mbps WDM visible light communication systems," *Optics Express*, vol. 20, no. 9, pp. 9919-9924, 2012.

[2] J. Wallace, "Semiconductor sources: Laser plus phosphor emits white light without droop," *Laser Focus World*, Jul. 2013.

[3] B. Coxworth, "White laser light found to be just as easy on the eyes as LEDs," *Gizmag*, Oct. 2011.

[4] L. Ulrich, "BMW Laser Headlights Slice Through the Dark," *IEEE Spectrum*, Oct. 2013.

[5] (2012) TopGaN Lasers. [Online]. http://www.topganlasers.com

[6] Z. Gong, et al., "Size-dependent light output, spectral shift, and self-heating of 400 nm InGaN light-emitting diodes," *Journal of Applied Physics*, vol. 107, 2010.

[7] S. A. Gurevich, *High Speed Diode Lasers*. World Scientific Publishing Co. Pte. Ltd., 1998.

[8] J. M. M. Santos, et al., "Hybrid GaN LED with capillary-bonded II-VI MQW color-converting membrame for visible light communication," *Semiconductor Science and Technology*, vol. 30, 2015.

[9] H. Chun, et al., "Visible Light Communication Using a Blue GaN uLED and Fluorescent Polymer Color Converter," *IEEE Photonics Technology Letters*, vol. 26, no. 20, 2014.

[10] M. T. Sajjad, et al., "Novel Fast Color-Converter for Visible Light Communication Using a Blend of Conjugated Polymers," vol. 2, no. 2, pp. 194-199, 2015.

[11] O. Ueda, *Reliability and degradtion of III-V optical devices*. Boston: Artech House, 1996.

[12] J. W. Tomm, "Catastrophic optical damage in semiconductor lasers," *SPIE Newsroom*, vol. 10.1117/2.1200902.1495, Feb. 2009.

[13] M. Ziegler, et al., "Surface recombination and facet heating in high-power diode lasers," *Applied Physics Letters*, vol. 92, no. 20, 2008.

[14] O. Ueda and S. J. Pearton, *Materials and Reliability Handbook for Semiconductor Optical and Electron Devices*. New York: Springer, 2013.

[15] S. Watson, et al., "Visible light communications using a directly modulated 422 nm GaN laser diode," *Optics Letters*, vol. 38, no. 19, pp. 3792-3794, 2013.

# Chapter 5

# Fibre measurements

Fibre-optic communication has been an important method of transmitting data since the 1970s [1]. Telecommunication applications such as phone lines, cable TV and internet connections all make use of this technology. Early advancements were using light around wavelengths of 800 nm but later it was found that working at 1.3 μm and 1.55 μm was more desirable due to the lower attenuation at these wavelengths using glass fibre, as seen in Figure 5.1.1.

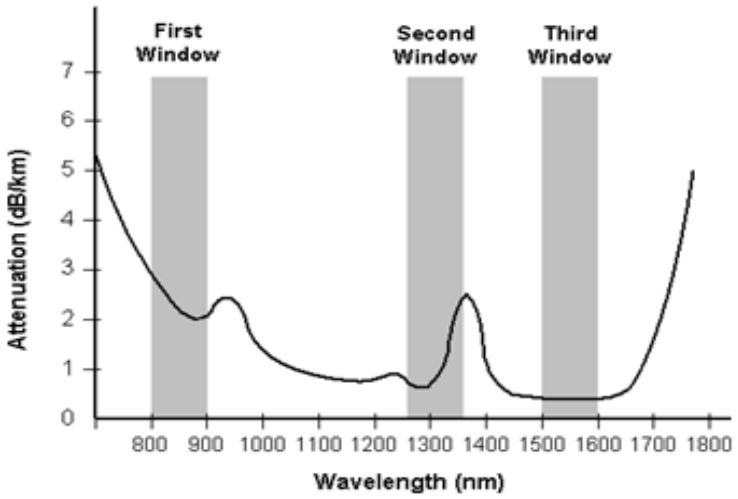


**Figure 5.1.1 Attenuation vs wavelength for glass fibre [2].**

However, plastic optical fibre (POF) has a different attenuation graph. There is a low loss window in the green part of the spectrum which can be exploited for transmission purposes, as seen in Figure 5.1.2. Plastic optical fibre has a number of advantages over glass fibre. Firstly, the fibre itself is much lower in price and the installation costs are lower too due to the lower precision required. These fibres have a much greater flexibility and resilience to bending, shock and vibration. They are easier to handle and connect to test equipment, and can be used with visible light. Plastic optical fibres have much larger core diameters, typically 1 mm, which makes alignment easier. However, much higher losses are seen through plastic optical fibre in comparison to the glass fibre [3].

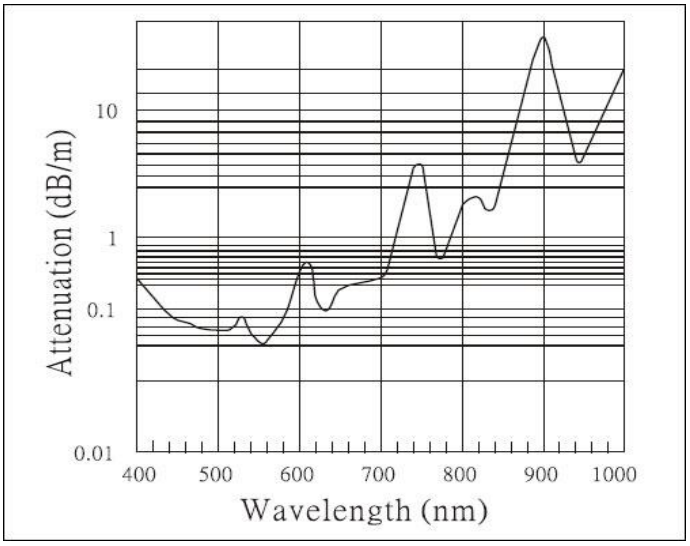


**Figure 5.1.2 Attenuation vs wavelength for plastic optical fibre [4].**

In chapter 4, a blue GaN laser diode was used for high speed measurements. A similar device was used here to analyse the effects of dispersion in plastic optical fibre, both standard fibre and some novel multi-core fibre. More high speed measurements were conducted using the different types fibre and an in depth look at the limitations of them is explored. A comparison of the two types of fibre is presented showing the benefits of each one. Previously, it has been seen that using resonant cavity LEDs emitting at 650 nm, communication can be achieved over plastic optical fibre [5]. However, more recently work has been carried out using laser diodes to achieved higher data rates over longer distances. By exploiting higher order modulation schemes such as discrete multi-tone modulation (DMT), much higher data rates have been achieved [6] [7]. There has been a lack of research on fibre communications at wavelengths below 450 nm so work has been carried out to explore this topic.

## 5.1 Dispersion in optical fibre

When light is sent from one end of a fibre to the other, not all the light is received at the other end due to attenuation. If a short light pulse travels the length of a fibre, the pulse will broaden which reduces the transmission bandwidth. Figure 5.1.3 shows this process.

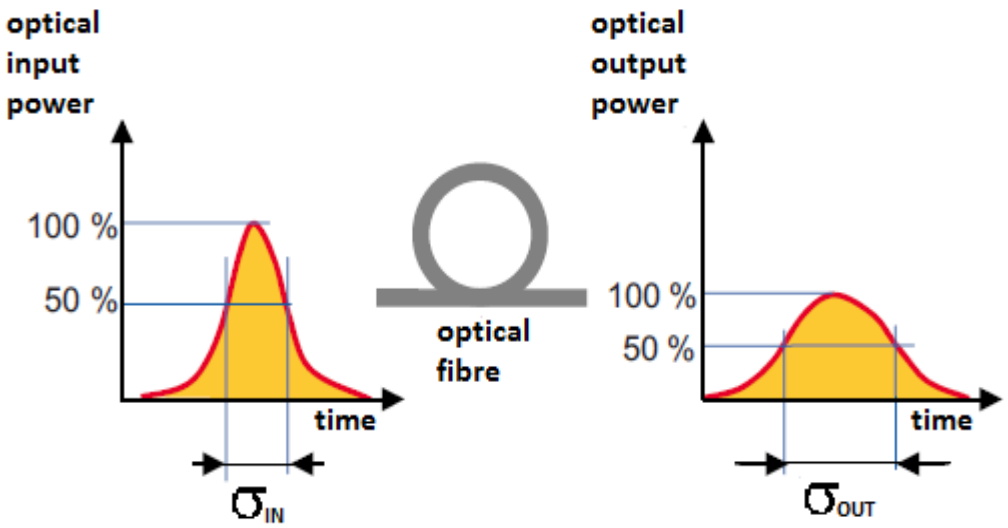


**Figure 5.1.3 Pulse broadening due to dispersion [8].**

In the following section, similar measurements were carried out to analyse the dispersion through different types of fibre. Measurements in the frequency domain and the time domain were conducted in order to analyse the performance of each fibre.

## 5.2 Experiments

Frequency response experiments were conducted using step-index plastic optical fibre (SI-POF) with a core diameter of 1 mm, in order to analyse its bandwidth and hence dispersion. A blue laser diode was used to exploit the low-loss window. As in previous chapters, an RF signal from the network analyser was combined with a DC bias and used to drive the laser diode, with the output focused onto the high speed photo-receiver. The free space response of the laser was measured before the inclusion of the fibre after the lenses as shown in Figure 5.2.1.

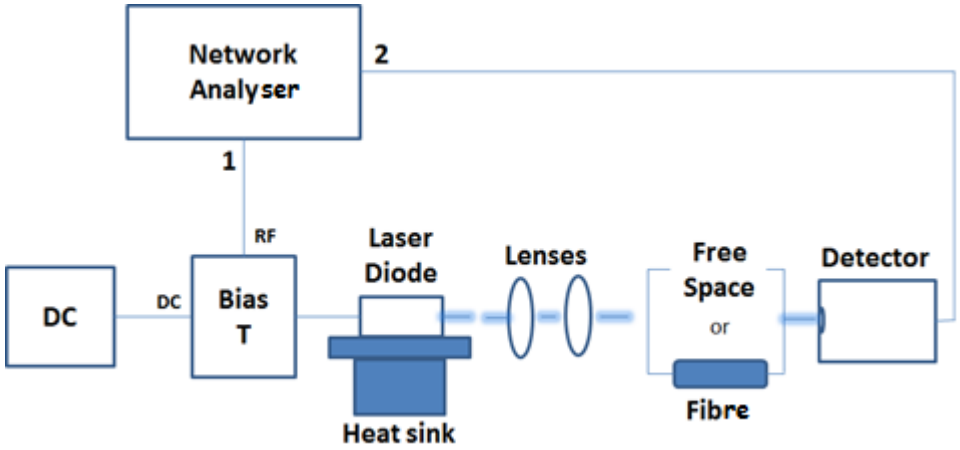


**Figure 5.2.1 Experimental setup.**

The frequency responses of varying lengths of SI-POF were measured with the -3 dB bandwidths shown as a function of current in Figure 5.2.2. The output of the fibre was butt-coupled straight to the photodetector.

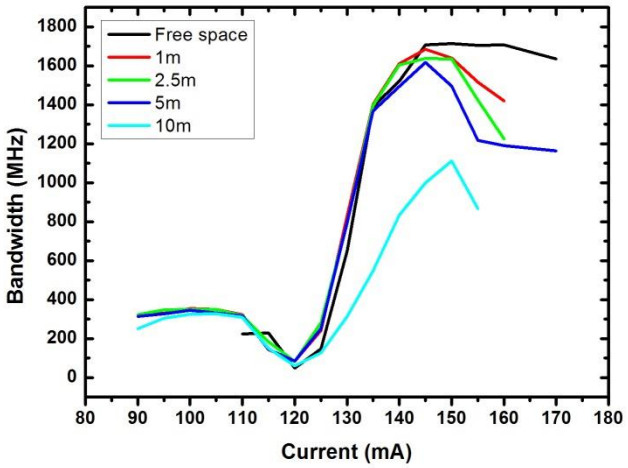


**Figure 5.2.2 Current vs bandwidth for varying lengths of step index plastic optical fibre.**

The maximum bandwidths achieved in free space and through 1 m, 2.5 m, 5 m and 10 m are 1.71 GHz, 1.68 GHz, 1.63 GHz, 1.62 GHz and 1.1 GHz, respectively. The maximum bandwidth values achieved up to 5 m of fibre are very similar, showing that the system bandwidth – i.e. the photodetector - is the limiting factor. After this, a drop of 700 MHz is seen going from the free space response to the 10 m fibre response.

The free space response was subtracted from that of each length of fibre, in order to work out the bandwidth of the fibre itself.

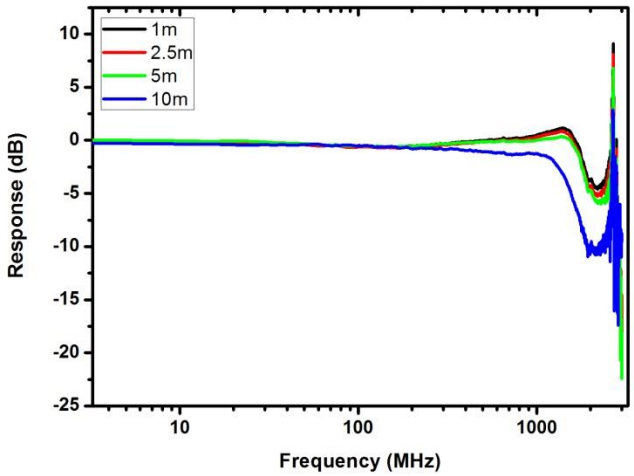


**Figure 5.2.3 Frequency response of the varying lengths of step index plastic optical fibre.**

As shown in Figure 5.2.3, the -3 dB bandwidth of 1 m, 2.5 m and 5 m of fibre is very similar. The 5 dB drop seen at higher frequencies is believed to be due to the increase in noise at these frequencies and hence the subtraction results in some fluctuations. It is expected that the frequency response plot for 1 m, 2.5 m and 5 m will be flat up past 3 GHz. However, a reduction of bandwidth is seen for 10 m of fibre as it drops to 1.38 GHz. This drop is real and is due to the higher levels of modal dispersion with increased length. This suggests a bandwidth-distance product of 13.8 MHz per km i.e. the fibre could carry a 13.8 MHz signal for 1 km.

Further experiments were carried out using multi-core fibre and a different blue laser from the same batch. This type of fibre is not predominantly used to increase the bandwidth capabilities of a system but rather for its advantages of low bend loss. This makes it an ideal solution for in-vehicle applications or on aircrafts where space may be limited. The fibre used here had cleaved ends, allowing all the cores to be illuminated for the experiments. A cross-section of the fibre, showing the layout of the cores, can be seen in Figure 5.2.4.

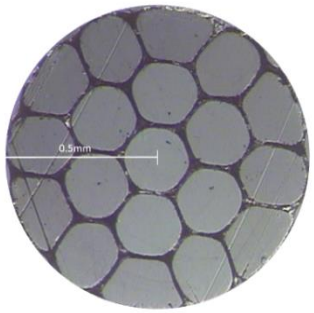


**Figure 5.2.4 A cross section showing the core layout of the fibre.**

Again, the frequency response of the laser was measured on its own in free space, in order to have a comparison against the different lengths of fibre. The network analyser provided an RF signal which was combined with a DC bias and sent to the laser diode, like before. The setup is the same as shown in Figure 5.2.1, the only difference is the type of fibre being used.

The optical bandwidth of the laser diode was plotted as a function of drive current, with a maximum bandwidth of 840 MHz achieved in free space. In order to analyse the effect of the fibre on the transmission, different lengths of fibre were measured versus laser bias. Fibre lengths of 1 m, 3 m, 5 m, 10 m and 15 m were tested in order to see the dependence of bandwidth on fibre length. Maximum bandwidths of 654 MHz, 577 MHz, 324 MHz, 252 MHz and 150 MHz were achieved for fibre lengths of 1 m, 3 m, 5 m, 10 m and 15 m of fibre, respectively, which can be seen clearly in Figure 5.2.5.

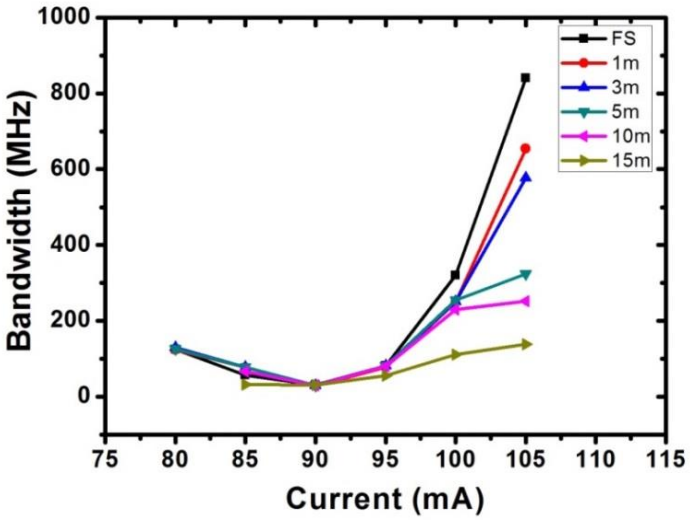


**Figure 5.2.5 Current versus bandwidth for varying lengths of multi-core fibre.**

Figure 5.2.5 shows the system bandwidth as a function of drive current, and as expected, at currents below the laser threshold, the system is limited by the laser bandwidth as it behaves like an LED. Above this current, the system bandwidth can be seen to be a strong function of fibre length, indicating the presence of dispersion. Using the 15 m fibre, the system bandwidth has been reduced from the free space value of 840 MHz down to 150 MHz.

In order to analyse the effect of dispersion from the fibre itself, the free space response was subtracted from that measured through the varying lengths of fibre and an average of the fibre responses at different currents was taken. Figure 5.2.6 shows the steps taken to do this. Figure 5.2.6 (a) shows the free space response at different currents and Figure 5.2.6 (b) shows the 10 m fibre response at the same currents. Figure 5.2.6 (c) then subtracts the fibre response from the free space response with an average of these subtracted responses shown in Figure 5.2.6 (d).

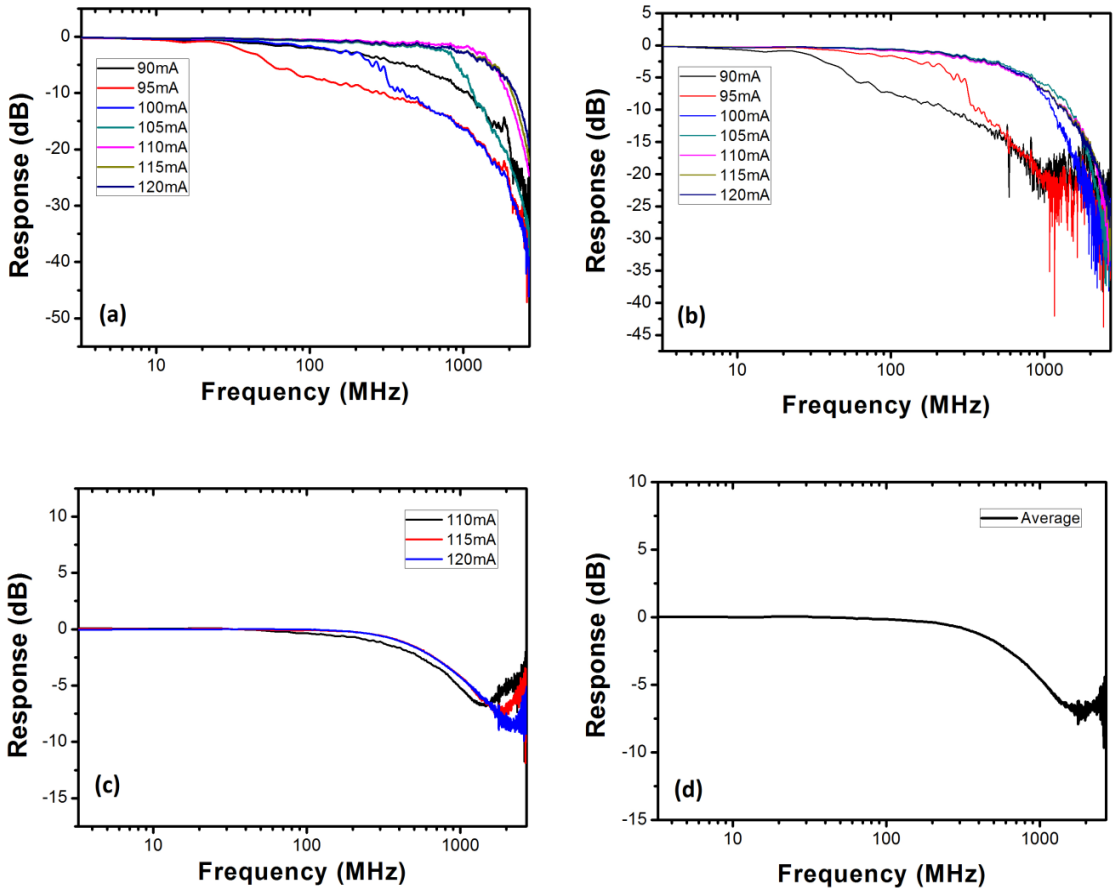


**Figure 5.2.6 (a) Frequency response through free space, (b) frequency response measured through 10m of fibre, (c) free space response subtracted from the fibre response at different currents and (d) the average response calculated from (c).**

Figure 5.2.6 (d) is used to calculate the -3dB bandwidth of the fibre and although an average has been taken, the similarity of the responses in Figure 5.2.6 (c) at different currents, and hence different system bandwidths, gives confidence that a robust measurement of the fibre bandwidth is being presented. For 5 m, 10 m and 15 m of fibre, bandwidth values of 1.29 GHz, 724 MHz and 360 MHz are measured. The linear reduction in bandwidth with respect to length is consistent with the significant dispersion in the fibre. The bandwidth-distance product works out at about half the value of the step-index plastic optical fibre (SI-POF). This reduction is seen in both types of fibre meaning that the transmission distance will be limited when working at these wavelengths. However, this would be an ideal, cheaper alternative for short distance transmission such as in-vehicle or in-room situations. Also, the bend loss was found to be very minimal and have no effect on the bandwidth.

To verify these results, further experiments were carried out using a pulse generator, where an optical pulse was transmitted through the varying lengths of fibre to examine dispersive effects directly in the time domain. The rise and fall times were measured for the electrical drive signal, through free space and then through the varying lengths of fibre. It can be seen in Figure 5.2.7 that the rise and fall times increases as the fibre length increases.

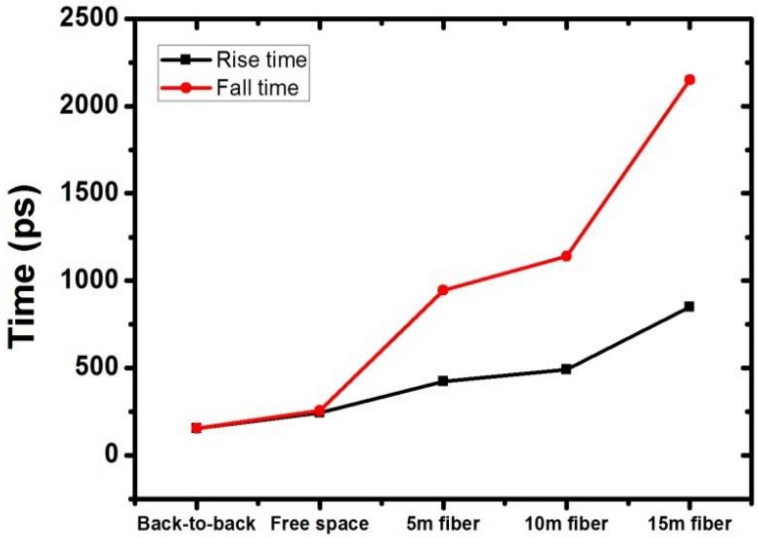


**Figure 5.2.7 The change in rise and fall times as transmission distance is increased.**

As the pulse broadens, the fall time increases much more dramatically than the rise time [9]. The effect of frequency chirping in interaction with dispersion distorts the signal as it travels along the fibre resulting in this phenomenon [10], with the large increase in pulse width supporting the results shown earlier.

The measurement of dispersion below 450 nm is still a relatively unexplored topic. In these experiments, the modal dispersion was calculated in order to find out if this was the dominating factor or whether other effects such as chromatic dispersion affect the signal. The equation to work out $\Delta t_{mod}$ takes into consideration the fastest and slowest routes in which the light can travel along the fibre and is given as [11]:

$$\Delta t_{mod} = \frac{L}{2 \times c \times n_{clad}} (NA)^2 \qquad [5.1]$$

where L is the length of fibre, c is the speed of light, $n_{clad}$ is the refractive index of the cladding material and NA is the numerical aperture of the fibre. The multi-core fibre has an NA of 0.6 and for 5 m of fibre this results in a $\Delta t_{mod}$ of 4.18 ns. In order to work out the corresponding bandwidth, equation 5.2 is used.

$$Bandwidth = \frac{0.44}{\Delta t_{mod}} \qquad [5.2]$$

This results in a bandwidth of 201.6 MHz. For 10 m and 15 m of fibre, $\Delta t_{mod}$ values of 4.36 ns and 6.55 ns are found resulting in bandwidths of 100.8 MHz and 67.2 MHz, respectively. This matches the values seen in the literature as shown in Figure 5.2.8.

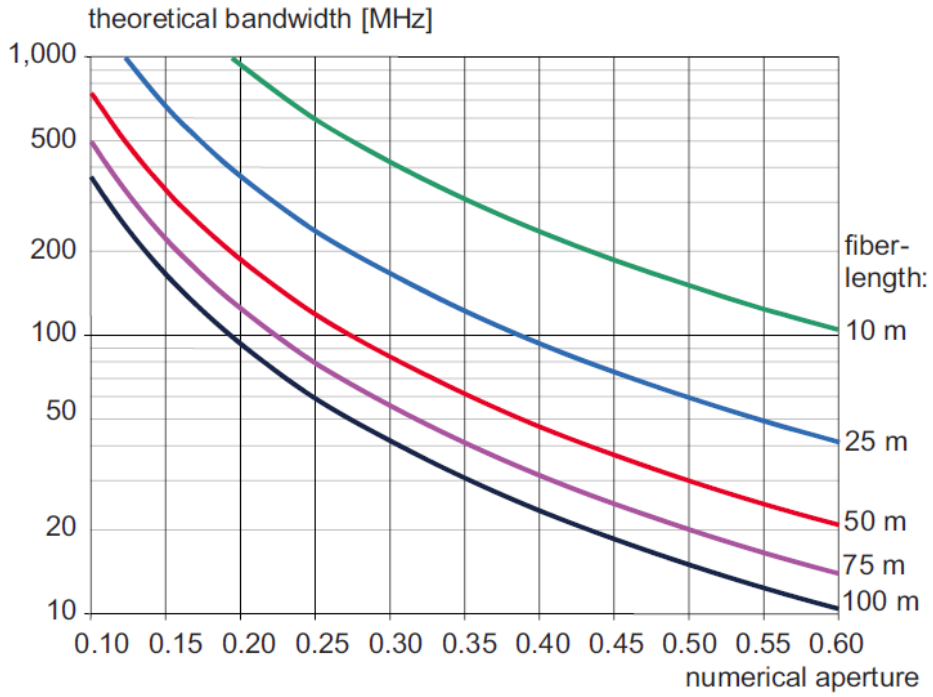


**Figure 5.2.8 Expected bandwidth for fibres of varying length as a function of numerical aperture [11].**

As seen earlier, the fibre bandwidths measured for 5 m, 10 m and 15 m of multi-core fibre were 1.29 GHz, 724 MHz and 360 MHz, respectively. These values are much higher than the calculated bandwidths which could be due to a few reasons. However, the main explanation for this is that the laser light is not optimised for perfect alignment and hence, not all the modes are being taking into consideration. The offset launch technique, which only excites a subset of the modes, results in lower dispersion and hence higher bandwidth [12] [13].

Equation 5.1 assumes that all modes from the fastest to the slowest are considered. There is no way to confirm which modes are being excited in the experiment and if only the fastest modes are being illuminated, then a higher bandwidth is seen.

Furthermore, by using the equations above, the step-index fibre results in a $\Delta t_{mod}$ value of 2.968 ns and a bandwidth of 148.2 MHz for 10 m of fibre. The measured bandwidth value was 1.38 GHz. The same theory applies here, however, it can be seen that the step-index fibre is slightly better than the multi-core fibre. This could be due to the shape of the different cores in the multi-core fibre as seen in Figure 5.2.4 earlier. Also, the step index fibre has a numerical aperture of 0.5 compared to 0.6, which improves the bandwidth as seen in Figure 5.2.8.

Further work could be conducted to look at the data transmission characteristics of both types of fibre using these laser diodes.

## 5.3 Summary and conclusions

In summary, this chapter has looked at the use of fibres for communications. Initial measurements were discussed, which involved step-index plastic optical fibre, in conjunction with a blue laser diode. Further measurements using multi-core fibre were carried out to measure the effect of dispersion on the bandwidth through varying lengths of fibre. As expected, the bandwidth of the fibre is inversely proportional to its length. Following this, measurements were carried out by propagating an optical pulse through the fibre and evaluating how it changed due to the dispersion present. The equations used to calculate the dispersion were given before a comparison of these results and results in the literature was presented. It can be concluded that the presence of dispersion is very high when working at these wavelengths and that this system may only be practical over short distances or to accompany existing systems. It has been shown at the beginning of the chapter that the attenuation at blue wavelengths and red wavelengths are very similar. However, by exploiting the high bandwidth blue devices, measurements were conducted to compare. High speed characterisation using blue light through fibre has been shown which can complement, and be used simultaneously, with the work done using red light.

Chapter 6 looks at another interesting application of these laser diodes. It will present the use of laser diodes for underwater communications.

# References


[1] G. P. Agrawal, *Fiber-Optic Communication Systems*, 3rd ed. John Wiley & Sons, 2002.

[2] Museu das comunicacoes. (2014) Museu das comunicacoes. [Online]. http://macao.communications.museum/eng/main.html

[3] P. Polishuk, "Plastic Optical Fibers Branch Out," *IEEE Communications Magazine*, vol. 44, no. 9, pp. 140-148, 2006.

[4] Riko Opto-Electronics Technology Ltd. (2010) Riko. [Online]. http://www.riko.com/application/e_fiber-spectral-attenuation.html

[5] M. M. Dumitrescu, M. J. Saarinen, M. D. Guina, and M. V. Pessa, "High-Speed Resonant Cavity Light-Emitting Diodes at 650 nm," *IEEE Journal on Selected Topics in Quantum Electronics*, vol. 8, no. 2, pp. 219-230, 2002.

[6] S. C. J. Lee, F. Breyer, S. Randel, H. P. A. van den Boom, and A. M. J. Koonen, "High-speed transmission over multimode fiber using discrete multitone modulation," *Journal of Optical Networking*, vol. 7, no. 2, pp. 183-196, 2008.

[7] S. C. J. Lee, et al., "Discrete Multitone Modulation for Maximising Transmission Rate in Step-Index Plastic Optical Fibers," *Journal of Lightwave Technology*, vol. 27, no. 11, pp. 1503-1513, 2009.

[8] O. Ziemann, "Optical fibers," in *POF Handbook: Optical Short Range Transmission Systems*. Springer, 2008, ch. 2, p. 57.

[9] R. Olshanksy and D. B. Keck, "Pulse broadening in graded-index optical fibers," *Applied Optics*, vol. 15, no. 2, pp. 483-491, 1976.

[10] P. Krehlik, "Characterization of semiconductor laser frequency chirp based on signal distortion in dispersive optical fiber," *Opto-Electronics Review*, vol. 14, no. 2, pp. 123-128, 2006.

[11] O. Ziemann, J. Krauser, P. E. Zamzow, and W. Daum, *POF Handbook: Optical Short Range Transmission Systems*, 2nd ed. Springer, 2008.

[12] L. Raddatz, I. H. White, D. G. Cunningham, and M. C. Nowell, "An Experimental and Theoretical Study of the Offset Launch Technique for the Enhancement of the Bandwidth of Multimode Fiber Links," *Journal of Lightwave Technology*, vol. 16, no. 3, pp. 324-331, 1998.

[13] H. R. Stuart, "Dispersive Multiplexing in Multimode Optical Fiber," *Science*, vol. 289, no. 5477, pp. 281-283, 2000.

# Chapter 6

# Underwater communications

There has become a demand for further technology to advance underwater communication systems. Security and defence industries and oil and gas companies have the need to communicate with unmanned vehicles under the ocean, whether it is two vehicles communicating underwater or equipment on land communicating with an underwater vehicle. Radio frequency (RF) communication is not applicable in sea water as the propagation of electromagnetic waves is limited due to the high conductivity. Currently, acoustic and fibre optic methods are used but these are limited in bandwidth and the use of fibre optics involves complex, expensive setups which are not very practical [1]. Moving towards visible light communication under the water will offer high bandwidth transmission over short distances as it exploits the low-loss transparency window of water, especially using blue and green devices. The use of visible lasers under the water and the ability to track the laser light is investigated in this chapter. Due to the novelty of this application, there are few other publications on this specific topic. However, some systems are in place such as Neptune's underwater communication system from SA Photonics [2] and another from S. Cowen *et al.* [3]. SA Photonics have shown data transmission rates up to 250 Mbit/s over a distance of 200 m in an optical tracking system. S. Cowen et al. have shown a system which can be used to guide an autonomous vehicle underwater and track its progress based on the scattering of the light. Also, B. Cochenour *et al.* have conducted frequency response measurements in different water conditions, showing that these measurements are possible [4]. Using our novel blue laser sources, frequency response measurements were carried out in this chapter. This chapter looks at another optical tracking system using the blue laser diodes, emitting at 422 nm. It begins by exploring the tracking capabilities before looking at the effect of scattering. The ability to carry out frequency response measurements and ultimately data transmission is shown in an underwater environment, with some of the best results in the field presented here. These measurements are conducted over a few metres, however, despite the shorter distance there are still many applications which this is suited to. Deep sea divers can exploit this technology to communicate with one another whilst underwater or they could transmit or receive

information from unmanned underwater vehicles when they get to a certain distance from it.

## 6.1 Optical tracking

When carrying out experiments under the water, the most important aspect is for the detector to pick up the signal. Tests were carried out using a tracking, quadrant detector in order to establish whether or not the laser signal could be picked up. The quadrant detector is position sensitive and when it detects some light, will readjust to find the centre of the incoming beam. Many setups are in place using LEDs as they offer a low cost and low power solution which will provide ~Mbit/s data rates over short distances. However, the signal to noise ratio will be much lower as the beam diverges through the water. Laser diodes provide a collimated, more powerful output meaning they are more suited for longer distances and at much higher data rates which will be explored later in this chapter. Figure 6.1.1 shows the experimental setup making use of a blue GaN laser diode, similar to devices used in previous chapters, and Figure 6.1.2 shows the two ends of the setup in more detail with the detector setup shown on the left hand side and the laser setup with the temperature controller on the right.

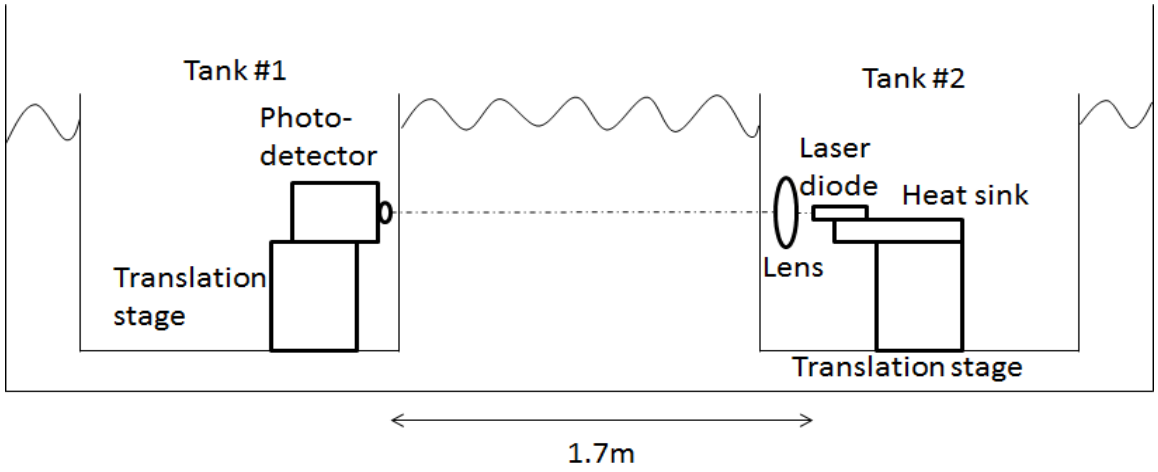


**Figure 6.1.1 Experimental setup.**

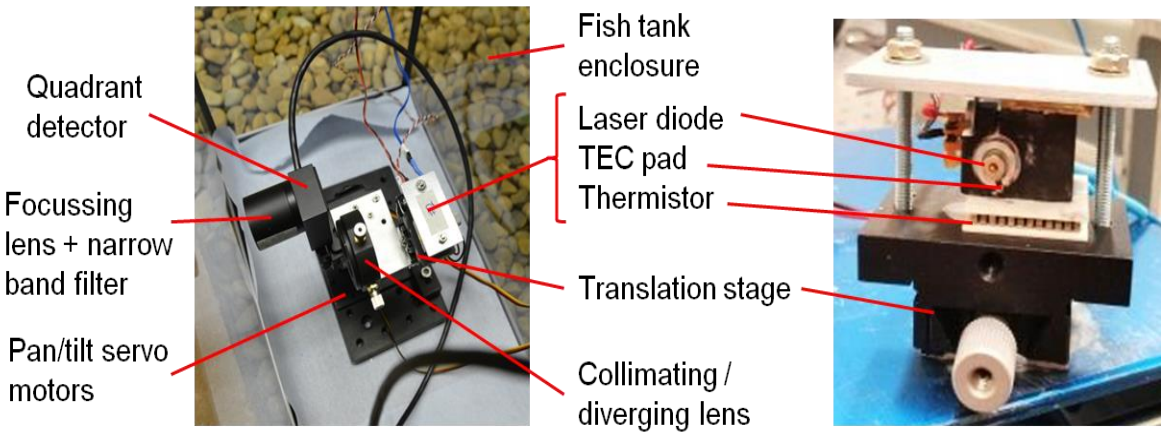


**Figure 6.1.2 The left hand side shows the detector used to track the signal and the right hand side shows the laser and temperature controller setup.**

For this experiment, the two parts of the setup were placed approximately 2 m apart in individual glass tanks. This allows the optical path to be submerged but without damaging the equipment. For the initial measurements the water quality was as good as possible, i.e. without the addition of light scattering material. Subsequently, a commercial antacid consisting of magnesium hydroxide and aluminium hydroxide was used to mimic the different qualities of sea water and analyse how the scattering affected the experiment. Despite the low sensitivity of the quadrant detector (~ -6.2 dBm), the tracking system was able to pick up the laser beam and would readjust itself to find it when the laser was moved. A commercial CCD array camera was then put in place of the quadrant detector in order to image the laser spot. This was able to detect a much larger range of powers than the tracking system and hence, was able to pick up the signal over larger distances.

In order to investigate the scattering properties of sea water, Maalox was used to mimic the effect of sea water particles. Other light-scattering experiments under the water have found Maalox to replicate this scattering behaviour very well [5] [6]. This experiment was conducted over 1 m, to ensure there was sufficient optical power at the detector after the largest amount of Maalox was added. The setup can be seen in Figure 6.1.4.

**Figure 6.1.4 Collimated laser beam under the water from transmitter to detector at a distance of 1 m.**

Doses of Maalox were added in stages so that the increase in scattering could be analysed and attenuation coefficient calculated. Each time a dosage of Maalox was added to the water, the water was stirred for approximately 5 minutes to circulate it and then left to settle for 20 minutes to ensure there was an equal spread of Maalox throughout the tank. It was estimated that there were 8000 litres of water circulating in the tank. Initially dosages of 200 ml were added to the tank to see what effect this had on the laser beam transmission. For Maalox doses of up to 600 ml, the quadrant detector still tracked as expected. It was still able to move and detect the laser beam. Once 1 litre of Maalox had been added, the detector began to lose sensitivity to the beam and did not track the laser as accurately as before. At 2 litres of Maalox, the tracking system no longer functioned as the laser was attenuated to below the noise floor of the detector. A graph showing how the laser transmission is affected with increased Maalox is shown in Figure 6.1.5.

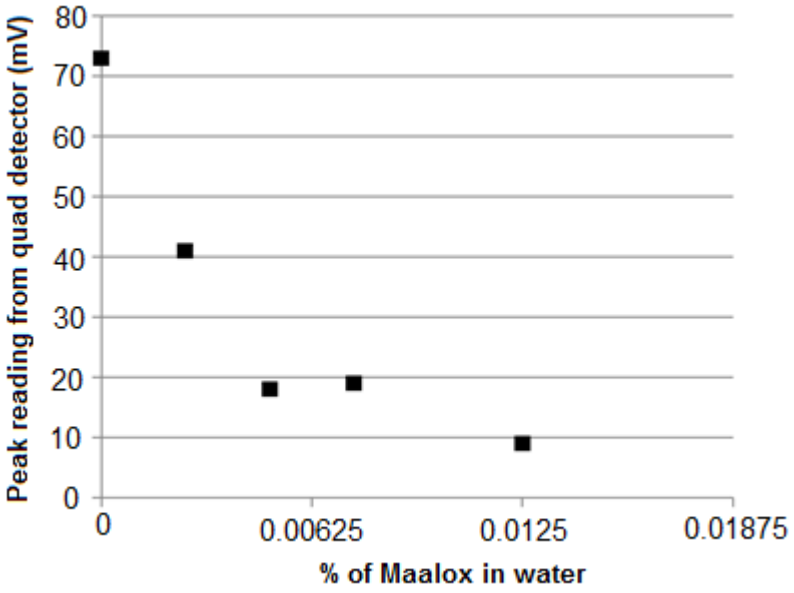


**Figure 6.1.5 Peak voltage reading from quadrant detector as the dose of Maalox added to the water is increased.**

It is clear to see that as the dose of Maalox is increased, the laser scattering is increased. It still functioned with 1 litre of Maalox added but at 2 litres (i.e. 2.5 parts Maalox to $10^4$ water) the signal was undetectable with this photo-receiver. This exponential decrease follows the trends seen using Beer's Law [7]. An image comparing the two extreme levels of scattering can be seen in Figure 6.1.6.

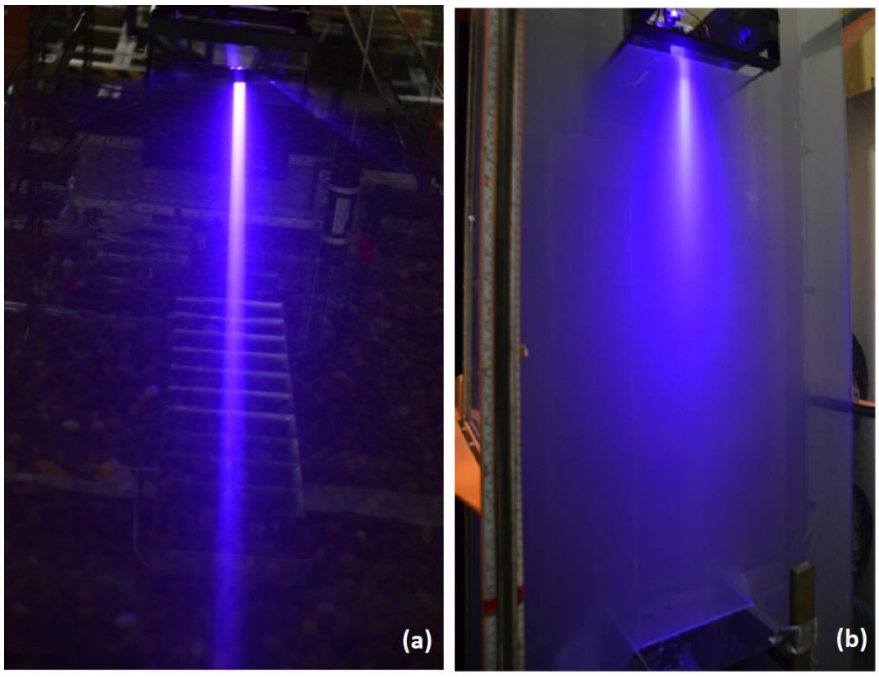


**Figure 6.1.6 Laser transmission over 1 m of water with (a) no Maalox added and (b) 4 litres of Maalox.**

The beam becomes more diverse with an increase in the amount of Maalox added and hence the signal cannot be detected. The experiments suggest a loss of ~24 dB/m per 1 in $10^4$ parts Maalox at this wavelength. This figure is similar to transmission results seen in other experiments [8]. Even before Maalox was added, the water is estimated to be similar in quality to relatively murky coastal water, i.e. an attenuation coefficient of approximately 1.2 $m^{-1}$ [9].

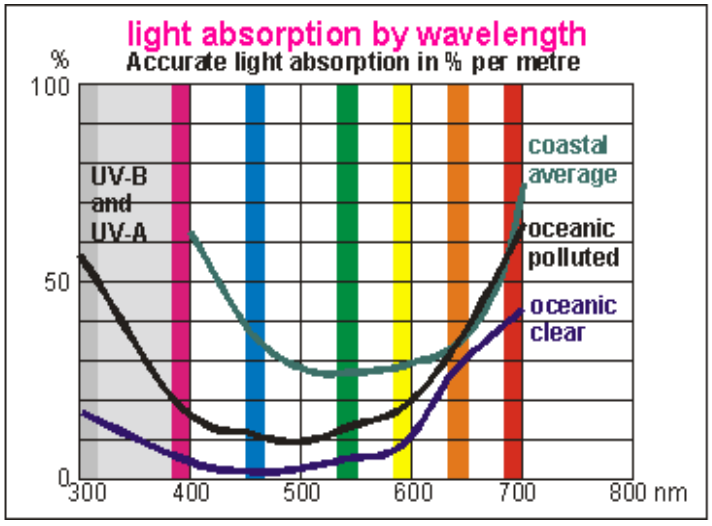


**Figure 6.1.7 Light absorption in water vs wavelength [10].**

Figure 6.1.7 shows that over 40% of the light is absorbed per metre at these wavelengths before the addition of Maalox, and therefore better results could be achieved in clear, oceanic water.

## 6.2 High speed measurements

By using a similar laser diode, high speed measurements were conducted under the water. The water was emptied out of the tank and refilled without any Maalox. The frequency response was measured and data transmission experiments were carried out to analyse the underwater behaviour. The underwater path was approximately 1.7 m in length and the frequency response was measured as a function of drive current. As in previous chapters, the laser diode was driven with a combination of a bias current from a constant current source and an RF signal from a network analyser, and the collimated beam was directed onto a high speed PIN photo-receiver in order to measure the bandwidth. No additional optics were required in order to pick up a signal on the photo-receiver.

In order to compare the effects of the frequency response plot above and below water, a measurement was taken using the same setup but with no water in the tank. The laser used here had a threshold current of 100 mA. The bandwidth values above threshold are very similar with and without the addition of water, showing that the water path has no effect on the measured bandwidth of the laser. This can be seen in Figure 6.1.8.

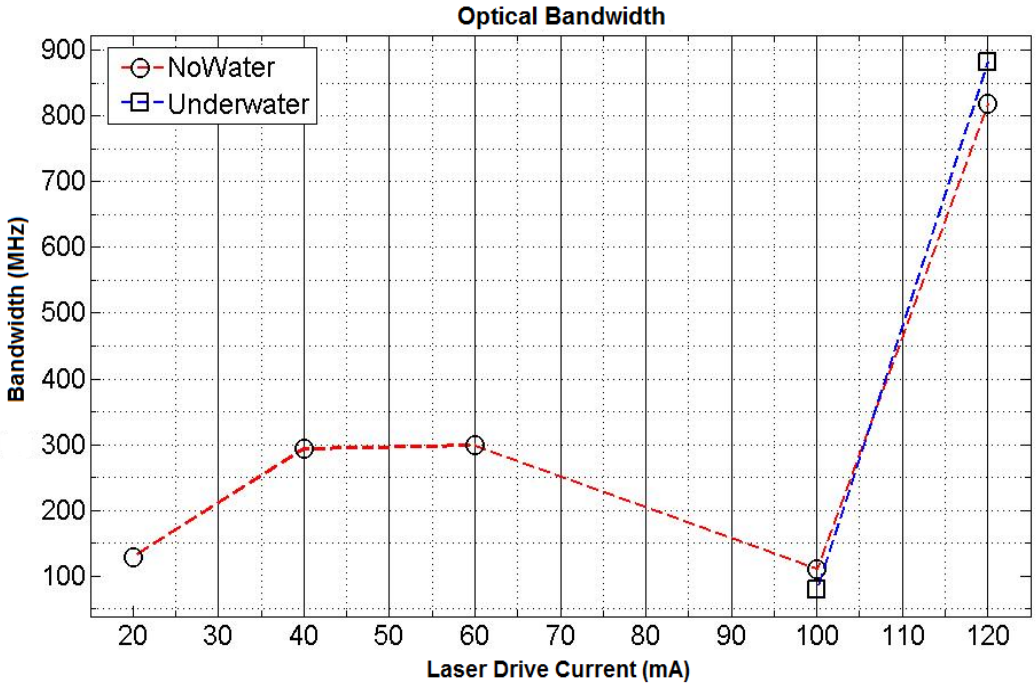


**Figure 6.1.8 Comparison of frequency response measurement with and without water.**

The maximum bandwidth achieved using this device was 883 MHz at 120 mA. As shown in Figure 6.1.8, only values above the laser threshold are given for the case underwater. This is because the power is too low below threshold in order to measure the frequency response at the photo-receiver, due to the losses in the water. Figure 6.1.9 shows two frequency response plots at 120 mA. The black line is the signal without any water and the red line is the signal with water in the tank. Despite the difference in signal strength, the same value of -3 dB bandwidth is seen in both cases.

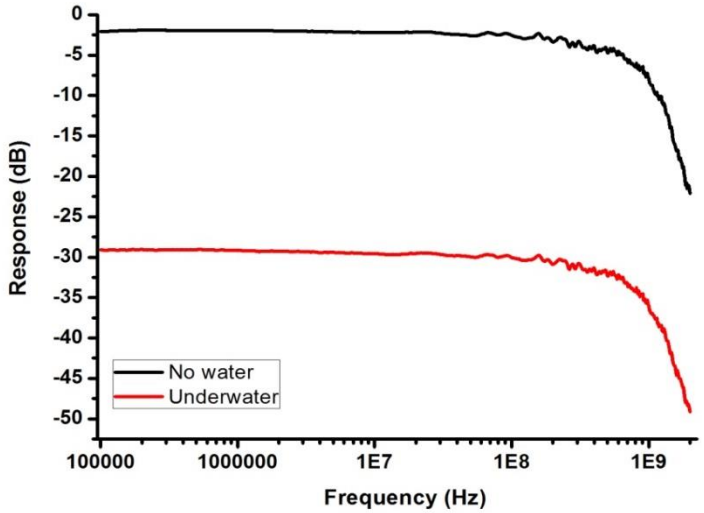


**Figure 6.1.9 Frequency response plots at 120 mA with and without water.**

In practise, the laser would almost always be used above threshold for underwater applications. Further measurements were carried out underwater using this device as a source for data transmission experiments. A bit-error rate test (BERT) system was used to provide a pseudo-random bit sequence (PRBS) of $2^7$-1 bits in length, with a peak-to-peak amplitude of 2 V. This was then combined with a DC bias and used to modulate the device.

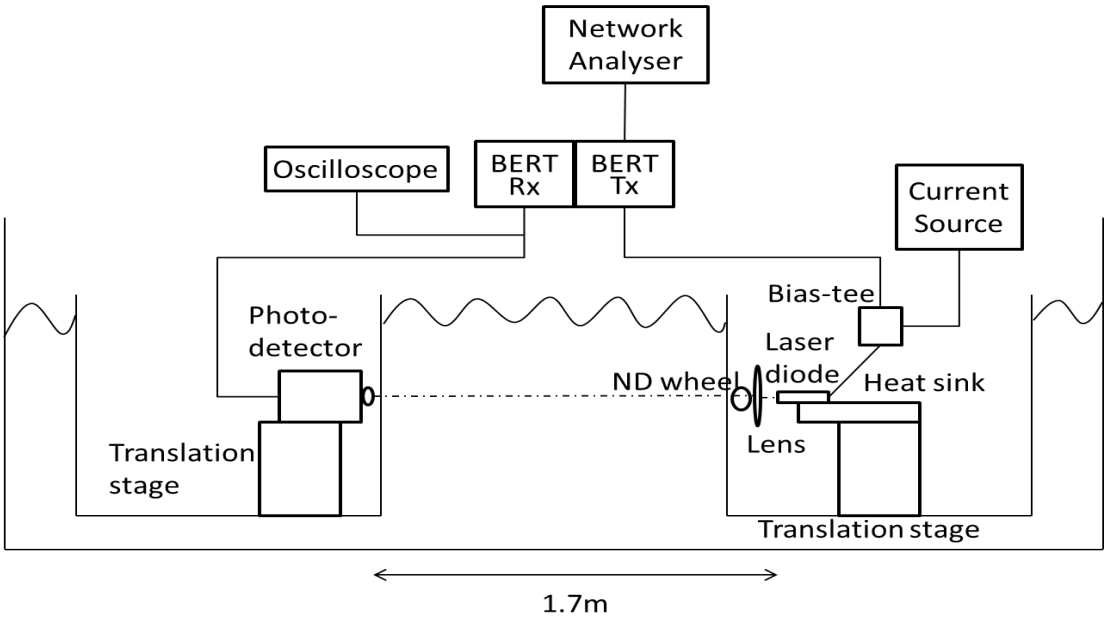


**Figure 6.1.10 Experimental setup for data transmission underwater.**

In order to visualise the underwater performance, the output of the photo-receiver was connected to a fast oscilloscope to examine the eye diagrams.

Figure 6.1.10 shows the experimental setup for data transmission experiments with the eye diagrams at different bit rates shown in Figure 6.1.11.

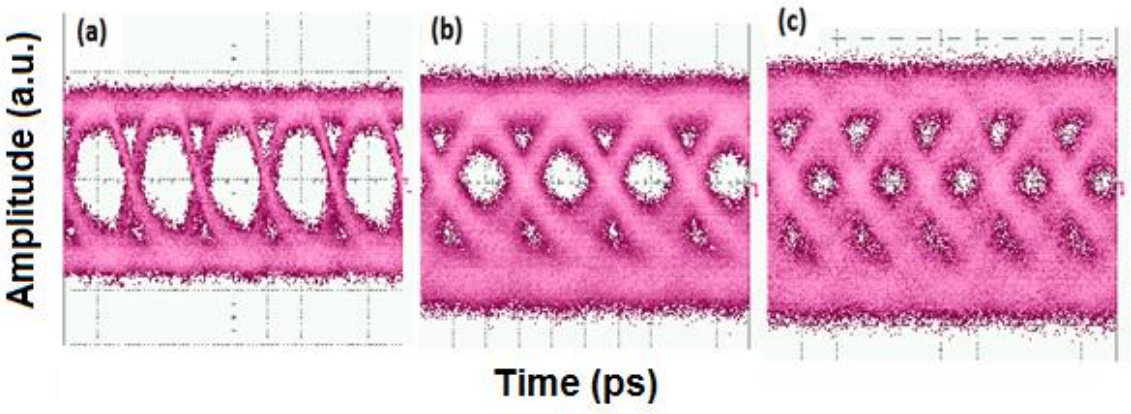


**Figure 6.1.11 Eye diagrams showing data transmission under the water at (a) 1 Gbit/s at 125 mA, (b) 2 Gbit/s at 132 mA and (c) 2.488 Gbit/s at 132 mA.**

As the bit-rate is increased, the 'eye' begins to close. The lower the signal-to-noise ratio, the more noise that is displayed. At a data rate of 2.488 Gbit/s, the eye diagram is noisy but still open showing that data transmission can be achieved. Indeed, the signal was retrieved by the BERT, confirming that error-free data transmission could be carried out. Figure 6.1.12 shows the bit-error rate plotted against the received optical power for the three bit rates.

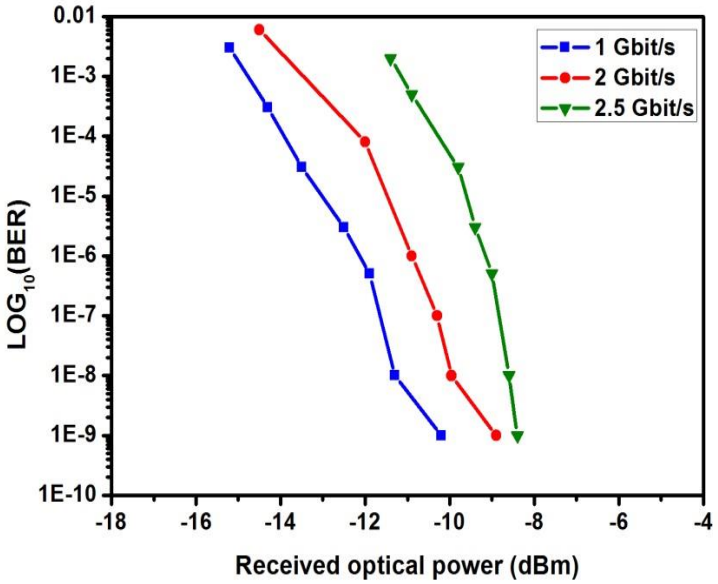


**Figure 6.1.12 Bit-error rate vs received optical power at 1, 2 and 2.5 Gbit/s.**

Sensitivities of -10.2, -8.9 and -8.4 dBm are seen at bit rates of 1, 2 and 2.5 Gbit/s, respectively. These power values are slightly higher than the free space measurements as the alignment and focussing of the light underwater is different. The beam spot is bigger when trying to focus the light onto the detector underwater and hence, more power is needed to reach the same bit-error rates.

## 6.3 Summary and conclusions

A range of experiments have been conducted in this underwater setup from optical tracking to data transmission. Above-water and below-water measurements have been carried out to compare the tracking mechanisms and optical communication properties. For the experiments in this chapter, a single, blue laser diode has been used as the source for both tracking and communications and this is desirable for a number of reasons. Firstly, it has been shown that it is capable of high bandwidth modulation, not only above water, but underwater too. This leads itself to desirable properties in terms of data transmission with data rates of 2.488 Gbit/s achieved under the water. Also, the laser beam has a degree of divergence control and the stimulated emission output after threshold makes it appropriate for this purpose. It has been seen that there is low attenuation around the blue part of the spectrum and the laser diodes used have exploited this.

An underwater optical tracking system was realised making use of a blue laser diode and quadrant detector as mentioned in this chapter. Experiments were conducted where scattering solution was added to the water in order to determine how this affected the laser transmission. Maalox, the solution which was used, is known to mimic the scattering properties of seawater particles. As expected, the more solution that was the added, the laser transmission through the water was reduced. The beam became more divergent and the optical power reaching the detector was small or non-existent. A loss of 24 dB/m per 1 in $10^4$ parts Maalox was measured. Further distances could be achieved through clear water. However, it has been proved that this tracking system is fully operational and can achieve high data rates under the water.

# References


[1] W. C. Cox Jr. (2008) NCSU Libraries. [Online]. http://www.lib.ncsu.edu/resolver/1840.16/1696

[2] SA Photonics. (2015) Neptune Underwater Communications. [Online]. http://www.saphotonics.com/high-bandwidth-optical-communications/underwater/

[3] S. Cowen, S. Briest, and J. Dombrowski, "Underwater docking of autonomous undersea vehicles using optical terminal guidance," in *OCEANS 97 MTS/IEEE Conference*, vol. 2, 1997, pp. 1143-1147.

[4] B. Cochenour, L. Mullen, and J. Muth, "Temporal Response of the Underwater Optical Channel for High-Bandwidth Wireless Laser Communications," *IEEE Journal of Oceanic Engineering*, vol. 38, no. 4, pp. 730-742, 2013.

[5] F. Hanson and S. Radic, "High Bandwidth Underwater Optical Communication," *Applied Optics*, vol. 47, no. 2, 2008.

[6] A. Laux, et al., "The a, b, c's of oceanographic lidar predictions: a significant step toward closing the loop between theory and experiment," *Journal of Modern Optics*, vol. 49, no. 3-4, pp. 439-451, 2002.

[7] A. Beer, "Bestimmung der Apsorption des rothen Lichts in fabrigen Flussigkeiten (Determination of the absorption of red light in coloured liquids)," *Annalen der Physik und Chemie*, vol. 86, pp. 78-88, 1852.

[8] P. A. Hiskett, R. Struthers, R. Tatton, and R. Lamb, "A photon-counting optical communication system for underwater data transfer," in *SPIE Security and Defence Europe*, vol. 8542, Edinburgh, 2012.

[9] M. A. Watson, et al., "Assessment of Laser Tracking and Data Transfer for Underwater Optical Communications," in *SPIE Unmanned/Unattended Sensors and Sensor Networks X*, vol. 9248, 2014.

[10] J. F. Anthoni. (2000-2005) Seafriends: Water and light in underwater photography. [Online]. http://www.seafriends.org.nz/phgraph/water.htm

# Chapter 7

# Conclusions

This thesis has presented the system measurements which have been conducted using gallium nitride light-emitting diodes and laser diodes and the applications that they are useful for. Measurements which have been carried out include LVI measurements to characterise the devices, spectral measurements to establish their emission wavelength, frequency response measurements to explore their modulation characteristics and data transmission experiments to see at what rates the data can be transmitted. Both micro-LEDs and laser diodes have showed great potential for applications in communications amongst many other things.

Chapter 1 provided a general introduction to the thesis. It set out the different topics which were covered and gave a brief introduction to the devices that were used. LEDs have developed over the last 50 years and a look at their development and different structures is introduced at the start of chapter 1. This chapter then introduces laser diodes before portraying the use of LEDs and laser diodes for communication applications. A short introduction to the fibre measurements and the underwater measurements was given to conclude this introductory chapter.

An in depth study of the relative theory and corresponding literature review was given in chapter 2. A study of the work that has been done using LEDs for visible light communications was presented before an analysis of their limitations was given. There are many different types of LED and there are lots of different modulation schemes which have been explored to advance data rates. A review of eye diagrams and crosstalk was shown before a study of the work carried out using laser diodes was reported. Different types of fibre were explored and their characteristics explained in detail. Finally in chapter 2, a review of work that has been carried out underwater in the topic of communications was presented.

Chapter 3 looked at the use of micro-LEDs for communications. It introduced the different ways to drive these devices. For high speed measurements, it was shown that using a probe to drive the LEDs directly was the best method to get

the highest modulation bandwidths and data transmission rates. However, the ability to externally control the LEDs using complementary metal oxide semiconductor (CMOS) technology was explored and proven to simplify the way the LEDs are driven. There were two main results sections in chapter 3: parallel data transmission using a blue micro-LED and a novel CMOS controlled colour tuneable micro-LED. The results achieved were presented showing the potential of a multi-colour display from a single LED which can provide a communication link. Parallel data transmission was also presented using a blue micro-LED which was shown to be a good way to increase the overall data rate. The fastest data rates for this work were recorded and published. Other methods have been considered and further work could achieve some better results.

The use of laser diodes for communications in free space was explored in chapter 4. High speed measurements using a blue laser diode were carried out to explore the potential of laser diodes for visible light communications. A look at the structure of such devices was given before the LVI and spectral characteristics were presented. The bandwidth measurements and data transmission experiments were shown before an analysis of the reliability of these devices was given. Error free data transmission was shown initially at 2.5 Gbit/s and then at 3.4 Gbit/s showing the potential of these devices for communications. These laser diodes were also used to drive some colour converting materials which showed fast modulation characteristics.

Fibre communications is another important topic and the use of these blue laser diodes was explored for this purpose in chapter 5. The fibre itself was described before more high speed measurements were conducted. An in depth analysis of the dispersion in the fibre was conducted showing that the transmission distance may be limited when working at this wavelength.

Finally, chapter 6 looks at the prospect of underwater communications. Measurements were conducted under the water to evaluate the ability to track a laser signal and ultimately to determine its bandwidth and data transmission characteristics in an underwater environment. The frequency response proved to be very similar to the above-water measurements and a data rate of 2.488 Gbit/s was achieved. Different water qualities were tested and the results presented in chapter 6 were also published.

Overall, this thesis has presented the high speed measurements using GaN LEDs and laser diodes for communications. It has been shown that there are a number of relevant applications using this technology. The devices have shown great potential to become leading sources for this work. Some novel results have been presented here, with some of the work being published in worldwide journal and conference papers.

## 7.1 Future work

There are still a number of measurements which could be carried out to advance this work further. It has been shown that the limiting factor in the high speed measurements of laser diodes was the bandwidth limit of the photo-receiver. With a much faster photo-receiver, which is responsive in the visible spectrum, I believe higher bandwidths and higher data transmission rates will be achieved. Many free space photo-receivers which work at higher speeds tend to lose their responsivity to lower wavelengths in the visible spectrum. Fibre can be used to couple the light onto the detector but then there are losses associated with the fibre. I feel more work could be done to advance this and ultimately achieve better results. Also, I think further study is needed to analyse the degradation of the laser diodes. It has been shown that the laser diodes performance degrades over time which is usually due to its structure. Therefore, further analysis should be done on the fabrication of these laser diodes to try and improve their reliability.

The bulk of the measurements presented in this thesis have been using blue-emitting devices. There is the potential to use ultra-violet (UV) devices for short-range communications amongst other things. Ultra-violet light has many advantages for applications such as contamination control, medical treatments and fluorescent inspection [1]. It would be interesting to explore the performance of UV based devices for these applications.

Single frequency lasers are another area of interest. These are lasers which operate on a single resonator mode with a very small linewidth and low noise. They can be used to exploit the Fraunhofer lines for communication purposes [2] in situations where communication may not have been possible before.

Chapter 3 looked at the concept of parallel data transmission. It may be of interest to look at isolating each of the beams using micro-lenses or spatial light modulators, as well as increasing the number of detectors used. Multiple-input multiple-output (MIMO) systems would be one way to improve on the results presented in this thesis. However, looking at improvements of the transmitters and corresponding circuitry may also be beneficial in terms of reducing ground bounce from the CMOS circuitry and by increasing the power from the devices.

As mentioned in Chapter 5, there is still some work to be completed using the fibre for communications. Bit-error rate measurements should be conducted to determine the data transmission characteristics using blue laser diodes through the varying types and varying lengths of fibre. It was concluded from chapter 5 that there are very high levels of dispersion when working at this wavelength, however it will still be possible to carry out data transmission experiments to see how the different kinds of fibre perform.

# References

[1] UV Light Technology. UV Light Technology. [Online]. http://www.uv-light.co.uk/applications/overview.php

[2] E. L. Kerr, "Fraunhofer filters to reduce solar background for optical communications," California Institute of Technology, 1986.